https://doi.org/10.15388/vu.thesis.740
https://orcid.org/0000-0002-9361-6562

VILNIUS UNIVERSITY

Rokas Stulpinas

HCC Prognostic Modeling Using AI-Based Tissue Analysis

DOCTORAL DISSERTATION

Medicine and Health Sciences,
Medicine M 001

VILNIUS 2025

The dissertation was prepared between 2020 and 2024 at Vilnius University. The research was in part funded by the *European Social Fund* resources allocated for the project *Development of Doctoral Studies* implemented by the Research Council of Lithuania, project No. 09.3.3-ESFA-V-711-01-0001, under the Specific objective *Strengthen the Skills and Capacities of Public Sector Researchers for Engaging in High Level R & D Activities* of Priority Axis 9 *Educating the Society and Strengthening the Potential of Human Resources* within the framework of the *Operational Programme for the European Union Funds' Investments in 2014–2020*.

Academic supervisor – Prof. Dr. Arvydas Laurinavičius (Vilnius University, Medicine and Health Sciences, Medicine – M 001).

This doctoral dissertation will be defended in a public meeting of the Dissertation Defence Panel:

Chairperson:
Prof. Dr. Janina Tutkuvienė (Vilnius University, Medicine and Health Sciences, Medicine – M 001).

Members:
Assoc. Prof. Dr. Vaida Baltrūnienė (Vilnius University, Medicine and Health Sciences, Medicine – M 001),
Assoc. Prof. Dr. Justinas Besusparis (Vilnius University, Medicine and Health Sciences, Medicine – M 001),
Prof. Dr. Dainius Characiejus (Vilnius University, Medicine and Health Sciences, Medicine – M 001),
Prof. Dr. Sandra Lejniece (Rīga Stradiņš University, Medicine and Health Sciences, Medicine – M 001).

The dissertation shall be defended at a public meeting of the Dissertation Defence Panel at 14:00 on 27 March 2025 at the Medical Science Centre of Vilnius University Faculty of Medicine. Address: Žaliųjų Ežerų 2, LT-08406, Vilnius, Lithuania

The text of this dissertation can be accessed at Vilnius University Library, as well as on the website of Vilnius University at
www.vu.lt/lt/naujienos/ivykiu-kalendorius

https://doi.org/10.15388/vu.thesis.740
https://orcid.org/0000-0002-9361-6562

VILNIAUS UNIVERSITETAS

Rokas Stulpinas

Hepatoceliulinės karcinomos (HCC) prognostinis modeliavimas dirbtinio intelekto metodais

DAKTARO DISERTACIJA

Medicinos ir sveikatos mokslai,
Medicina M 001

VILNIUS 2025

Disertacija rengta 2020–2024 metais Vilnaus universitete.

Mokslinius tyrimus iš dalies rėmė Europos socialinis fondas, skyręs lėšas Lietuvos mokslo tarybos vykdomam projektui „Doktorantūros studijų plėtra“, projekto Nr. 09.3.3-ESFA-V-711-01-0001, priemonė „Mokslininkų ir kitų tyrėjų gebėjimų stiprinimas“, 9 prioritetinė kryptis „Visuomenės švietimas ir žmogiškųjų išteklių potencialo didinimas“ pagal Europos Sąjungos fondų investicijų 2014–2020 m. veiksmų programą.

Mokslinis vadovas – prof. dr. Arvydas Laurinavičius (Vilniaus universitetas, medicinos ir sveikatos mokslai, medicina – M 001).

Gynimo taryba:

Pirmininkė:
Prof. dr. Janina Tutkuvienė (Vilniaus universitetas, medicinos ir sveikatos mokslai, medicina – M 001).

Nariai:
Doc. dr. Vaida Baltrūnienė (Vilniaus universitetas, medicinos ir sveikatos mokslai, medicina – M 001),
Doc. dr. Justinas Besusparis (Vilniaus universitetas, medicinos ir sveikatos mokslai, medicina – M 001),
Prof. dr. Dainius Characiejus (Vilniaus universitetas, medicinos ir sveikatos mokslai, medicina – M 001),
Prof. dr. Sandra Lejniece (Rygos Stradinio universitetas, medicinos ir sveikatos mokslai, medicina – M 001).

Disertacija ginama viešame Gynimo tarybos posėdyje 2025 m. kovo mėn. 27 d. 14:00 val. Vilniaus universiteto Medicinos fakulteto Medicinos mokslo centre. Adresas: Žaliųjų Ežerų g. 2, 08406, Vilnius, Lithuania

Disertaciją galima peržiūrėti Vilniaus universiteto bibliotekoje ir VU interneto svetainėje adresu:
https://www.vu.lt/naujienos/ivykiu-kalendoriu

ACKNOWLEDGEMENTS

First and foremost, I am grateful to my supervisor, Prof. Dr. Arvydas Laurinavičius, for his guidance, support, and feedback throughout this research process, while also allowing me the freedom to make my own decisions.

I would like to extend my sincere thanks to Dr. Mindaugas Morkūnas, Dr. Aistė Gulla, Julius Drachneris, Dr. Dovilė Žilėnaitė-Petrulaitienė, Dr. Allan Rasmusson, Renaldas Augulis and Prof. Dr. Kęstutis Strupas for their collaborative efforts and expertise. They laid the foundations for this research and worked side by side with me without hesitation throughout the entire process of conducting my research and writing this thesis.

I am particularly grateful to Prof. Dr. Dainius Characiejus, Assoc. Prof. Dr. Vaida Baltrūnienė, and Assoc. Prof. Dr. Vincas Urbonas for serving as reviewers of my thesis. Their insightful comments and constructive feedback have significantly enhanced the quality of this work.

My appreciation also goes to the staff at the National Center of Pathology for their technical assistance and support with the sample preparation and digital pathology infrastructure. I am grateful to Vilnius University Hospital Santaros Clinics and the National Center of Pathology for providing the necessary resources and environment to conduct this research.

I extend my heartfelt thanks to my dear friend and colleague Ugnius Mickys for his moral support and motivation throughout this journey.

Finally, I am deeply grateful to my beloved family for their unwavering support and endless patience during this challenging journey. To my wife Živilė, thank you for being my pillar of strength, for your understanding during the long hours of work, and for keeping our family together through it all. To my wonderful children, Rytis and Meda, your smiles and hugs have been my greatest motivation. Your love and belief in me have made all the difference.

LIST OF ABBREVIATIONS

AI	Artificial intelligence
AIC	Akaike information criterion
BCLC	Barcelona Clinic Liver Cancer
CD8	Cluster of differentiation 8
CI	Confidence interval
C-index	Concordance index
CM	Center of mass
CNN	Convolutional neural networks
CSM	Collagen segmentation mask
EE	Epithelial edge
FFPE	Formalin-fixed paraffin-embedded
GMM	Gaussian mixture model
GSPS	Gordon and Sweet's silver impregnation with picric acid–Sirius red
H&E	Hematoxylin-eosin
HCC	Hepatocellular carcinoma
HR	Hazard ratio
ID	Immunodrop
IZ	Interface zone
LASSO	Least absolute shrinkage and selection operator
ML	Machine learning
NAFLD	Non-alcoholic fatty liver disease
OS	Overall survival
RFS	Recurrence-free survival
SD	Standard deviation
SHG	Second harmonic generation
TE	Tumor edge
TIL	Tumor-infiltrating lymphocyte
WSI	Whole slide image

TABLE OF CONTENTS

INTRODUCTION

Background on HCC and current prognostic challenges

Hepatoellular Carcinoma (HCC) ranks as the third leading cause of cancer-related deaths worldwide, with a staggering 70% increase in incidence from 1990 to 2019 [1]. The global burden of HCC is significant, resulting in 480,000 attributable deaths in 2019, and this situation is further exacerbated by late diagnoses and advanced disease stages at presentation [2]. While early detection can lead to a five-year survival rate exceeding 70%, this rate plummets to a mere 18% in the later stages, underscoring the critical importance of an early diagnosis and accurate prognostication [3]. Liver cirrhosis, often induced by viral hepatitis B and C, alcohol consumption, chemical toxins, or metabolic liver diseases, precedes HCC in at least 80% of cases [4]. Furthermore, the global rise of obesity and type 2 diabetes has led to an increased incidence of *Non-Alcoholic Fatty Liver Disease* (NAFLD), which has emerged as a primary cause of HCC even in the absence of cirrhosis [5].

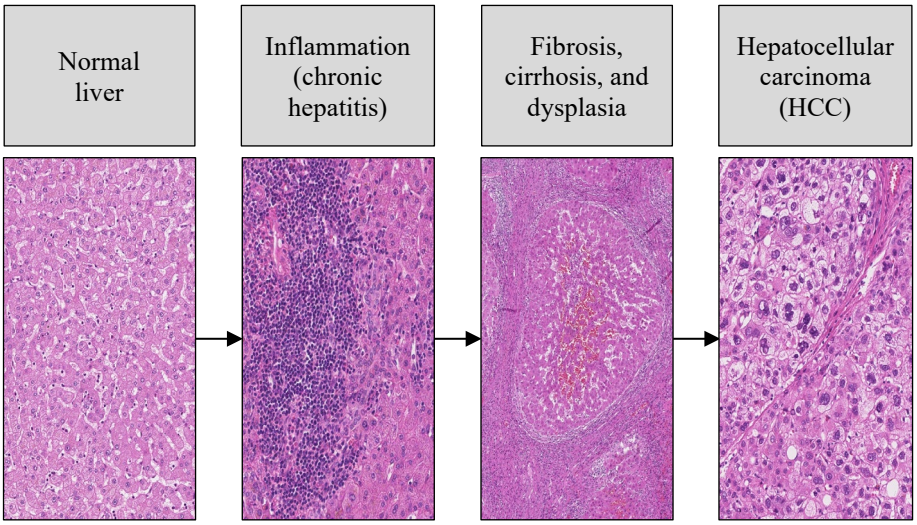

Figure 1. HCC is a prototypical inflammation-associated cancer; in 80% of the cases, the disease follows a similar pattern of evolution

The current prognostic models for HCC are facing several challenges. Unlike many other cancers, post-treatment clinical outcomes in HCC patients do not rely solely on the tumor properties and the success of its therapy [6]. An equally important determinant is the pathology and functional capacity of the residual liver tissue, thus highlighting the need for comprehensive

assessment of both tumor and non-tumor components [7]. The *Barcelona Clinic Liver Cancer* (BCLC) staging system attempts to address this complexity by incorporating multiple parameters of the tumor burden, liver function, and cancer-related symptoms [8]. However, even this system suffers from limitations in an attempt of accurately predicting the loss of the liver function specifically in the context of HCC [9].

The heterogeneity of HCC in terms of its etiology, molecular characteristics, and clinical presentation further complicates prognostication [10]. Additionally, the dynamic nature of the disease, with the potential for rapid progression and the development of portal vein invasion or extrahepatic spread, poses challenges for any long-term outcome prediction [11]. These factors collectively highlight the urgent need for more refined and personalized prognostic tools in HCC management.

Brief overview of AI and machine learning in pathology

The field of pathology is witnessing a paradigm shift with the integration of *Artificial Intelligence* (AI) and *Machine Learning* (ML) technologies, offering new avenues for diagnosis, prognosis, and personalized medicine [12]. Digital pathology, which involves the digitization of *Whole Slide Images* (WSI), has paved the way for the application of advanced computational techniques to histopathological analysis [13].

Convolutional Neural Networks (CNNs), a class of deep learning algorithms, have shown remarkable success in tasks such as automated tissue segmentation, cell detection, and classification of histological patterns [14]. These AI models can process vast amounts of visual data, while identifying subtle patterns and features that may get missed even by the best-trained human observers [15]. In the context of HCC, CNNs have been employed for tasks ranging from automated detection of tumor regions to the assessment of the histological grade and microvascular invasion [16].

Beyond simple classification tasks, AI techniques are being used to extract quantitative features from histological images, which is a field known as computational pathology [17]. These approaches can capture complex tissue architectures, cellular distributions, and morphological characteristics, providing a vast array of potential biomarkers [18]. For instance, AI-based analysis of tumor-infiltrating lymphocytes and stromal features has shown promise in predicting patient outcomes across various cancer types [19].

Machine learning algorithms, including support vector machines, random forests, and gradient boosting methods, are being used to integrate these image-derived features with the clinical and molecular data, creating

comprehensive prognostic models [20]. These models offer the potential to outperform the traditional staging systems and provide more personalized risk stratification [21].

Despite these advancements, the integration of AI in the pathology practice faces several challenges, including the need for large, diverse datasets for training, issues of interpretability and explainability of AI decisions, and the requirement for rigorous validation before clinical implementation [22]. Nonetheless, the continued development of AI tools in pathology holds great potential for enhancing the diagnostic accuracy, improving prognostic predictions, and ultimately guiding personalized treatment decisions in diseases like HCC [23].

Multimodal tissue analysis in HCC prognostication

The complex interplay between tumor cells, the immune system, and the extracellular matrix in HCC necessitates a multifaceted approach to prognostication. Our study focuses on three key aspects of the tumor microenvironment: CD8 lymphocytes, collagen (Type I and Type III) architecture, and the overall tissue patterns. Each of these components offers unique and complementary insights into the tumor biology and the potential disease outcomes.

CD8 lymphocytes play a crucial role in the anti-tumoral immune response and have shown prognostic significance across various cancer types [24]. In HCC specifically, the density and spatial distribution of CD8 cells have been associated with the patient outcomes, although the results have been somewhat inconsistent [25,26]. By employing advanced spatial analytics to characterize CD8 infiltration patterns, we aimed to resolve these inconsistencies and extract more nuanced prognostic information [27].

The extracellular matrix, particularly Type I collagen and Type III collagen (also called reticulin) fibers, forms a critical component of both the tumor microenvironment and the surrounding liver tissue. In HCC, alterations in the reticulin framework are a key diagnostic feature, while changes in the collagen deposition reflect both tumor-associated processes and underlying liver fibrosis [28,29]. Quantitative analysis of these fiber patterns by using AI-based approaches offers the potential to capture subtle architectural changes that may be of prognostic relevance [30].

Lastly, the concept of tissue ‘fingerprinting’ using deep learning algorithms aims to capture specific tissue patterns that may be complicated and challenging to quantify through predefined features. This approach has shown promise in other cancer types for identifying subtle prognostic signatures [31]. By applying

this technique to HCC, we sought to potentially uncover novel tissue characteristics associated with the disease outcomes.

By integrating these diverse aspects of tissue analysis – immune cell infiltration, extracellular matrix architecture, and the overall tissue patterns – we aimed to develop a more comprehensive and robust approach to HCC prognostication. This multimodal strategy reflects the complex biology of HCC and has the potential to provide a more accurate and personalized risk stratification for patients [32].

Study hypothesis

The integration of artificial intelligence-based analyses of tumor microenvironment, immune response, and tissue architecture will improve the prognostic accuracy for hepatocellular carcinoma compared to the traditional clinicopathological factors alone.

Objective of the study

To develop comprehensive AI-driven prognostic models for hepatocellular carcinoma by integrating digital pathology analyses of tumor microenvironment, immune response, and tissue microarchitecture in patients after surgical treatment.

Tasks of the study

1. To develop a prognostic model based on the spatial distribution and density of CD8 lymphocytes at the tumor and residual parenchyma tissue compartments using AI-driven image classification and hexagonal grid subsampling techniques.
2. To develop a prognostic model for hepatocellular carcinoma by employing AI-driven morphometric analysis of collagen patterns in the tumor microenvironment and the adjacent liver parenchyma.
3. To develop a prognostic model for hepatocellular carcinoma by using deep learning neural networks with the objective to identify and analyze distinctive microarchitectural signatures (‘fingerprints’) of the tumor.
4. To integrate the developed models and assess their combined prognostic performance for hepatocellular carcinoma.

MATERIALS AND STAINING

Bioethics permit and funding

Vilnius Regional Biomedical Research Ethics Committee approved (permit number 2021/6-1354-843, issued 29 June 2021) the study design. Patient consent was waived according to the *International Ethical Guidelines for Health-Related Research Involving Humans*.

This research is in part funded by the *European Social Fund* resources allocated for the project *Development of Doctoral Studies* implemented by the *Research Council of Lithuania*, project No. 09.3.3-ESFA-V-711-01-0001, under the Specific Objective *Strengthen the Skills and Capacities of Public Sector Researchers for Engaging in High Level R&D Activities* of Priority Axis 9 *Educating the Society and Strengthening the Potential of Human Resources* within the framework of the *Operational Program for the European Union Funds' Investments in 2014–2020*.

Patient cohort and sample collection

The complete cohort of the study included a total of 134 patients with *Hepatocellular Carcinoma* (HCC) who underwent a surgical intervention – either a liver resection or transplantation – at Vilnius University Hospital Santaros Clinics (Vilnius, Lithuania) between 2007 and 2020. The patient characteristics are presented in Table 1.

Table 1. Summary of patient characteristics

Characteristic	**Value**
Gender	Male: 101 (75.4%) Female: 33 (24.6%)
Age	Mean: 60.45 years (range: 13–82)
Tumor Grade	G1: 13 (9.7%) G2: 101 (75.4%) G3: 20 (14.9%)
pT Stage	T1: 53 (39.6%) T2: 73 (54.5%) T3: 7 (5.2%) T4: 1 (0.7%)
Intravascular Invasion	Present: 59 (44%) Absent: 75 (56%)

Characteristic	Value
Cirrhosis	Present: 89 (66.4%) Absent: 45 (33.6%)
Multiple Tumors	Yes: 37 (27.6%) No: 97 (72.4%)
Tumor Size	>2cm: 108 (80.6%) >5cm: 30 (22.4%)
Viral Status	HBV: 12 (9%) HCV: 74 (55.2%)
Liver Transplantation	Yes: 28 (20.9%) No: 106 (79.1%)
Recurrence After Treatment	Yes: 57 (42.5%) No: 77 (57.5%)

The initial analysis revealed significant (p=0.0011) *Overall Survival* (OS) differences between the transplanted (N=28) and the non-transplanted (N=106) patient subgroups.

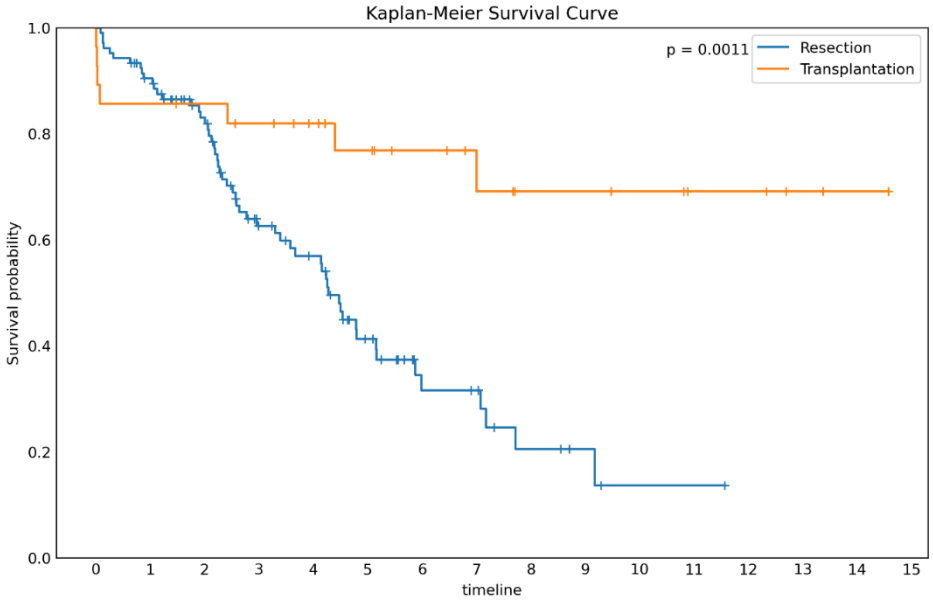

Figure 2. Overall survival following liver transplantation versus resection in hepatocellular carcinoma patients

The decision was made to analyze the transplanted and non-transplanted HCC patients separately in further prognostic modeling. This decision is backed by several arguments:

1. Patients selected for transplantation often have different disease characteristics compared to those undergoing resection. They may have more advanced cirrhosis but earlier stage tumors due to adherence to the Milan criteria which define patients eligible for transplantation.
2. Liver transplantation and resection are fundamentally different treatments with different risks involved, as well as different impacts on the tumor microenvironment and the residual liver tissue.
3. The subsequent univariate analysis of prognostic factors revealed that the predictors of outcomes may differ between these groups. For instance, the tumor size was more predictive in the transplanted group, while the immune response parameters were more relevant in the non-transplanted group.
4. With only 28 transplanted patients compared to 106 non-transplanted, combining the groups could mask important prognostic factors specific to the larger resection cohort.
5. Separate models for transplanted and non-transplanted patients could provide more tailored prognostic information, potentially guiding treatment decisions between these two options.
6. The immune microenvironment and its prognostic significance may differ in the context of total liver replacement (transplantation) versus partial liver resection.

Tissue selection, preparation and staining techniques

Archived *Formalin-Fixed Paraffin-Embedded* (FFPE) tissue samples stored at the *National Center of Pathology* (Vilnius, Lithuania) were utilized in this study. A pathologist (Rokas Stulpinas, the author of this thesis) reviewed the available archived slides for each case to select the single most representative FFPE block, aiming to include both the viable tumor and the adjacent non-neoplastic liver tissue (i.e., containing the tumor-liver interface), for the subsequent specialized staining and analysis. The selected FFPE blocks were cut, mounted on positively charged slides, and stained while using the following techniques:

1. *Hematoxylin-Eosin* (H&E) staining was performed by using a standard protocol: sections were deparaffinized in xylene, rehydrated through a graded ethanol series, and stained with Harris hematoxylin solution. After differentiation in acid alcohol and washing, the sections were

counterstained with eosin solution. Finally, the slides were dehydrated, cleared in xylene, and mounted with a permanent mounting medium. H&E staining provides a general morphological overview of the tissue, with cell nuclei stained in blue, and cytoplasm and extracellular matrix appearing in shades of pink.

2. The *Gordon and Sweet's silver impregnation with Picric Acid–Sirius Red* (GSPS) staining was performed as follows: sections were deparaffinized, hydrated, oxidized with potassium permanganate, decolorized with oxalic acid, and sensitized with ammonium iron sulfate. After impregnation with ammoniacal silver solution and toning with gold chloride, the sections were fixed with sodium thiosulfate. The slides were then stained with Weigert's iron hematoxylin and Picric Acid–Sirius Red solution. Finally, the sections were dehydrated, cleared, and mounted. This staining procedure results in black reticulin fibers and red Type I collagen fibers, providing a clear contrast for the assessment of the connective tissue architecture in HCC and the adjacent liver tissue.
3. Immunohistochemical staining for CD8 was performed by using an automated staining platform: sections were subjected to heat-induced epitope retrieval and then incubated with a primary monoclonal anti-CD8 antibody (clone C8/144B, *Dako*) at a 1:100 dilution. Detection was performed by using a universal DAB detection kit, followed by counterstaining with hematoxylin. This immunohistochemical staining procedure specifically highlights CD8-positive cytotoxic T lymphocytes within the tumor (tumor-infiltrating lymphocytes) and the surrounding liver tissue (liver-infiltrating lymphocytes), allowing for the assessment of the local immune response in HCC.

All stained slides were digitized at 20× magnification (0.5 μm/pixel resolution) while using a *Leica Aperio AT2* scanner to generate whole slide images. The generated digital images were then annotated by a pathologist to mark the regions of interest – HCC and the adjacent liver tissue – and exclude the necrotic tumor areas or tissue artifacts. This ensured that only informative regions were included in the downstream computational analysis pipelines.

TASK 1: CD8 LYMPHOCYTE SPATIAL DISTRIBUTION ANALYSIS

The spatial distribution of CD8 lymphocytes within the tumor microenvironment provides valuable insights into the local immune response, which has been shown to have prognostic significance in various cancers. However, the precise quantification and characterization of this spatial distribution remains a challenge due to the complexity of the tumor-stroma interface and the limitations of manual annotation methods. To address these challenges, Rasmusson et al. [33] developed a novel computational approach called the *Immunogradient* method, which enables automated detection of the tumor-stroma *Interface Zone* (IZ) and the extraction of the immune cell density profiles. The *Immunogradient* analysis was utilized in this study with some minor alterations (most notably, because of using two – the tumor-stroma and the liver-stroma – interface zones).

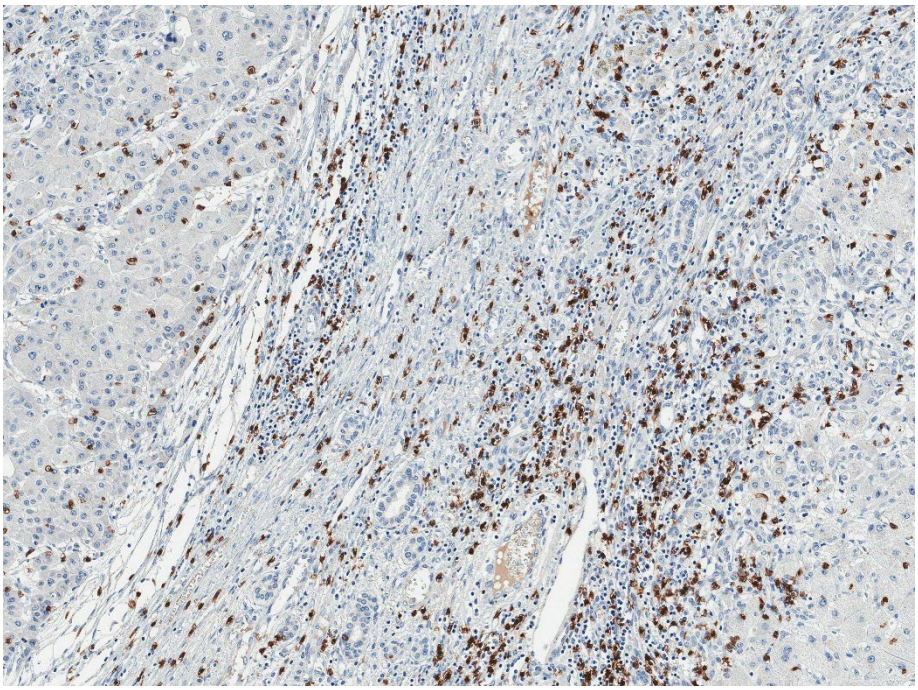

Figure 3. CD8 immunohistochemistry. CD8-positive cytotoxic lymphocytes (brown-stained cells) are the main effectors involved in both the antitumoral response (left) and hepatocyte damage in the remaining functional liver parenchyma (right)

The pipeline begins by training the *HALO*® AI (*Indica Labs*, USA) system to segment the tissue into hepatocytes (both malignant and non-malignant), stroma (fibrous tissue including the vasculature and the bile ducts), and background/debris classes, with a subsequent segmentation of CD8 cells via the *HALO*® *Multiplex IHC* algorithm (*Indica Labs*, USA); see Figure 4. Analysis continues with applying a hexagonal grid to subsample the classified tissue regions into hexagonal tiles. The use of a hexagonal grid offers several advantages over the traditional rectangular grids, thus including an improved spatial resolution and more isotropic sampling [34]. The optimal hexagon size was determined to be 65 μm based on empirical evaluation and previous experience.

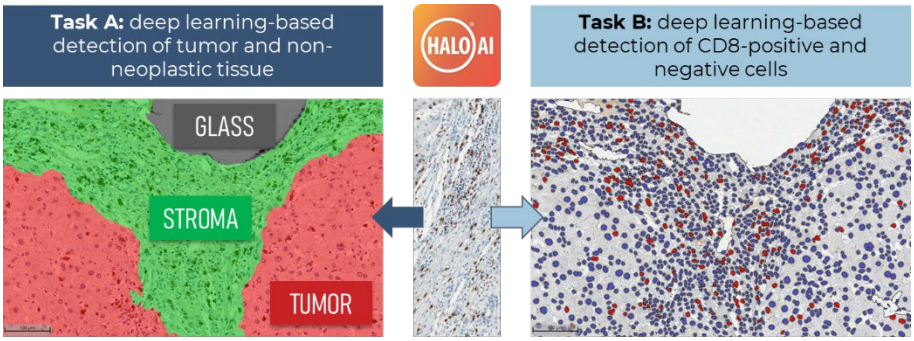

Figure 4. Commercial artificial intelligence-based tool *HALO*® AI (*Indica Labs,* USA) was utilized to A) detect the different parts of the tissue (tissue segmentation) and B) detect the CD8-positive cells with their coordinates

Next, the method automatically extracts the *Epithelial Edge* (EE, originally called *Tumor Edge* (TE), but in this study we were detecting malignant and benign edges, see Figure 5) by using a set of explicit, data-driven rules based on abrupt changes in the epithelial and stroma area fractions across the hexagonal grid. This automated EE extraction eliminates the need for time-consuming precise manual annotations and ensures reproducibility across different samples and studies. The rules for EE detection are based on the principle that the interface between the epithelium and the stroma regions exhibits sharp transitions in the tissue composition, which can be detected by analyzing the area fractions of epithelium and stroma within each hexagonal tile [33].

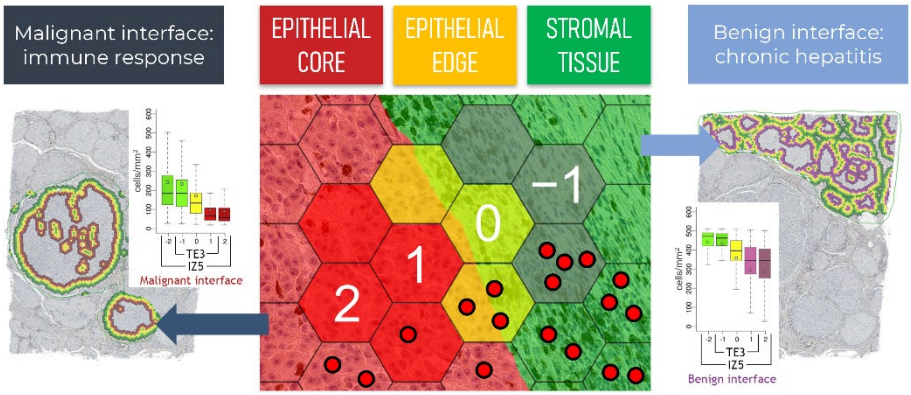

Figure 5. Hexagonal grid-based cell density analysis. We have defined two separate interface zones for each case: one for the border between the tumor and the surrounding fibrous stroma (representing the antitumoral immune response) and one more for the border between the non-neoplastic hepatocytes and the fibrous tissue (representing chronic hepatitis)

Once the EE has been identified, the hexagonal tiles are ranked on each side of the EE based on their shortest distance to the EE. The EE itself is assigned a rank of *0*, while the tiles on the epithelial (meaning either a tumor or liver parenchyma; it depends on the area of the slide that is being analyzed) side are assigned positive ranks, whereas those on the stromal side are assigned negative ranks. We then aggregate the CD8 cell counts within the hexagons of each rank to generate CD8 density profiles across the IZ. Subsequently, the Immunogradient indicators representing the whole IZ are calculated, including the *Center of Mass* (CM) and *Immunodrop* (ID). The CM can serve two purposes: it either represents an increase in the CD8 density toward the epithelial aspect when calculated by using the means, or indicates a higher CD8 variance along the IZ when using the standard deviation. The ID indicator functions as a ratio between the mean CD8 density in ranks *-1* (the stromal aspect) and *1* (the epithelial aspect), capturing an abrupt decrease in the CD8 density across the tumor edge – hence the term 'Immunodrop'. These indicators provide a concise, quantitative characterization of the immune cell density gradient and can be utilized as biomarkers for further modeling [33].

The automated, data-driven nature of the 'Immunogradient' method offers several advantages over the manual edge annotation approaches. First, it allows for comprehensive and reproducible assessment of the immune response at the epithelial-stromal interface, while eliminating the subjectivity and variability associated with manual annotations of the precise tumor edge. Second, it enables high-throughput analysis of large cohorts of samples, thus

facilitating the discovery of robust biomarkers and the validation of clinical applications. Finally, by providing a quantitative characterization of the spatial distribution of immune cells, the method opens up new opportunities for integrating spatial information with other omics data to gain a more comprehensive understanding of the tumor-immune ecosystem.

Statistical analysis

The statistical analysis in our studies focused on investigating the associations between the immunogradient indicators, clinicopathological variables, and the patient outcomes (*Overall* (OS) and/or *Recurrence-Free* (RFS) survival). Due to the left-skewed distribution of CD8 cell densities, a logarithmic transformation was applied to these variables before conducting parametric statistical tests. To dichotomize the patient cohorts for univariate survival analysis, optimal cut-off values for each indicator were determined by using the *Cutoff Finder* tool [35].

Survival analysis was performed by using the Kaplan-Meier method, and log-rank tests were employed to assess differences in survival between patient subgroups. Multivariate Cox proportional hazards regression models were constructed to evaluate the independent prognostic value of the CD8 spatial indicators while accounting for the conventional clinicopathological parameters. Variable selection for these models was performed by using a stepwise likelihood ratio test with a value of $p<0.05$.

The statistical analyses were carried out by using *SAS* and *R* software packages. Computation of the hexagonal grid subsampling, IZ detection, and immunogradient indicators was implemented in *C++* using the *OpenCV* and *Boost* libraries.

Key findings

In the resected HCC cohort, a higher variance (represented by the *Standard Deviation* (SD)) of CD8 density at the tumor edge was found to be an independent predictor of a longer *Overall Survival* (OS). This finding suggests that irregular CD8 cell infiltrates along the tumor edge may represent localized, denser immune cell clusters, potentially indicating a more effective anti-tumoral response. In contrast, a higher mean CD8 density in the epithelial aspect of the non-neoplastic liver parenchyma was associated with worse OS, possibly reflecting ongoing liver damage driven by the immune system in the context of chronic viral hepatitis.

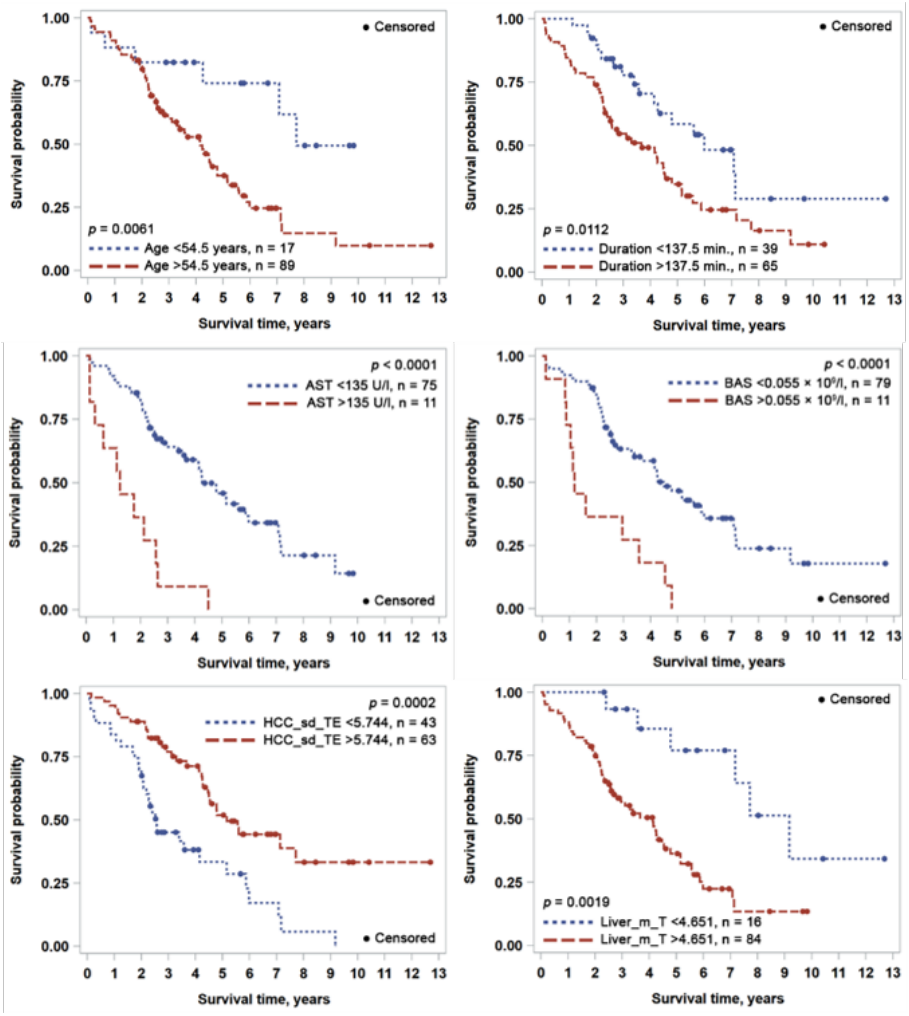

Figure 6. Kaplan-Meier *Overall Survival* (OS) plots for independent prognostic indicators identified by multiple Cox regression analysis [36]: patient age; duration of surgery; *Aspartate Transaminase* (AST); peripheral blood basophil count; standard deviation of CD8 density at the tumor edge (HCC_sd_TE); mean CD8 density within the epithelial aspect of the perineoplastic liver-stroma interface (Liver_m_T)

The study developed a comprehensive overall survival scoring system which integrates five independent prognostic variables: the duration of the surgery, the aspartate transaminase level, the blood basophil count, the standard deviation of CD8 density at the tumor edge, and the mean CD8 density in the epithelial aspect of non-neoplastic liver. For each variable, patients received a

score of *0* (indicating good prognosis) or *1* (indicating poor prognosis). These individual scores were then combined to create a total risk score. Based on their total score, patients were stratified into three distinct prognostic categories: low risk (total score *0–1*), intermediate risk (total score *2*), and high risk (total score *3–5*). This stratification system demonstrated a strong prognostic value, with 4-year overall survival rates of 100% for low-risk, 51% for intermediate-risk, and 12% for high-risk patients. These results validate the effectiveness of combining CD8 spatial distribution indicators with the traditional clinicopathological parameters in order to create a more accurate prognostic model for HCC patients following resection.

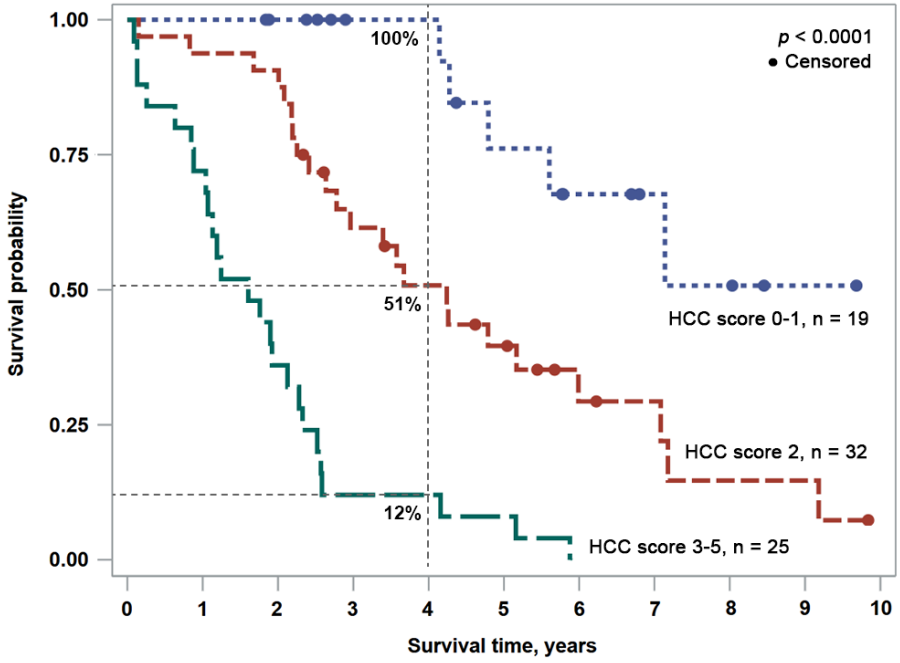

Figure 7. OS risk stratification based on combined prognostic scores [36]: a comprehensive HCC OS score derived from five independent predictors

In the transplanted HCC cohort, two parameters emerged as independent predictors of a better overall survival: a higher mean CD8 cell density at the epithelial edge of the non-malignant interface in the explanted liver parenchyma (HR: 0.15, 95% CI: 0.03–0.82, p=0.01) and a higher preoperative peripheral blood platelet count (HR: 0.15, 95% CI: 0.03–0.81, p=0.01). Specifically, patients with platelet counts above 70.8 x 10^9/L and a higher CD8 density showed significantly better survival outcomes. Both parameters demonstrated equal hazard ratios, indicating that higher values of either

predictor were associated with a similar magnitude of the survival benefit. This finding emphasizes the potential prognostic value of both immune cell infiltration patterns and basic hematological parameters in predicting the outcomes after liver transplantation for HCC patients.

Furthermore, in a subgroup of resected HCC patients meeting the Milan criteria preoperatively, low standard deviation of the CD8 density along the tumor edge and a positive (R1) resection margin were identified as independent predictors of early post-resection recurrence. Notably, patients presenting with both adverse predictors exhibited a 100% risk of relapse within 200 days. This finding suggests that integrating CD8 spatial distribution indicators with the resection margin status could help identify high-risk patients who might benefit from prioritization for liver transplantation, potentially improving the overall treatment outcomes.

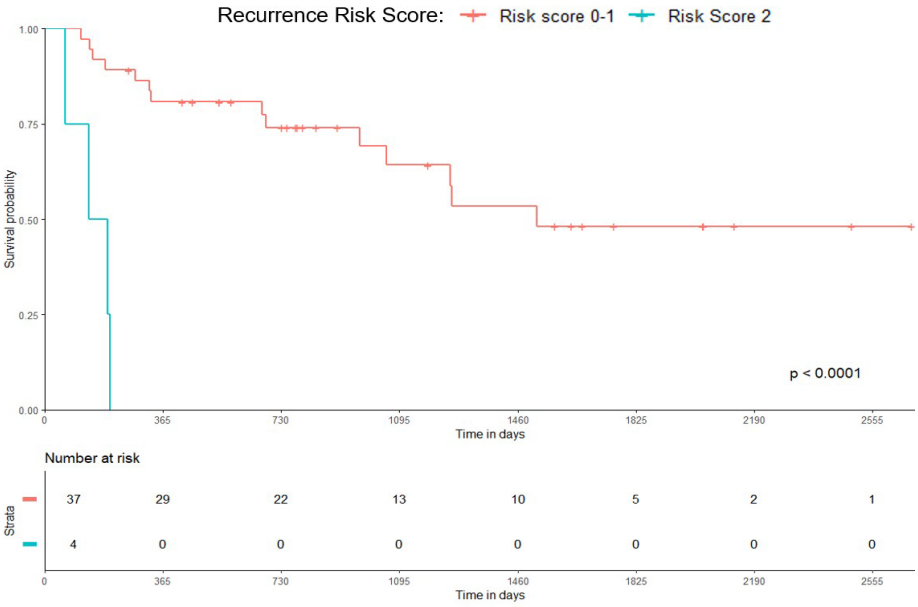

Figure 8. HCC Recurrence Risk Score in the subgroup of patients fulfilling the Milan criteria preoperatively [37]. Risk Score 0–1 indicates patients with either no risk factors or one risk factor (low CD8 density variation or R1 resection margin), while Risk Score 2 indicates patients with both risk factors present.

Limitations

Our research has several limitations that should be acknowledged. First, the sample sizes of the cohorts, particularly the transplanted HCC cohort (N=28)

and the subgroup of Milan criteria-fulfilling resected HCC patients (N=41), are relatively small, which may limit the generalizability of the findings. Second, the retrospective nature of the studies and the heterogeneity of the patient cohorts could introduce potential biases and confounding factors that might impact the robustness of the results. Third, the lack of complete data on the viral hepatitis status and the cause of death in the resected HCC cohort limits the ability to investigate their potential influence on disease-specific survival and to further discriminate the impact of both neoplastic and non-neoplastic components of the liver disease. Finally, as the studies were based on surgical resection and explanted liver samples, the applicability of the immunogradient method to the preoperative biopsy material remains to be validated. Despite these limitations, we believe that these studies provide proof-of-concept for the prognostic value of CD8 spatial distribution indicators in HCC and highlight the potential for their integration with the conventional clinicopathological parameters to improve the risk stratification and guide the treatment decisions.

TASK 2: AI-EXTRACTED TISSUE FIBER FRAMEWORK MORPHOMETRICS

Type I collagen and Type III collagen, despite their structural similarities, play distinct roles in the progression of chronic liver disease and hepatocellular carcinoma. While the accumulation of Type I collagen characterizes advancing fibrosis and cirrhosis, the disruption of the delicate Type III collagen (reticulin) network is a hallmark of HCC development (see Figure 9). By virtue of recognizing the prognostic potential of these microarchitectural changes, our study aimed to quantitatively assess the spatial patterns of both collagen types within the tumor and the surrounding liver tissue, seeking to uncover novel predictors of the outcomes in patients undergoing liver resection for HCC.

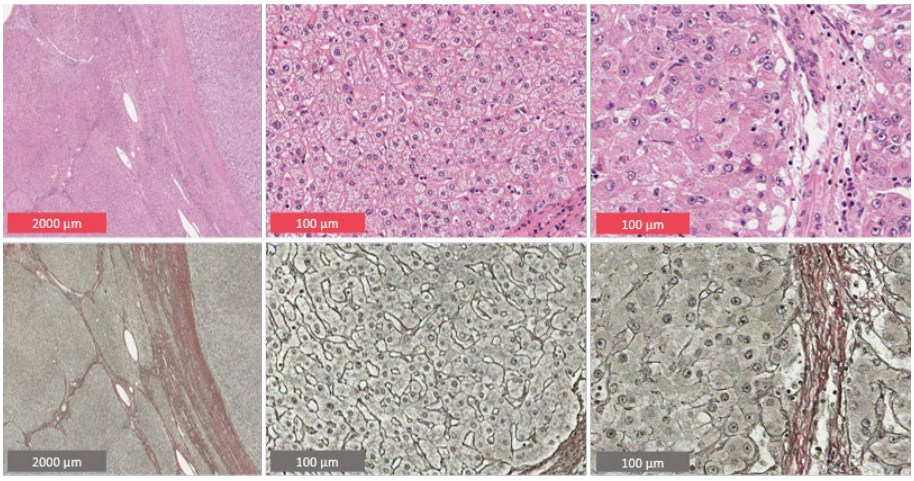

Figure 9. Conventional H&E staining (top row) is not highly suitable to visualize the fibrous structures; to highlight them, we use the GSPS staining protocol (bottom row), based on silver impregnation and picric acid–Sirius Red. GSPS stains Type III collagen (reticulin) is shown in black, and Type I collagen is visualized in red

Methodology

At the second leg of our study, we aimed to extract prognostic information from the fiber architecture in the tumor microenvironment of HCC by using a *Convolutional Neural Network* (CNN) from bright-field histology images, building upon the methodology developed by Morkunas et al. for breast

carcinoma [38]. A key aspect was the differentiation between reticulin (black silver-impregnated fibers) representing Type III collagen, and thicker red-staining fibers in the fibrous septae representing Type I collagen. Similar to Morkunas et al., we have trained a modified U-net (a fully convolutional encoder-decoder network originally developed for biomedical image segmentation) CNN architecture to segment these two fiber types, generating pixel-precise collagen segmentation masks (CSMs, see Figure 10). Our modifications included the use of exponential linear units instead of rectified linear units in the convolutional layers, and adding a 'bottleneck' block to the encoder path after each max-pooling layer. This block splits the tensor into two parallel flows before concatenating, allowing the network to learn both compressed and expanded representations.

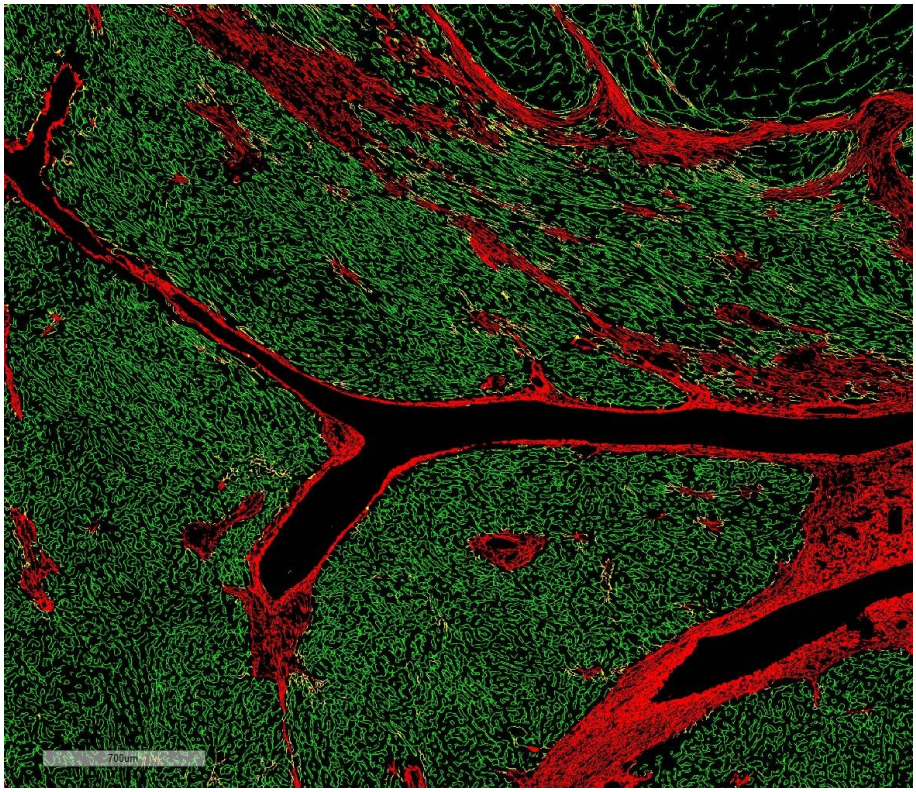

Figure 10. The resulting *Collagen Segmentation Mask* (CSM) of red (Type I collagen), green (Type III collagen or reticulin) and yellow (ambiguous areas) fibers set against a contrasting black background, optimized for viewing and morphometric feature extraction. Note the reduction of green fibers in the HCC area (top right)

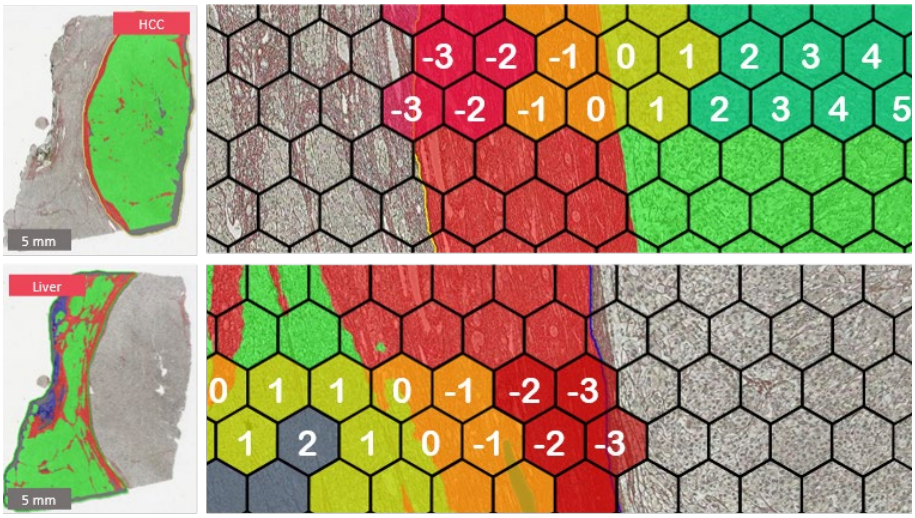

Figure 11. Hexagonal tiling and ranking: (left) *HALO*® AI (*Indica Labs*, Albuquerque, NM, USA) classifier result on the manually placed HCC (top) and peritumoral liver (bottom) annotations; (right) ranking of the hexagonal tiles according to their shortest distance from the epithelial edge (rank *0*), with positive ranks for epithelial-side, and negative ranks for stromal hexagons

The ground truth for training was generated by the manual annotation of image patches by two blinded experts capturing the direction of collagen fibers, as well as a semi-automated thresholding approach. We augmented the training data with rotations, flips, blurring, zooming and varying amounts of dilation applied to the annotations. Inference was done by splitting whole-slide images into overlapping patches, running the CNN on each patch, and merging the probability maps with thresholding to generate the final CSMs for reticulin and Type I collagen.

In parallel, we again applied the hexagonal grid subsampling to the whole slide images, as described in detail in the previous section, by ranking each tile based on its distance from the automatically detected epithelial-stromal interface. Briefly, in the ranking process, hexagons at the epithelial-stromal boundary (including both benign hepatocytes and neoplastic HCC cells) are assigned rank *0*, with positive ranks for epithelial-side hexagons and negative ranks for stromal hexagons, based on their shortest distance from the interface. This approach offers two crucial advantages over the whole-image analysis. First, it enables localized analysis of tumor features, while capturing gradual changes and heterogeneity that might otherwise be overlooked. Second, the spatially ranked tiles allow targeted extraction of specific regions of interest.

In the next step, we sampled the mapped hexagonal tiles from the CSMs for further analysis. From each hexagonal region, we computed 11 features at the pixel, fiber, and image levels to characterize the fiber microarchitecture. These features were selected based on their potential relevance and interpretability from a larger set of 37 features previously used by Morkunas et al. in their study of breast cancer collagen networks [38]. The selected features (see Table 2) included metrics related to fiber orientation, morphology, density, texture, and fractal properties, aiming to capture key aspects of the fiber microarchitecture within each hexagonal tile. During the data aggregation process, the mean and the standard deviation of each feature measurement were calculated for every case, considering all hexagons within each region of interest. This compiled case-level dataset contained the potential fiber-derived predictors, which were derived as follows:

- 2 annotations per case (tumor and peritumoral liver);
- 3 regions per annotation (core, epithelial edge, and stroma);
- 2 summary metrics (mean and standard deviation) per region;
- 2 types of fibers (reticulin and collagen Type I) per summary metric;
- 11 fiber features per fiber type.

The combination of these factors ($2 \times 3 \times 2 \times 2 \times 11$) resulted in the total of 264 potential predictors for each case.

Table 2. List of features used to characterize the fibrous matrix, calculated twice per each hexagon: for green (reticulin or Type 3 collagen) and red (Type 1 collagen) fibers separately

Feature	Description
Orientation:	
Circular Standard Deviation (CSD)	Dispersion of circular angles of the individual fibers
Magnitude, mean (mMag)	Average strength or intensity of vectors (e.g., gradients) in the fiber mask
Morphometry:	
Fiber length, mean (mFL)	Average Euclidean distance between the endpoints of each skeletonized fiber
Fiber path, mean (mFP)	Average pixel length of a line dividing a fiber into two equal parts along its longer axis
Fiber straightness, mean (mFS)	A ratio of fiber length over fiber path

Feature	Description
Density:	
Fiber density (FD)	Number of pixels in the mask
Endpoints (nENDP)	Number of fiber endpoints in the hexagon mask
Texture (Haralick's):	
Homogeneity (hom)	The closeness of the distribution of elements in the gray-level co-occurrence matrix to the matrix diagonal
Entropy (ent)	Amount of information or randomness in the texture
Correlation (cor)	Linear dependency of gray levels on those of neighboring pixels
Fractal:	
Lacunarity (lac)	A measure of both gaps and heterogeneity: the variation in space around objects in the image and their irregular distribution

Statistical analysis

An updated comprehensive statistical analysis pipeline was utilized to identify prognostic features and build predictive models for the overall survival in the cohort of 105 HCC patients (one patient was lost from the initial pool of 106 due to the poor quality of the tissue), of whom, 56 died during the follow-up period. The 264 fiber-derived features were first scaled by using min-max normalization to a range of *0* to *1*. Univariate Cox regression with LASSO regularization was then applied to assess the performance of individual variables, and the tumor stage T2–T4 (vs. T1) was identified as the strongest individual predictor of a worse overall survival (HR 4.81, 95% CI 2.40–9.64, $p<0.0001$). From the initial analysis, we selected 36 features which showed a potential prognostic value ($p<0.1$) for inclusion in the subsequent modeling steps. These were combined with clinicopathological variables including the age, stage, gender, lymphovascular invasion, and tumor multifocality. Adhering to the 'rule of ten' guideline of having at least 10 events per variable in the model, all possible combinations of up to 6 features were systematically generated, resulting in over 2.8 million candidate models. These models were evaluated by using multivariate Cox regression with LASSO penalization and

5-fold cross-validation. Only 139 models (approximately 0.005%) in which all the variables had $p<0.05$ were retained. The concordance index (C-index) on the test split was used as the performance metric to rank these models, with two models achieving a C-index above 0.7, indicating good discriminative ability. The variables comprising these 139 models were further analyzed by counting the number of occurrences of each unique feature, revealing 30 key features that were recurrently selected. Factor analysis was additionally performed on the fiber-derived features in order to identify latent relationships and the underlying biological processes.

Key findings

We developed two comparable penalized Cox regression models which incorporated the patient age, tumor multifocality, and fiber-derived features to predict the overall survival in patients with *Hepatocellular Carcinoma* (HCC). Both models achieved a concordance index (C-index) greater than 0.7, indicating good discriminative ability. These models outperformed those solely reliant on the conventional clinicopathologic parameters, emphasizing the utility of AI-extracted microarchitectural features for the management of HCC.

Table 3. Fiberomics-derived *Overall Survival* (OS) models with a C-index above 0.7

Features	**HR**	**95% CI**	***p*-value**
Model A, test set C-index 0.7094, AIC 359.3840			
Age ≥55 years	4.05	1.67–9.80	0.00194
Multiple tumors	1.92	1.11–3.31	0.01895
Green_mean_lacunarity_HCC_IZ3	6.36	1.69–23.87	0.00615
Red_mean_correlation_LVR_IZ3	0.21	0.05–0.92	0.03802
Model B, test set C-index 0.7061, AIC 359.2425			
Age ≥55 years	4.33	1.73–10.81	0.0017
Multiple tumors	2.24	1.30–3.83	0.0035
Green_mean_lacunarity_HCC_IZ3	5.58	1.48–21.06	0.0113
Red_sd_mean_straightness_LVR_IZ3	0.02	0.00–0.84	0.0396

Interestingly, we discovered that the prognostic value at the tumor edge was derived from the reticulin structure, while Type I collagen characteristics were significant at the epithelial edge of the peritumoral liver. Specifically, the high mean lacunarity of the reticulin framework at the tumor edge was associated with a shorter OS. In contrast, Type I collagen features in the peritumoral liver – a high mean texture correlation, a high variance in density, and a high variance of fiber straightness – emerged as significant predictors of longer OS.

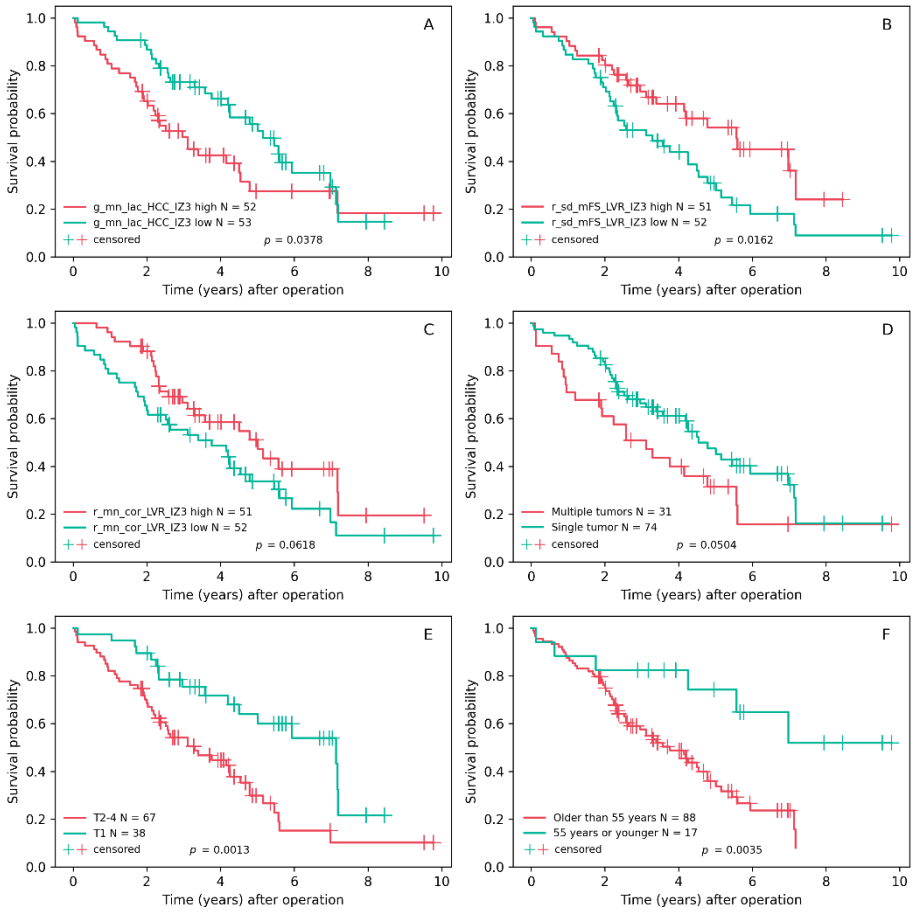

Figure 12. Kaplan-Meier overall survival plots and the cutoff values for the components of models with good discriminative ability (C-index >0.7). Tumor stage T2–T4 (vs. T1), which was the strongest predictor in univariate analysis (HR 4.81, p<0.0001), is also included for comparison

All of these indicators were measured at the interface zone between the epithelial and fibrous tissue, highlighting the importance of assessing the

spatial aspects of collagen deposition in the context of liver fibrosis and cirrhosis.

In the factor analysis, we identified six factors which explained 85.12% of the variance in the data, revealing the underlying relationships among the fiber-derived features.

Although the first five factors exhibited cutoff values that divided the cohort into groups with statistically significant differences in the overall survival duration, as indicated by $p<0.05$ in univariate analysis, they did not outperform the individual features in the multivariate Cox regression models. After applying the LASSO Cox regression, none of these factors were found to be significant predictors of the overall survival.

Limitations

Besides the same limitations that were discussed in the previous section on CD8 lymphocyte infiltration, further validation using other collagen-specific imaging techniques, such as *Second Harmonic Generation* (SHG) microscopy or polarized light microscopy, would strengthen our findings. These techniques could provide additional insights into the collagen fiber architecture and serve as a reference for evaluating the performance of our CNN-based approach.

TASK 3: DEEP LEARNING-BASED TISSUE 'FINGERPRINT' EXTRACTION

The following sections (Task 3 and Task 4) present preliminary findings from the final phases of our study, which are still ongoing. This part of the research is not yet complete, and the data have not been formally published. The information provided here is intended to offer insights into the direction and the potential outcomes of this leg of the study. However, it should be noted that these results are subject to change as the research is progressing and undergoing further analysis and peer review.

Methodology

Initial MISL approach

Before settling on our current methodology, we explored an attention-guided *Multiple Instance Survival Learning* (MISL) approach, building upon the base pipeline that was successfully employed by Drachneris et al. to predict a relapse of non-muscle invasive papillary urothelial carcinoma [39]. This method involved simultaneously feeding patches and survival data into the model. However, this approach did not produce satisfactory results, prompting us to develop the current feature extraction and clustering pipeline.

Data preparation and feature extraction

The third leg of our study utilized the conventional hematoxylin and eosin-stained *Whole Slide Images* (WSIs) from 105 patients who underwent liver resection for HCC. The patch selection process was again guided by the manual annotations marking all viable HCC tissue within each WSI. We then employed a systematic sampling approach:

- The annotated regions were split to create 256×256-pixel patches.
- Patches containing less than 95% tissue were discarded to ensure the quality and relevance of the analyzed areas.
- Vahadane (library: tiatoolbox version 1.5.1) color normalization was applied.

This process resulted in a collection of 416,928 high-quality 256×256-pixel patches representing a viable HCC tissue for each patient (range 384–8656, median 3568 patches/patient). We then employed *CTransPath* [40], a hybrid deep learning foundation model integrating *Convolutional Neural Networks* (CNNs) and multi-scale Swin Transformers, that is pretrained on a large set

of unlabeled histopathological images to learn domain-specific feature representations. This model served as a general feature extractor, capturing both fine-grained and contextual information from our histopathological images (HCC patches). Specifically, we extracted 768 features corresponding to the activations of the penultimate layer of the *Convolutional Neural Network* (CNN). No fine tuning of the model, or any post-processing of the results were applied.

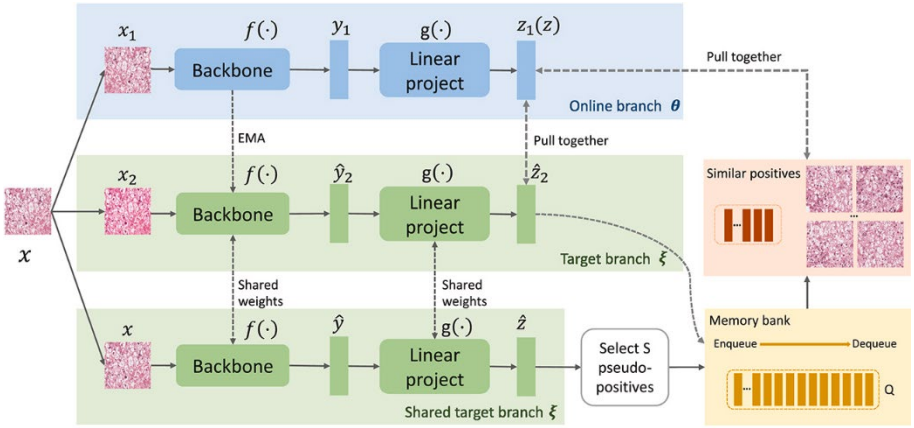

Figure 13. *CTransPath* designed by integrating a *Convolutional Neural Network* (CNN) and a multi-scale Swin Transformer architecture, diagram shown as originally published by Xiyue Wang et al. [40]

Clustering

To identify distinct tissue 'fingerprints' within the HCC samples, we applied two clustering algorithms to the extracted feature vectors of the patches:

- *Gaussian Mixture Model* (GMM) (*Python* 'scikit-learn' library version 1.3.2, default settings)
- K-means clustering (*Python* 'scikit-learn' library version 1.3.2, default settings)

For each algorithm, we explored a range of patch cluster numbers (k=2, 3, 4, 5, 6, 7, 8, 9, 10) to determine the optimal granularity of tissue classification. This approach allowed us to capture various levels of tissue heterogeneity within the tumor samples.

Patient-Level Fingerprint Quantification

Following the clustering process, we quantified the tissue composition for each patient by calculating the percentage of patches assigned to each cluster. This resulted in a patient-specific 'fingerprint' represented as a vector of cluster proportions. For instance, in a 4-cluster analysis, if a patient's tissue has the following composition:

- Cluster 1: 10%
- Cluster 2: 0%
- Cluster 3: 35%
- Cluster 4: 55%

it might be represented as a 'fingerprint' vector (0.1, 0.0, 0.35, 0.55) in the double-precision floating-point format.

Statistical Analysis

To investigate the prognostic significance of these tissue 'fingerprints', we conducted univariate Cox proportional hazards regression analyses. We examined two primary clinical outcomes, the *Overall Survival* (OS) and the *Recurrence-Free Survival* (RFS). For each cluster in each clustering scheme, we assessed whether a higher proportion of patches belonging to that cluster was associated with improved survival outcomes. This approach allowed us to identify specific tissue patterns which may serve as prognostic indicators in HCC.

All statistical analyses were performed by using *R* version 4.4.1 (*Race for Your Life).* Cox regression models were fitted using the survival package. The statistical significance was set at $p<0.05$, and hazard ratios with 95% confidence intervals were reported for each analyzed cluster proportion.

Results

Clustering Maps

As evident from the clustering result maps (see Figure 14), the identified clusters represent specific tissue types or microenvironments within HCC, thereby demonstrating that this unsupervised approach yields interpretable and biologically meaningful results. The spatial distribution and composition of these clusters reveal distinct patterns which likely correspond to different tumor regions, tissue classes, or histological features.

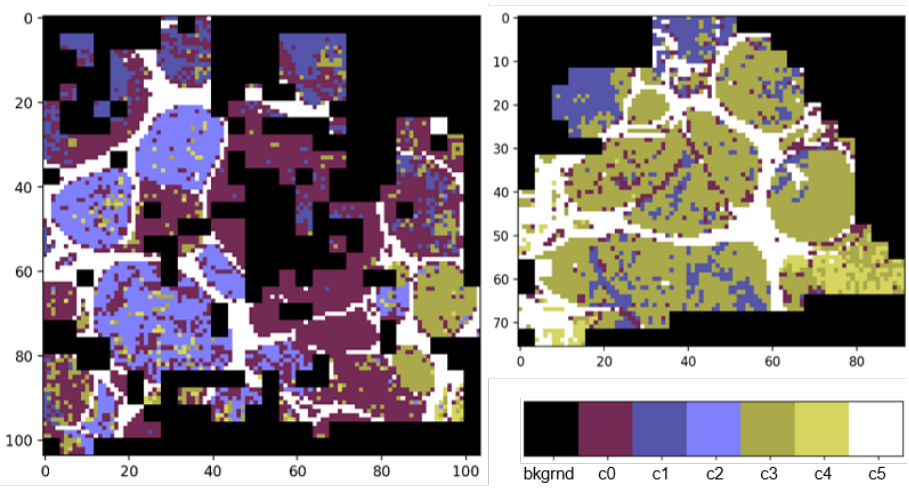

Figure 14. Spatial distribution of tissue microenvironments in *Hepatocellular Carcinoma* (HCC) using Gaussian Mixture clustering with 6 clusters (GM6). Each image represents an annotated HCC tissue part of the *Whole Slide Image* (WSI), where patches are color-coded according to their assigned cluster (c0–c5). The black areas represent background or non-tissue regions. These maps reveal distinct spatial patterns and heterogeneity within HCC tumors

Overall Survival

The analysis identified three variables with $p<0.05$: gm6_c0 (HR 4.05, 95% CI: 1.40–11.75, $p=0.010$), gm9_c1 (HR 9.24, 95% CI: 1.23–69.63, $p=0.031$), and km10_c1 (HR 3.54, 95% CI: 1.10–11.44, $p=0.034$).

Subsequent multivariate Cox regression including these three variables revealed that only gm9_c1 remained statistically significant (HR 8.67, 95% CI: 1.21–62.36, $p=0.032$). The overall multivariate model was significant (LR $p=0.014$).

Table 4. Multivariate Cox regression for *Overall Survival* (OS), clustering variables only

Variable	HR	HR 95% CI		Wald *p*	LR *p*
gm6_c0	2.7620	0.7304	10.4448	0.1344	0.0143
gm9_c1	8.6747	1.2067	62.3581	**0.0318**	0.0143
km10_c1	2.2841	0.5506	9.4751	0.2552	0.0143

Recurrence-Free Survival

Univariate Cox regression for recurrence-free survival identified two variables with $p<0.05$: km9_c1 (HR 4.07, 95% CI: 1.29–12.90, $p=0.017$) and gm6_c0 (HR 3.32, 95% CI: 1.11–9.99, $p=0.032$).

In the multivariate Cox regression, both variables remained statistically significant: km9_c1 (HR 3.81, 95% CI: 1.19–12.13, $p=0.024$) and gm6_c0 (HR 3.20, 95% CI: 1.03–9.97, $p=0.045$). The overall multivariate model was significant (LR $p=0.013$).

Table 5. Multivariate Cox regression for *Recurrence-Free Survival* (RFS), clustering variables only

Variable	HR	HR 95% CI		Wald *p*	LR *p*
km9_c1	3.8069	1.1947	12.1310	**0.0238**	0.0134
gm6_c0	3.1985	1.0260	9.9715	**0.0450**	0.0134

Conclusion

In conclusion, the preliminary results reveal the potential of unsupervised clustering approaches to identify prognostically relevant tissue microenvironments in HCC. The findings suggest that the quantification of the proportion of specific tissue types within tumors could provide valuable information for patient stratification and personalized treatment strategies.

The emergence of new foundation models in computational pathology opens up exciting opportunities for extending this work through transfer learning and comparative analysis of different model architectures. A multi-resolution approach, integrating both high (cytologic) and low (architecture) magnification tissue features, could provide a more comprehensive understanding of tumor heterogeneity and its prognostic implications. Additionally, incorporating fingerprints of the residual liver parenchyma into the analysis could offer valuable insights into the relationship between tumor characteristics and the surrounding tissue environment, potentially revealing new prognostic markers.

TASK 4: INTEGRATION OF MACHINE LEARNING APPROACHES

We developed comprehensive prognostic models incorporating clinical parameters, laboratory data, and computational tissue features derived from both CD8 lymphocyte spatial analysis and tissue fiber framework analytics. These are unpublished calculations that are still subject to change, as we aim to integrate the 'fingerprints' data when it is complete.

Methodology

Our modeling strategy employed a two-step approach. First, all variables were evaluated by using univariate Cox proportional hazards regression, with those achieving $p<0.05$ selected for further analysis. In the second phase, we systematically generated all possible combinations containing up to 7 variables, adhering to the 'rule of ten' events per variable given our cohort size. These combinations underwent LASSO-penalized multivariate Cox regression with 5-fold cross-validation to minimize overfitting. The models were ranked according to their performance on test splits using the concordance index (C-index).

Results

Recurrence-Free Survival Models

The analysis of *Recurrence-Free Survival* (RFS) revealed several complementary modeling approaches. In the complete cohort analysis, the top-performing model achieved a test set C-index of 0.718 (AIC: 333.12) and included three independent predictors: resection margin status (R1 vs. R0: HR 4.23, 95% CI: 2.29–7.81, $p<0.0001$), preoperative Milan criteria status (HR 0.56, 95% CI: 0.32–0.98, $p=0.042$), and mean lacunarity of Type I collagen at the tumor edge (HR 0.20, 95% CI: 0.06–0.63, $p=0.006$).

Given the dominant impact of the resection margin status on recurrence, we performed a subgroup analysis focusing only on patients with complete (R0) resections. In this refined cohort, the optimal model (C-index: 0.706, AIC: 231.97) identified just two independent predictors: CD8 density variation at the tumor edge (HR 0.15, 95% CI: 0.03–0.61, $p=0.008$) and the tumor multifocality (HR 2.45, 95% CI: 1.30–4.62, $p=0.006$). This suggests that, in cases where complete surgical resection is achieved, immune response

patterns and the tumor architectural features become more relevant for predicting recurrence.

Table 6. Performance metrics of top three *Recurrence-Free Survival* (RFS) models in full cohort

Model Components	Test C-index	AIC
R0/R1 + Fulfills Milan criteria prior to rection + Type 1 collagen lacunarity at the tumor edge	0.718	333.12
R0/R1 + Fulfills Milan criteria prior to resection + Type 1 collagen lacunarity at the tumor edge + Variance (SD) of CD8 density at the tumor edge	0.712	331.52
R0/R1 + Fulfills Milan criteria prior to resection + CD8 Factor 1* at the tumor edge	0.702	336.62

* As originally described by Rasmusson et al. [33], Factor 1 (from the factor analysis of CD8 variables) was characterized by strong positive loadings of the variables, which reflected the level of CD8 + density within all interface zone aspects and was therefore interpreted as the interface zone CD8 + density level factor, also referred to as the CD8 + density factor.

Overall Survival Models

The analysis of the *Overall Survival* (OS) revealed remarkable complexity in prognostic modeling, with 132 different variable combinations achieving test set C-indices above 0.70. This finding highlights the multifaceted nature of HCC progression, where numerous factors contribute relatively equally to the long-term outcomes. The optimal model achieved a test C-index of 0.782 (AIC: 299.90) by integrating clinical, laboratory, and computational tissue parameters.

The identification of multiple high-performing models for OS prediction suggests several important implications for HCC management. First, it demonstrates that the disease course is influenced by a complex interplay of factors, with no single dominant predictor. Second, it suggests that clinicians may have the flexibility in choosing which parameters to monitor, as different combinations of variables can provide similar prognostic accuracy. Third, it reinforces the value of integrating computational tissue analysis with the conventional clinical parameters, as all top-performing models included both types of features.

Table 7. Components of best-performing OS model

Variable	HR	95% CI	*p*-value
Age ≥55 years	2.96	1.19–7.39	0.020
Lymphovascular invasion	2.58	1.44–4.63	0.001
Preoperative AST level	15.49	4.28–56.09	<0.0001
Preoperative GGT level	13.36	1.63–109.75	0.016
Variance (SD) of CD8 density at the tumor edge	0.25	0.07–0.90	0.033
Reticulin (green), mean correlation at the tumor edge	0.10	0.01–0.78	0.028
Reticulin (green), CSD variation at the tumor edge	3.38	1.09–10.50	0.035

Several limitations of our modeling approach should be noted. The relatively small cohort size (N=106) limited the number of variables which could be included in any single model. The retrospective nature of the study may introduce selection bias. Additionally, external validation in independent cohorts will be needed to confirm the generalizability of these models.

The findings from this integrated analysis demonstrate that a combination of clinical parameters with computational tissue features can significantly improve the prognostic accuracy in HCC. The identification of multiple viable modeling approaches, particularly for OS prediction, reflects the complex nature of HCC progression and suggests that personalized risk assessment may benefit from considering multiple complementary sets of predictors.

Conclusion

Notably, both RFS and OS models incorporated computational markers derived from tissue analysis alongside the established clinical parameters, with CD8 lymphocyte distribution and fiber characteristics, both performing as independent prognostic factors. Interestingly, some established conventional prognostic factors, such as the tumor grade and size, did not show a significant prognostic value in our cohort.

DISCUSSION

The integration of artificial intelligence-based analyses of tumor microenvironment, immune response, and tissue architecture has demonstrated a significant potential for improving the prognostic accuracy in *Hepatocellular Carcinoma* (HCC). This study employed multiple computational approaches to extract and analyze various features from digitized histopathology slides, with the objective of providing novel insights into HCC biology and patient outcomes.

CD8 lymphocyte spatial distribution analysis

Our investigation into the spatial distribution of CD8 lymphocytes within the HCC microenvironment revealed several important findings. In the resected HCC cohort, a higher variance (standard deviation) of CD8 density at the tumor edge emerged as an independent predictor of a longer overall survival [27]. This observation suggests that irregular CD8 cell infiltrates along the tumor edge may represent localized, denser immune cell clusters, potentially indicating a more effective anti-tumoral response. This finding aligns with recent studies in other cancer types, such as breast cancer, where the spatial heterogeneity of immune infiltrates has been associated with improved outcomes [41].

In our analysis, we explored multiple Immunogradient parameters. Several additional measures, specifically, the *Center of Mass* (CM) and *Immunodrop* (ID) ratios which characterize changes in the CD8 density across the interface zones, demonstrated significant correlations with the patient outcomes in univariate analyses. However, these parameters did not retain independent prognostic significance when evaluated alongside other clinical and pathological variables in multivariate Cox regression models, as the most robust prognostic information emerged from other metrics.

Interestingly, we observed contrasting prognostic implications for CD8 infiltration in different tissue compartments. While a higher CD8 density variance at the tumor edge was associated with better outcomes, a higher mean CD8 density in the epithelial aspect of the non-neoplastic liver parenchyma was associated with the worse overall survival [27]. This dichotomy highlights the complex role of CD8 T cells in HCC, where they may contribute to both anti-tumoral immunity and liver damage in the context of chronic inflammation. The negative prognostic impact of high CD8 density in non-neoplastic liver tissue may reflect ongoing immune-mediated damage, particularly in the context of viral hepatitis [42].

The development of a comprehensive overall survival score combining the CD8 spatial distribution indicators with the conventional clinicopathological parameters demonstrated the potential for improved risk stratification in HCC patients [27]. This integrated approach, which achieved a clear separation of patient groups with 5-year overall survival probabilities ranging from 76% to 8%, underscores the value of combining tissue-based computational biomarkers with established clinical factors.

In the context of liver transplantation for HCC, our study identified two independent predictors of the overall survival: preoperative platelet counts and the mean CD8 cell density at the epithelial edge of the non-neoplastic liver parenchyma-stroma interface [43]. Notably, while previous research focused primarily on the prognostic significance of tumor-infiltrating lymphocytes within HCC, our findings highlight the importance of assessing the CD8 cell distribution in the surrounding liver tissue as well. These results suggest that the evaluation of the CD8 lymphocyte-mediated inflammatory response in the non-neoplastic liver parenchyma may provide a better prognostic value than the assessment of the anti-tumoral immune response within the HCC lesions, particularly in the setting of liver transplantation where the malignant tissue is completely removed. The validation of these results in preoperative liver biopsy samples could offer a significant translational potential, enabling the use of CD8 cell spatial distribution data to guide treatment decisions and optimize the outcomes for HCC patients undergoing liver transplantation. For example, patients with a more pronounced inflammatory response in the non-neoplastic liver might benefit from a closer post-transplant monitoring.

Different predictors emerged from our analysis of a subgroup of resected HCC patients meeting the Milan criteria preoperatively. In this subgroup of early-stage HCC, low standard deviation of CD8 density along the tumor edge and a positive (R1) resection margin were identified as independent predictors of early post-resection recurrence [37]. It is a striking observation that the fact that patients with both of these adverse factors exhibited a 100% risk of relapse within 200 days has significant clinical implications. Validating the findings in patient cohorts who underwent core biopsy could provide valuable information about the distribution of CD8 cells before surgery. This preoperative data could help guide treatment decisions, particularly in identifying patients at higher risk of incomplete tumor resection (R1). For these high-risk patients, prioritizing liver transplantation over surgical resection may significantly improve the overall treatment outcomes.

AI-extracted tissue fiber framework morphometrics

Our analysis of the tissue fiber framework using AI-based morphometrics revealed distinct prognostic roles for different types of fibers in HCC. The study demonstrated that the reticulin structure at the tumor edge and collagen characteristics at the epithelial edge of the peritumoral liver provided independent prognostic information [32]. This finding underscores the importance of analyzing both the tumor and its surrounding microenvironment for comprehensive prognostic assessment.

The mean lacunarity of the reticulin framework at the tumor margin emerged as a key prognostic feature derived from the HCC tissue, followed closely by the variance (SD) of the reticulin lacunarity at the core of the tumor [32]. Lacunarity, as a fractal parameter capturing both gaps and heterogeneity in a pattern, likely reflects the disruption and distortion of the reticulin framework associated with HCC progression. This aligns with the established role of reticulin loss as a diagnostic hallmark of HCC [44]. The prognostic significance of reticulin lacunarity extends beyond the simple quantification of the reticulin content, suggesting that the spatial arrangement and heterogeneity of the reticulin framework may provide more insight into the tumor behavior than the overall reticulin density alone.

Our findings also highlight the independent prognostic significance of the peritumoral liver parenchyma in HCC, particularly, the role of Type I collagen in fibrous tissue accumulation during persistent liver damage. We identified three collagen-derived features – a mean texture correlation, a high variance of the fiber straightness, and a high variance in the fiber density – as significant predictors of the overall survival, all measured at the interface between the remaining functional hepatocytes and fibrous stroma. These features may reflect the balance between the regions of dense, compact fibrosis and the areas of relatively intact liver parenchyma, with high variability of collagen deposition alongside the maintained overall tissue structure potentially indicating an ongoing successful tissue repair and a sufficient residual liver function, which is crucial for the patient survival.

The development of penalized Cox regression models incorporating the patient age, tumor multifocality, and fiber-derived features achieved a good discriminative ability for predicting the overall survival, outperforming models based solely on the conventional clinicopathologic parameters [32]. This again highlights the potential of AI-extracted microarchitectural features so that to enhance prognostic modeling in HCC.

Deep learning-based tissue ‘fingerprint’ extraction

Our exploratory analysis using deep learning-based tissue ‘fingerprinting’ revealed promising results for identifying prognostically relevant tissue microenvironments in HCC. The use of a pretrained transformer network (CTransPath) for feature extraction, followed by unsupervised clustering, allowed for the identification of distinct tissue patterns associated with the patient outcomes.

The multivariate analysis identified specific cluster proportions (gm9_c1 for the overall survival; km9_c1 and gm6_c0 for the recurrence-free survival) as independent predictors of the patient outcomes [unpublished data]. These findings suggest that certain tissue microenvironments, identifiable through deep learning approaches, may represent distinct tumor-stromal interactions or epithelial-stromal transitions which influence the disease course. While the biological interpretation of these clusters requires further investigation, the ability to stratify patients based on these computational tissue ‘fingerprints’ demonstrates the potential of this approach for enhancing prognostic modeling in HCC.

Integration of machine learning approaches

The integration of multiple machine learning approaches, incorporating clinical, pathological, laboratory, and computational tissue analysis data, resulted in predictive models for both the recurrence-free survival and the overall survival in HCC patients. The recurrence-free survival model, which included factors such as the resection margin status, the fulfillment of the Milan criteria, the CD8 density variance at the tumor edge, and the collagen fiber lacunarity, achieved good predictive performance (c-index of 0.712) [unpublished data]. This integrated approach demonstrates the potential for combining the traditional clinical parameters with advanced computational tissue analysis to improve risk stratification in HCC.

The development of multiple overall survival models with comparable performance suggests that there may be several valid approaches to prognostic modeling in HCC, potentially reflecting the complex and heterogeneous nature of the disease. The consistent inclusion of computational markers derived from tissue analysis alongside the established clinical parameters in these models underscores the value of integrating AI-based tissue analysis into prognostic assessment for HCC.

In conclusion, this comprehensive study demonstrates the potential of integrating artificial intelligence-based analyses of the tumor

microenvironment, the immune response, and the tissue architecture to enhance prognostic modeling in hepatocellular carcinoma. A combination of CD8 spatial distribution analysis, AI-extracted tissue fiber framework morphometrics, and deep learning-based tissue ‘fingerprinting’ provides a multifaceted approach to capturing the complex biology of HCC. While further validation in larger, prospective cohorts and/or biopsy material is needed, these findings lay the groundwork for the development of more accurate and more personalized prognostic tools in HCC management.

CONCLUSIONS

This doctoral thesis investigated the prognostic modeling of *Hepatocellular Carcinoma* (HCC) through artificial intelligence-based tissue analysis, studying a cohort of 134 patients who underwent surgical intervention (of which, 106 liver resections and 28 liver transplantations) at Vilnius University Hospital Santaros Clinics between 2007–2020. The study employed multiple computational approaches to analyze digitized histopathology slides, while focusing on three main analytical strategies.

CD8 lymphocyte spatial distribution analysis

By using a hexagonal grid-based computational approach combined with *HALO*® AI tissue segmentation, we analyzed the spatial distribution of CD8 lymphocytes at both tumor-stroma and liver-stroma interfaces. The key findings of the present research include:

- In resected HCC patients:
  - A higher standard deviation of CD8 density at the tumor edge independently predicted a longer overall survival (HR 0.39, 95% CI: 0.24–0.65, p=0.0002).
  - A higher mean CD8 density in the epithelial aspect of perineoplastic liver predicted a worse survival likelihood (HR 3.65, 95% CI: 1.54–8.67, p=0.0019).
- In transplanted HCC patients:
  - A mean CD8 density at the epithelial edge of the non-malignant interface emerged as an independent predictor (HR 0.15, 95% CI: 0.03–0.82, p=0.01).
  - Combined with the preoperative platelet count (HR 0.15, 95% CI: 0.03–0.81, p=0.01), these factors have been found to create a robust prognostic model.

AI-extracted collagen framework analysis

By employing a modified U-Net convolutional neural network architecture, we analyzed the architectural patterns of both reticulin (Type III collagen) and Type I collagen fibers. Our notable findings include:

- In the HCC tissue:
  - Mean lacunarity of reticulin at the tumor edge emerged as a key predictor of shorter OS (HR 6.36, 95% CI: 1.69–23.87, p=0.006).

- Correlation of Type I collagen in peritumoral liver showed a protective OS effect (HR 0.21, 95% CI: 0.05–0.92, p=0.038).
- Two prognostic OS models achieved C-indices of >0.70, combining:
  - Model A: Age ≥55 years (HR 4.05, 95% CI: 1.67–9.80, p=0.00194), multiple tumors (HR 1.92, 95% CI: 1.11–3.31, p=0.01895), reticulin lacunarity (HR 6.36, 95% CI: 1.69–23.87, p=0.00615), and collagen correlation (HR 0.21, 95% CI: 0.05–0.92, p=0.03802).
  - Model B: Similar variables, but replacing collagen correlation with fiber straightness variance.

Deep learning-based tissue 'fingerprint' analysis

By using the CTransPath foundation model and unsupervised clustering approaches, we have identified distinct tissue patterns associated with the patient outcomes:

- For the *Overall Survival* (OS):
  - Gaussian mixture model cluster gm9_c1 showed an independent prognostic value (HR: 8.67, 95% CI: 1.21–62.36, p=0.032).
- For the *Recurrence-Free Survival* (RFS):
  - Two clusters emerged as significant predictors: km9_c1 (HR: 3.81, p=0.024) and gm6_c0 (HR: 3.20, p=0.045).

Integration of machine learning approaches

Our integrated prognostic models combine clinical, laboratory, and computational tissue features to enhance prediction accuracy for both the *Recurrence-Free Survival* (RFS) and the *Overall Survival* (OS) in HCC. Our key insights include:

- *Recurrence-Free Survival* (RFS):
  - Full Cohort: The top RFS model, achieving a C-index of 0.718, identified the resection margin status (R0 vs R1), the Milan criteria status, and collagen lacunarity at the tumor edge as independent predictors (HR 4.23, p<0.0001 for the resection status; HR 0.56, p=0.042 for fulfilling the Milan criteria prior to resection; HR 0.20, p=0.006 for collagen).
  - Subgroup Analysis (R0-only): In patients with complete resections, the immune cell spatial distribution and the tumor architectural features were key, with CD8 density variation at the tumor edge (HR 0.15, p=0.008) and tumor multifocality (HR 2.45, p=0.006) driving the predictive performance (C-index: 0.706).

- *Overall Survival* (OS):
  - The optimal OS model reached a C-index of 0.782 by integrating seven variables: age ≥55 years, lymphovascular invasion, AST and GGT levels, CD8 density standard deviation at the tumor edge, reticulin correlation, and reticulin CSD variation. Notably, immune (CD8 spatial variation, HR 0.25, p=0.033) and tissue features (reticulin fiber correlation, HR 0.10, p=0.028) complemented the clinical markers, underscoring their prognostic value.

This multimodal approach demonstrates that a combination of the clinical data with tissue-specific computational features, especially CD8 lymphocyte distribution and collagen/reticulin framework analytics, provides a significant improvement in the prognostic accuracy, thus supporting more personalized HCC management strategies.

Summary

These findings represent significant advances in computational pathology for HCC prognostication. The study demonstrates that the integration of AI-based tissue analysis with the conventional clinical parameters can provide a more accurate risk stratification than the traditional methods alone. The developed methods have potential clinical applications in the treatment planning, particularly in decisions between liver resection and transplantation.

Future validation of these findings in larger, prospective cohorts and the investigation of their applicability to preoperative biopsy specimens could facilitate their translation into the clinical practice. This work lays the foundation for more personalized approaches to HCC management, potentially improving the patient outcomes through better-informed treatment decisions.

SANTRAUKA LIETUVIŲ KALBA

PREAMBULĖ

Ši mokslų daktaro disertacija pateikiama ginti kaip mokslinių straipsnių rinkinys, kai kurios jos dalys cituojamos iš anksčiau publikuotų straipsnių, pateikiamų šio darbo pabaigoje.

Mūsų atliktas tyrimas nukreiptas į dirbtinio intelekto įrankių panaudojimą mikroskopinių vaizdų analizei, siekiant prognozuoti hepatoceliuline karcinoma (HCC) sergančių pacientų išgyvenamą laiką iki ligos atkryčio (RFS) ir bendrą išgyvenamumą (OS). Tyrimo metu analizavome 134 HCC pacientų, kuriems buvo atlikta kepenų rezekcija (106 pacientai) arba kepenų transplantacija (28 pacientai) Vilniaus universiteto ligoninės Santaros klinikose 2007–2020 metais, grupę.

Atliekant tyrimą taikytos trys viena kitą papildančios analitinės strategijos:

1. CD8 limfocitų infiltracijos analizė. Jos metu pritaikytas šešiakampiu tinkleliu grįstas skaičiavimo ir vizualizavimo metodas citotoksinių limfocitų erdviniam pasiskirstymui abipus epitelio ir stromos ribos ištirti.
2. Kolageno skaidulų analizė. Ją atliekant buvo tiriama tiek III tipo (retikulino), tiek I tipo kolageno skaidulų mikroarchitektūra panaudojant modifikuotą neuroninį tinklą.
3. Giliu mokymusi paremta audinių „pirštų atspaudų“ analizė. Jos metu taikytas neprižiūrimo mokymosi metodas ir klasterizavimas skirtingoms audinių struktūroms, susijusioms su ligos baigtimis, nustatyti.

Mūsų tyrimas atskleidė, kad dirbtiniu intelektu pagrįstos audinių analizės integravimas į modelius su įprastiniais klinikiniais parametrais gali reikšmingai pagerinti prognozavimo tikslumą. Pavyzdžiui, nustatėme, kad maža CD8 limfocitų tankio variacija naviko krašte kartu su dideliu retikulino struktūrų lakūnariškumu (specifiniu tekstūros parametru) perinavikiniame audinyje leidžia prognozuoti trumpesnį išgyvenamumą. Mūsų sukurti kombinuoti prognostiniai modeliai, apimantys tiek klinikinius, tiek skaičiuojamuosius požymius, pasiekė geresnį prognozavimo tikslumą, lyginant su tradiciniais metodais.

Šis darbas – tai dar vienas nedidelis žingsnis link labiau individualizuoto HCC gydymo. Tikimės, kad dirbtiniu intelektu grįsta audinių analizė leis patobulinti tradicinius prognozavimo metodus ir galiausiai pagerinti priimamus terapinius sprendimus.

ĮVADAS

HCC prognozavimo iššūkių kontekstas

Hepatoceliulinė karcinoma (HCC) užima trečią vietą tarp visų piktybinių navikų sukeltų mirčių pasaulyje, 1990–2019 metais net 70 % padidėjo sergamumas šia liga [1]. Pasaulinei sveikatos apsaugos sistemai HCC kelia daug problemų, vien 2019 metais nuo šios ligos mirė 480 000 žmonių, o jos gydymą apsunkina nesavalaikė diagnostika, kai liga nustatoma jau esant vėlyvoms stadijoms [2]. Iš jau atliktų tyrimų žinoma, kad ankstyvos HCC atveju penkerių metų bendras išgyvenamumas viršija 70 %, tačiau esant vėlyvoms stadijoms šis skaičius krinta iki vos 18 % – tai aiškiai parodo, kaip yra svarbu kuo anksčiau diagnozuoti ligą ir turėti metodus kuo tiksliau ją prognozuoti [3]. Bent 80 % HCC atvejų šią ligą predisponuoja kepenų cirozė, dažniausiai sukelta virusinio hepatito B ir C, alkoholio vartojimo, cheminių toksinų ar metabolinių kepenų ligų [4]. Be to, pasaulyje nuolat augant žmonių, turinčių antsvorį, skaičiui ir plintant 2 tipo diabetui vis dažniau susergama nealkoholinėmis riebalinėmis kepenų ligomis (angl. *non-alcoholic fatty liver disease*, NAFLD), kurios laikomos pagrindine HCC priežastimi netgi tuomet, kai cirozės nėra [5].

Dabar taikomi HCC eigos prognozavimo modeliai nėra pakankamai tikslūs. Skirtingai nuo daugelio kitų vėžio formų, HCC pacientų gydymo rezultatai priklauso ne vien nuo paties naviko savybių ir jo atsako į skirtą gydymą [6]. Ne mažiau svarbus veiksnys yra likusių kepenų patologija bei funkciniai pajėgumai, tad siekiant tiksliau prognozuoti pacientų išeitis būtina visapusiškai įvertinti tiek naviko, tiek kepenų charakteristikas [7]. Pavyzdžiui, vienas plačiausiai naudojamų modelių yra Barselonos klinikinė kepenų vėžio (BCLC) stadijavimo sistema, ją taikant atsižvelgiama į kelis naviko išplitimo, kepenų funkcijos ir su vėžiu susijusių simptomų parametrus [8]. Tačiau netgi taikant šią sistemą ne visuomet galima pakankamai tiksliai prognozuoti kepenų funkcijos praradimą sergantiesiems HCC [9].

Tiksliai prognozuoti HCC išeitis sunku dėl šio naviko etiologijos, architektūros, molekulinių charakteristikų ir klinikinių simptomų heterogeniškumo [10]. Dinamiška ligos eiga, kuriai būdingas greitas progresavimas, vartų venos invazija ar ekstrahepatinis plitimas, virsta tikru iššūkiu prognozuojant ilgalaikius rezultatus [11]. Dėl visų šių veiksnių svarbu kuo labiau tobulinti ir individualizuoti HCC prognozavimo priemones.

Trumpa dirbtinio intelekto ir mašininio mokymosi patologijoje apžvalga

Šiuo metu, kai plačiai integruojamas dirbtinis intelektas (DI) ir mašininio mokymosi (MM) technologijos, patologijos srityje vyksta didžiulis paradigmos pokytis, atveriantis daugiau galimybių diagnostikai, prognozavimui ir individualizuotai medicinai [12]. Išvysčius viso mikropreparato vaizdo (angl. *whole slide imaging*, WSI) skenavimo galimybes sudaromos sąlygos pažangių skaičiavimo metodų taikymui atliekant audinių mikroarchitektūros tyrimus [13].

Konvoliuciniai neuroniniai tinklai (angl. *convolutional neural networks*, CNN), gilaus mokymosi algoritmų klasė, yra ypač efektyvūs atliekant tokias užduotis kaip automatinis audinių segmentavimas, ląstelių aptikimas ir histologinių struktūrų klasifikavimas [14]. Šios DI programos gali apdoroti didžiulius vaizdinių duomenų kiekius, identifikuodamos subtilius struktūrinius pokyčius ir ypatybes, kurių netgi labai patyrę gydytojai patologai gali nepastebėti [15]. HCC kontekste CNN yra sėkmingai naudojami labai įvairioms užduotims – nuo automatizuoto navikų sričių suradimo iki diferenciacijos laipsnio ar intravaskulinės invazijos aptikimo [16].

Be įprastų klasifikavimo užduočių, DI metodai naudojami ir kiekybiniams požymiams iš histologinių vaizdų išgauti (t. y. apskaičiuoti) [17]. Naudojantis DI galima automatizuotai išmatuoti sudėtingas audinių architektūros savybes, įvairių tipų ląstelių ar mikrostruktūrų pasiskirstymą bei kitas morfologines charakteristikas ir tokiu būdu išgauti daugybę potencialių biožymenų [18]. Pavyzdžiui, DI grįsta naviką infiltruojančių limfocitų analizė sėkmingai taikoma prognozuojant įvairių piktybinių navikų tipų išeitis [19].

Mašininio mokymosi algoritmai, tokie kaip atraminių vektorių klasifikatoriai (angl. *support vector machine*), atsitiktinių medžių (angl. *random forest*) ir palaipsnio stiprinimo (angl. *gradient boost*) metodikos, naudojami integruojant šiuos iš vaizdų išgautus požymius kartu su geriau pažįstamais klinikiniais ir molekuliniais parametrais, taip siekiama sukurti tikslesnius prognostinius modelius [20]. Šie modeliai labiau individualizuotai stratifikuoja riziką, todėl turi potencialą pranokti tradicines stadijavimo sistemas [21].

Nors atliekama daugybė sėkmingų eksperimentų, kurių rezultatai nuolat publikuojami, vis dėlto DI integracija į patologijos praktiką susiduria su iššūkiais, tokiais kaip mokymams būtini dideli ir įvairiapusiai duomenų rinkiniai, DI sprendimų interpretavimo, paaiškinamumo, atkartojamumo ir etiškumo problemos, taip pat būtinas griežtas validavimas prieš klinikinį įdiegimą [22]. Nepaisant to, nekyla abejonių, kad DI įrankių taikymas patologijoje gali padidinti diagnostinį tikslumą, pagerinti prognozes ir

galiausiai padėti pasirinkti individualizuotus gydymo sprendimus, kurie susiję su tokiomis ligomis kaip HCC [23].

Daugiamodalė audinių analizė

Esant sudėtingai HCC ląstelių, imuninės sistemos ir tarpląstelinio matrikso sąveikai būtinas kompleksinis požiūris į prognostinių modelių kūrimą. Šiame tyrime dėmesys sutelkiamas į tris pagrindinius naviko mikroaplinkos aspektus: CD8 citotoksinius T limfocitus, I bei III tipo kolageno skaidulų architektūrą ir bendruosius vizualinius audinių bruožus (angl. patterns). Kiekvienas šių komponentų suteikia unikalių ir vienas kitą papildančių įžvalgų apie naviko biologiją, aplinkinio kepenų audinio būklę ir galimas ligos baigtis.

CD8 limfocitai yra vienas svarbiausių priešnavikinio imuninio atsako elementų, todėl nestebina, kad jie yra prognostiniu požiūriu reikšmingi daugelyje piktybinių navikų tipų [24]. Kalbant konkrečiai apie HCC, CD8 ląstelių tankis ir specifinis jų erdvinis pasiskirstymas yra susijęs su pacientų išgyvenamumu, tačiau gaunami rezultatai yra šiek tiek nevienareikšmiai [25,26]. Pasitelkę pažangius erdvinės analizės metodus CD8 limfocitų infiltracijai į naviko ir kepenų audinius charakterizuoti, siekėme patikslinti iki šiol publikuotus rezultatus ir surinkti kuo detalesnę prognostinę informaciją [27].

Tarpląstelinis matriksas, ypač I tipo kolageno ir III tipo kolageno (dar vadinamo retikulinu) skaidulos, yra dar viena esminė naviko mikroaplinkos ir aplinkinio kepenų audinio dalis. HCC atveju normalaus retikulino tinklo pokyčiai yra svarbus diagnostinis požymis, o I tipo („randinis“) kolagenas tiek remodeliuojamas intra- / perinavikinėje aplinkoje, tiek parodo likutinių kepenų fibrozę [28, 29]. Kiekybinė šių skaidulų struktūros analizė, atliekama naudojant DI pagrįstus metodus, leidžia užfiksuoti subtilius architektūrinius pokyčius, galinčius turėti prognostinę reikšmę [30].

Trečioji koncepcija mūsų tyrime yra audinių „pirštų atspaudai“, išgauti naudojant giliojo mokymosi algoritmus. Šiuo metodu siekiama nustatyti specifines vizualines audinių savybes (angl. patterns), kurių neįmanoma lengvai įvertinti pagal iš anksto apsibrėžtus jų požymius. Naudojant šį metodą kitų navikų prognostinėse analizėse jau gauta perspektyvių rezultatų [31]. Taikydami minėtą metodiką HCC siekėme identifikuoti naujas audinių savybes, kurios gali būti susijusios su ligos baigtimis.

Integruodami šiuos tris audinių analizės komponentus – imuninių ląstelių infiltraciją, tarpląstelinio matrikso architektūrą ir bendrąsias vizualines audinių savybes – siekėme sukurti visapusiškai patikimą HCC prognostinį modelį. Toks daugiamodalis rizikos vertinimas geriau atspindi sudėtingą HCC biologiją, todėl yra potencialiai tikslesnis ir labiau personalizuotas [32].

Tyrimo hipotezė

Dirbtiniu intelektu pagrįsta imuninio atsako, naviko mikroaplinkos ir audinių architektūros analizė turėtų pagerinti hepatoceliulinės karcinomos prognostinius modelius, paremtus tik šiuo metu naudojamais klinikiniais ir patologiniais parametrais.

Tyrimo tikslas

Sukurti dirbtiniu intelektu pagrįstus hepatoceliulinės karcinomos prognostinius modelius, skirtus pacientams po chirurginio gydymo, į kuriuos būtų integruoti skaitmeninės patologijos duomenys apie imuninį atsaką, naviko mikroaplinką ir audinių mikroarchitektūrą.

Tyrimo uždaviniai

1. Sukurti prognostinį modelį, pagrįstą CD8 limfocitų erdviniu pasiskirstymu navike ir aplinkinėje kepenų parenchimoje, taikant DI audinių klasifikavimo ir šešiakampių gardelių segmentavimo metodikas.
2. Sukurti prognostinį modelį taikant DI pagrįstą kolageno skaidulų morfometrinę analizę naviko mikroaplinkoje ir aplinkinėje kepenų parenchimoje.
3. Naudojant giliojo mokymosi neuroninius tinklus sukurti prognostinį modelį, kuriuo būtų nustatomos ir analizuojamos specifinės naviko mikroarchitektūrinės ypatybės („pirštų atspaudus“).
4. Integruoti gautus duomenis į bendrą modelį ir įvertinti jo efektyvumą hepatoceliulinės karcinomos išeitims prognozuoti.

TIRIAMOJI MEDŽIAGA IR AUDINIŲ DAŽYMO METODAI

Bioetikos leidimas ir finansavimo šaltiniai

Vilniaus regioninis biomedicininių tyrimų etikos komitetas (leidimas Nr. 2021/6-1354-843, išduotas 2021 m. birželio 29 d.) patvirtino atlikto tyrimo protokolą, kuriuo tyrėjai buvo atleisti nuo pareigos gauti kiekvieno paciento sutikimą. Tyrimas iš dalies finansuotas Europos socialinis fondo pagal Lietuvos mokslo tarybos projektą Nr. 09.3.3-ESFA-V-711-01-0001, kurio tikslas – sustiprinti viešojo sektoriaus mokslininkų kompetencijas vykdant aukšto lygio MTTP veiklas.

Pacientų grupė ir mėginių surinkimas

Į tyrimą įtraukti 134 hepatoceliuline karcinoma (HCC) sergantys pacientai, kuriems 2007–2020 m. Vilniaus universiteto ligoninės Santaros klinikose buvo atlikta kepenų rezekcija arba kepenų transplantacija. Pagrindinės pacientų charakteristikos pateiktos 8 lentelėje. Transplantuotųjų pacientų (N=28) bendras išgyvenamumas buvo statistiškai reikšmingai (p=0,0011) ilgesnis nei pacientų iš rezekcijos grupės (N=106), todėl šios grupės toliau analizuotos atskirai.

8 lentelė. Pagrindinės pacientų charakteristikos.

Charakteristika	**Reikšmė**
Lytis	Vyrai – 101 (75,4 %) Moterys – 33 (24,6 %)
Amžius	Vidurkis – 60,45 metų (spektras – 13–82)
Naviko diferenciacijos laipsnis (G)	G1 – 13 (9,7 %) G2 – 101 (75,4 %) G3 – 20 (14,9 %)
pT stadija	T1 – 53 (39,6 %) T2 – 73 (54,5 %) T3 – 7 (5,2 %) T4 – 1 (0,7 %)
Intravaskulinė invazija	Yra – 59 (44 %) Nėra – 75 (56 %)
Cirozė	Yra – 89 (66,4 %) Nėra – 45 (33,6 %)
Daugiau nei vienas naviko židinys	Taip – 37 (27,6 %) Ne – 97 (72,4 %)
Naviko dydis	> 2 cm – 108 (80,6 %) > 5 cm – 30 (22,4 %)
Nustatytas virusinis sukėlėjas	HBV – 12 (9 %) HCV – 74 (55,2%)
Atlikta kepenų transplantacija	Taip – 28 (20,9 %) Ne – 106 (79,1 %)
Recidyvas po gydymo	Taip – 57 (42,5 %) Ne – 77 (57,5 %)

Audinių atranka ir dažymo technikos

Atliekant tyrimą panaudoti Valstybiniame patologijos centre archyvuoti formalinu fiksuoti ir į parafiną įlieti audinių mėginiai (FFPE). Iš kiekvienos grupės atrinktas vienas reprezentatyviausias FFPE blokas, kuriame (jei tik įmanoma) buvo ir naviko, ir aplinkinio kepenų audinio. Audiniai paruošti ir dažyti šiomis technikomis:

- Hematoksilino ir eozino (H & E) dažymas – naudotas bendrai audinio morfologijai apžvelgti.
- Gordon'o & Sweets'o sidabro impregnavimo ir pikro rūgšties ir Sirijaus raudonojo (GSPS) metodas – taikytas jungiamojo audinio architektūrai įvertinti, išryškinant III tipo kolageno (retikulino) skaidulas juoda spalva, o I tipo kolageno skaidulas – raudona spalva.
- CD8 imunohistochemija – taikyta citotoksiniams T limfocitams identifikuoti naviko ir aplinkiniuose kepenų audiniuose.

Visi dažyti mėginiai buvo skaitmenizuoti 20× padidinant (0,5 μm/pikseliui raiška), tam panaudotas „Leica Aperio AT2" skeneris. Skaitmenizuoti vaizdai buvo peržiūrėti pažymint dominančias naviko ir kepenų parenchimos sritis, bet vengiant nekrozės ir artefaktų zonų.

1 UŽDAVINYS. CD8 LIMFOCITŲ ERDVINIO PASISKIRSTYMO ANALIZĖ

CD8 limfocitų erdvinis pasiskirstymas naviko mikroaplinkoje reprezentuoja lokalų imuninį atsaką ir yra reikšmingas prognozuojant įvairius piktybinių navikų tipus.

Metodika

Rasmusson'o ir kt. [33] sukurtas „Immunogradient" metodas automatizuoja naviko ir stromos sąveikos zonos (angl. *interface zone*, IZ) nustatymą bei CD8 limfocitų (ar kitų tiriamų ląstelių) tankio profilių generavimą. Atliekant tyrimą šis metodas buvo modifikuotas ir pritaikytas analizuoti dvi sąveikos zonas: vienos zonos ribos buvo tarp naviko ir stromos, kitos – tarp kepenų parenchimos (hepatocitų) ir aplinkinio jungiamojo audinio. Komercine HALO® AI sistema (*Indica Labs*, Naujosios Meksikos valstija, JAV) naudotasi tiek segmentuojant audinius, tiek identifikuojant CD8 ląsteles.

Analizė buvo tęsiama taikant šešiakampių gardelių tinklą, kuris padalija klasifikuotas audinių sritis į šešiakampius segmentus. Remiantis empiriniais vertinimais ir ankstesne patirtimi, analizei pasirinkti 65 μm dydžio

šešiakampiai. Šešiakampių gardelių tinklas turi keletą privalumų, palyginti su tradiciniu vaizdo suskaidymu į stačiakampius, taip pat ir geresnę erdvinę raišką [34]. Kiekviename šešiakampiame segmente apskaičiuojamas kiekvienos audinio klasės plotas, ir sistema automatiškai aptinka naviko (ar kitos klasės audinio) kraštą laikydamasi aiškių taisyklių, kuriose yra numatyti staigūs naviko ir stromos plotų frakcijų pokyčiai. Ši automatinė naviko krašto identifikacija leidžia išvengti daug laiko reikalaujančių rankinių anotacijų ir užtikrina stabilius rezultatus tarp skirtingų mėginių ir tyrimų.

Kitame etape šešiakampiai abiejose naviko krašto (NK) pusėse reitinguojami pagal mažiausią atstumą iki NK. Šešiakampiams, kuriuose yra NK, skiriamas 0 rangas, šešiakampiai naviko pusėje (arba kepenų parenchimoje, priklausomai nuo analizuojamos srities) gauna teigiamus rangus (1, 2, 3 ir t. t.), o stromos pusėje – neigiamus (–1, –2, –3 ir t. t.). Galiausiai apibendrinami kiekvieno rango šešiakampiuose esančių CD8 limfocitų skaičiai ir sukuriami CD8 tankio profiliai sąveikos zonoje.

Statistinė analizė

Statistinė analizė atlikta siekiant identifikuoti sąsajas tarp CD8 tankio profilių, klinikinių bei patologinių kintamųjų ir pacientų išgyvenamumo (bendro – OS ir berecidyvio – RFS). CD8 ląstelių tankiai buvo logaritmuoti, o optimalios tolydžių kintamųjų ribinės vertės nustatytos naudojant „Cutoff Finder“ viešos prieigos įrankį [35]. Išgyvenamumo skirtumams palyginti naudotos Kaplano ir Meierio kreivės ir „Log-Rank“ testas. Daugiaparametrė Cox’o regresijos analizė taikyta siekiant nustatyti nepriklausomą prognostinę rodiklių reikšmę. Analizė atlikta su SAS ir R programomis, o šešiakampio tinklo apdorojimas ir rodiklių skaičiavimas – C++ kalba, naudojant „OpenCV“ ir „Boost“ bibliotekas.

Rezultatai

Nustatyta, kad rezekuotų HCC pacientų grupėje didesnė CD8 tankio variacija (standartinis nuokrypis) naviko krašte buvo nepriklausomas ilgesnio bendrojo išgyvenamumo (OS) prognozės rodiklis. Didesnis už vidutinį CD8 tankis kepenų parenchimos krašte siejosi su trumpesniu OS, tikėtina, tai lėmė imuninės sistemos sukeltas lėtinis hepatocitų pažeidimas (t. y. hepatitas). Transplantuotųjų pacientų grupėje aukštesnis CD8 tankis naviko krašte ir didesnis trombocitų kiekis kraujyje buvo nepriklausomi rodikliai, kurie siejosi su ilgesniu OS. Be to, Milano transplantacijos kriterijus atitikusioje, tačiau

rezekuotoje HCC pacientų grupėje mažesnė CD8 tankio variacija ir teigiamas rezekcijos kraštas (R1) buvo veiksniai, sietini su ankstyva recidyvo rizika.

Tyrimą riboja nedidelės imtys, retrospektyvinis analizės pobūdis ir tai, kad radiniai nėra verifikuoti biopsinėje medžiagoje. Nepaisant šių trūkumų tyrimas patvirtina, kad CD8 erdviniai rodikliai gali būti integruoti ir taikomi kartu su klinikiniais parametrais, tokiu būdu gaunant tikslesnius prognostinius modelius po chirurginio HCC gydymo.

2 UŽDAVINYS. KOLAGENO SKAIDULŲ MORFOMETRIJA PANAUDOJANT DIRBTINĮ INTELEKTĄ

I tipo kolagenas ir III tipo kolagenas (dar vadinamas retikulinu), nors ir turi struktūrinio panašumo, atlieka skirtingas funkcijas lėtinio hepatito ir hepatoceliulinės karcinomos (HCC) evoliucijoje. I tipo kolageno kaupimasis yra progresuojančios kepenų audinio fibrozės ir galiausiai cirozės pagrindas. O III tipo kolageno (retikulino) normalaus sinusoidus išklojančio tinklo pažeidimas yra vienas iš HCC požymių. Žinodami šių mikroarchitektūrinių pokyčių prognostinį potencialą, šiame tyrimo etape siekėme kiekybiškai įvertinti abiejų kolageno tipų struktūrą tiek navike, tiek aplinkiniame kepenų audinyje nagrinėdami naujų pacientų, kuriems buvo atliekama kepenų rezekcija dėl HCC, prognostinius rodiklius.

Metodika

Antrame tyrimo etape tyrėme kolageno skaidulų mikroarchitektūrą HCC aplinkoje naudodamiesi konvoliuciniais neuroniniais tinklais (angl. *convolutional neural networks*, CNN) ir remdamiesi Morkūno ir kt. aprašyta metodika, originaliai pritaikyta krūties karcinomai tirti [38]. HCC atveju mums buvo būtina atskirai įvertinti plonas juodas retikulino (III tipo kolagenas) ir storesnes raudonai dažytas skaidulas (I tipo kolagenas). Apmokėme modifikuotą „U-net“ architektūros tinklą atpažinti šių dviejų tipų skaidulas ir galiausiai sugeneruoti kolageno segmentacijos žemėlapius (angl. *collagen segmentation masks*, CSM), atitinkančius originalaus skenuoto vaizdo dydį. Mokymui panaudoti vaizdai buvo anotuoti rankiniu būdu ir vėliau papildyti vaizdus sukant, apverčiant, išblukinant ar keičiant mastelį.

Gauti segmentuotų kolageno skaidulų vaizdai toliau analizuoti pasitelkiant pirmoje užduotyje aprašytą šešiakampės gardelės metodą, kuris automatiškai aptinka naviko ribą ir įvertina rangais šešiakampius pagal jų atstumą nuo aptiktos ribos. Tai mums leido atlikti specifinių vaizdo regionų (sąveikos zonų) analizę ir identifikuoti kolageno skaidulų piešinio heterogeniškumą.

Skirtingai nuo pirmos užduoties, kai buvo tiriamas vienas parametras (CD8 limfocitų skaičius šešiakampyje), šiame etape, remdamiesi Morkūno ir kt. tyrimo patirtimi, analizavome po 11 abiejų tipų kolageno skaidulų mikroarchitektūros požymių kiekviename šešiakampyje [38]. Duomenų agregavimo metu apskaičiuotos vidutinės ir standartinio nuokrypio reikšmės kiekvienam šešiakampių rangui. Galutinį duomenų rinkinį sudarė 264 potencialūs prognostiniai rodikliai kiekvienam atvejui.

Statistinė analizė

Tirta 105 rezekuotų pacientų grupė (vienas atvejis iš pradinės 106 pacientų grupės buvo pašalintas dėl nepakankamos audinio kokybės), iš kurios 56 pacientai mirė stebėjimo laikotarpiu. 264 skaidulų morfometrija pagrįsti požymiai pirmiausia buvo normalizuoti į 0–1 intervalą. Vienparametrė Cox'o regresija su LASSO reguliarizacija buvo panaudota siekiant įvertinti individualių kintamųjų prognostinę reikšmę, o T2–T4 naviko stadija (palyginti su T1) buvo identifikuota kaip ryškiausias reikšmingas individualus blogesnio bendro išgyvenamumo prediktorius (HR 4,81, 95% PI 2,40–9,64, $p < 0,0001$).

Iš visų 36 charakteristikų, turinčių potencialią prognostinę vertę ($p < 0,1$ vienparametrėje analizėje) bei klinikinių ir patologinių kintamųjų (amžius, stadija, lytis, limfovaskulinė invazija ir naviko daugiažidiniškumas), buvo sugeneruoti visi galimi iki 6 požymių turintys deriniai. Iš daugiau nei 2,8 milijonų kandidatų atrinkti 139 modeliai (apie 0,005%), kuriuose visi kintamieji buvo reikšmingi ($p < 0,05$). Du iš jų pasiekė konkordancijos indeksą (C indeksą) virš 0,7, tai parodo geras diskriminacines modelio savybes. Atlikta faktorinė analizė siekiant identifikuoti latentinius ryšius ir bendruosius biologinius procesus.

Rezultatai

Gauti du daugiaparametrės Cox'o regresijos modeliai HCC pacientų bendram išgyvenamumui prognozuoti po atliktos kepenų rezekcijos, į šiuos modelius įtraukti paciento amžius, naviko daugiažidiniškumas ir kolageno skaidulų charakteristikos. Pirmajame modelyje (C indeksas – 0,7094) reikšmingais prediktoriais buvo amžius – ≥ 55 metai (HR 4,05, 95% PI 1,67–9,80, $p = 0,00194$), naviko daugiažidiniškumas (HR 1,92, 95% PI 1,11–3,31, $p = 0,01895$), retikulino skaidulų vidutinis lakūnariškumas HCC sąveikos zonoje (HR 6,36, 95% PI 1,69–23,87, $p = 0.00615$) ir vidutinė kolageno skaidulų tekstūros koreliacija kepenų sąveikos zonoje (HR 0,21, 95% PI 0,05–0,92, p

= 0,03802). Antrasis modelis (C indeksas – 0,7061) turėjo panašius prediktorius, tik vietoj kolageno skaidulų tekstūros koreliacijos į modelį pateko kolageno skaidulų tiesumas kepenų sąveikos zonoje. Šie modeliai pranoko tuos, kurie rėmėsi vien įprastiniais klinikiniais ir (ar) patologiniais parametrais, pabrėždami potencialią DI išskirtų mikroarchitektūrinių kolageno požymių naudą prognozuojant HCC išeitis.

3 UŽDAVINYS. GILIU MOKYMUSI PAGRĮSTA AUDINIŲ „PIRŠTŲ ANTSPAUDŲ“ ANALIZĖ

Skyriuose, kuriuose aprašomi su 3 ir 4 uždaviniais susiję darbai, pateikiami tik preliminarūs paskutinių etapų rezultatai. Ši tyrimo dalis dar nėra baigta, o duomenys nėra oficialiai publikuoti. Pateikiama informacija siekiant supažindinti su darbų kryptimis ir galimais rezultatais. Būtina pažymėti, kad šie duomenys gali keistis tolesnės analizės ir recenzavimo proceso metu.

Metodika

MISL metodas

Pirminiame darbo etape išbandėme dėmesiu valdomą dauginių pavyzdžių išgyvenamumo mokymąsi (angl. *attention-guided multiple instance survival learning*), paremtą sėkmingai Drachnerio ir kt. naudota metodika [39]. Tačiau taikant šį analizės būdą nepavyko gauti tenkinančių rezultatų, todėl sukūrėme alternatyvų požymių ištraukimo (angl. *feature extraction*) ir klasterizavimo modelį.

Duomenų paruošimas ir požymių ištraukimas

Šiame tyrimo etape buvo panaudoti 105 pacientų, kuriems atlikta HCC rezekcija, hematoksilinu ir eozinu dažyti viso pjūvio vaizdai (WSI). Pažymėtos HCC sritys buvo suskirstytos į kvadrato formos 256 × 256 pikselių dydžio segmentus. Suboptimalios kokybės pavyzdžiai pašalinti, o likusių vaizdų spalvų normalizavimas atliktas naudojant Vahadane'o algoritmą. Iš viso sugeneruota 416 928 aukštos kokybės vaizdo segmentų. Požymiams ištraukti panaudotas atvirosios prieigos „CTransPath“ modelis, kuris kiekvienam vaizdo segmentui sugeneravo po 768 požymius.

Klasterizavimas

Požymių vektoriai buvo suskirstyti į klasterius pagal audinių tipus taikant Gauso mišrųjį modelį (angl. *gaussian mixture model*, GMM) ir „K-means“ algoritmą skirtingiems klasterių skaičiams (k = 2–10). Kiekvieno paciento

mikropreparatui buvo apskaičiuota audinių sudėtis procentais, atsižvelgiant į aptiktus klasterius, tokiu būdu suformuotas unikalus vaizdo „pirštų atspaudas“.

Statistinė analizė

Taikant daugiaparametrę Cox'o regresijos analizę nustatyta klasterių proporcijų sąsaja su išgyvenamumu ir ligos atsinaujinimu. Statistinė reikšmingumo riba – $p < 0,05$.

Rezultatai

Vizualizuoti klasteriai parodė specifinius audinių piešinius ir struktūras. Remdamiesi jais siekėme nustatyti, ar didesnė tam tikro klasterio proporcija audinyje yra susijusi su ilgesniu ar su trumpesniu bendru išgyvenamumu (OS), taip pat ir išgyvenamumu be recidyvo (RFS).

Rezultatai parodė, kad yra trys reikšmingi kintamieji bendram išgyvenamumui: gm6_c0, gm9_c1 ir km10_c1, iš jų gm9_c1 liko statistiškai reikšmingas ir daugiaparametrėje regresijoje (HR 8,67, $p = 0,032$). Išgyvenamumui be recidyvo reikšmingi buvo du kintamieji: km9_c1 ir gm6_c0, kurie liko reikšmingi ir daugiaparametrėje analizėje, su HR reikšmėmis 3,81 ($p = 0,024$) ir 3,20 ($p = 0,045$). Tiek OS, tiek RFS modeliai buvo statistiškai reikšmingi (LR $p = 0,014$ ir $p = 0,013$).

Išvada

Iš preliminarių rezultatų matyti, kad audinių klasterizacija gali padėti identifikuoti prognostiniu požiūriu reikšmingas audinių klases (tipus).

4 UŽDAVINYS. MAŠININIO MOKYMOSI METODŲ INTEGRAVIMAS

Šis etapas skirtas sukurti kompleksinius prognostinius modelius, kurie sujungtų klinikinius parametrus, laboratorinius duomenis ir kompiuterinės audinių analizės rodiklius. Analizėje naudojome CD8 limfocitų erdvinį išsidėstymą ir audinių skaidulų struktūros charakteristikas.

Metodika

Taikėme dviejų etapų metodą. Per pirmąjį etapą visi kintamieji buvo įvertinti naudojant vienparametrę Cox'o regresijos analizę. Reikšmingi kintamieji ($p <$

0,05) buvo atrinkti tolesniam darbui. Per antrąjį etapą atlikta daugiaparametrė Cox'o regresija su LASSO reguliarizacija ir 5 kartų kryžmine validacija (angl. *cross validation*). Modeliai buvo vertinami pagal konkordantiškumo indeksą (C indeksą) ir Aikakės informacijos kriterijų (angl. *Akaike information criterion*, AIC).

Rezultatai

Bendrojo išgyvenamumo modeliai

Atlikus bendrojo išgyvenamumo analizę gauti net 132 skirtingi kintamųjų deriniai, kurių C indeksas buvo daugiau nei 0,70. Į geriausią modelį (C indeksas – 0,782, AIC – 299,90) buvo integruoti klinikiniai, laboratoriniai ir kompiuterinės audinių analizės parametrai:

- Amžius ≥ 55 metų (HR = 2,96, 95% PI: 1,19–7,39, $p = 0,020$);
- Intravaskulinė invazija (HR = 2,58, 95% PI: 1,44–4,63, $p = 0,001$);
- Priešoperacinė AST reikšmė (HR = 15,49, 95% PI: 4,28–56,09, $p < 0,0001$)
- Priešoperacinė GGT reikšmė (HR = 13,36, 95% PI: 1,63–109,75, $p = 0,016$);
- CD8 tankio variacija (standartinė deviacija) naviko krašte (HR = 0,25, 95% PI: 0,07–0,90, $p = 0,033$);
- Retikulino skaidulų tekstūros koreliacija naviko krašte (HR = 0,10, 95% PI: 0,01–0,78, $p = 0,028$);
- Retikulino CSD variacija naviko krašte (HR = 3,38, 95% PI: 1,09–10,50, $p = 0,035$).

Išgyvenamumo be recidyvo modeliai

Rezekuotų pacientų grupėje geriausias RFS modelis buvo toks: C indeksas – 0,718 (AIC – 333,12), o jo komponentai:

- Rezekcijos radikalumas (R1 vs R0: HR = 4,23, 95% PI: 2,29–7,81, $p < 0,0001$);
- Ikioperacinis atitikimas Milano transplantacijos kriterijams (HR = 0,56, 95% PI: 0,32–0,98, $p = 0,042$);
- Vidutinis kolageno skaidulų lakūnariškumas naviko krašte (HR = 0,20, 95% PI: 0,06–0,63, $p = 0,006$).

Subgrupėje, kurioje buvo tik radikalios (R0) rezekcijos pacientai, geriausias modelis (C indeksas – 0,706, AIC – 231,97) sujungė du nepriklausomus prognostinius veiksnius:

- CD8 tankio variaciją (standartinė deviacija) naviko krašte (HR = 0,15, 95% PI: 0,03–0,61, p = 0,008);
- Naviko daugiažidiniškumą (HR = 2,45, 95% PI: 1,30–4,62, p = 0,006).

IŠVADOS

Ši disertacija skirta hepatoceliulinės karcinomos (HCC) prognostiniam modeliavimui, kurio metu panaudojant dirbtinį intelektą atliekama audinių analizė, aprašyti. Į tyrimą buvo įtraukti 134 pacientai, kurie nuo 2007 m. iki 2020 m. gydyti Vilniaus universiteto ligoninės Santaros klinikose (106 kepenų rezekcijos ir 28 kepenų transplantacijos). Tyrime buvo taikomi trys pagrindiniai analitiniai metodai:

CD8 limfocitų erdvinio pasiskirstymo analizė

Naudojantis šešiakampių gardelių metodu ir HALO® AI audinių segmentavimu buvo analizuotas CD8 limfocitų erdvinis pasiskirstymas naviko–stromos ir kepenų–stromos sąveikos zonose.

- Rezekuotų HCC pacientų grupėje rezultatai buvo tokie:
  - CD8 tankio standartinis nuokrypis naviko krašte reikšmingai koreliavo su geresniu bendru išgyvenamumu (HR – 0,39, p = 0,0002).
  - Didelis vidutinis CD8 tankis kepenų parenchimoje siejosi su blogesniu bendru išgyvenamumu (HR – 3,65, p = 0,0019).
- Transplantuotų HCC pacientų grupėje rezultatai buvo tokie:
  - CD8 tankis ties kepenų parenchimos ir stromos riba buvo nepriklausomas prognostinis veiksnys (HR – 0,15, p = 0,01).
  - Kartu su priešoperaciniu trombocitų skaičiumi (HR – 0,15, p = 0,01) šie rodikliai buvo įtraukiami į statistiškai reikšmingą prognostinį modelį.

Kolageno skaidulų morfometrija panaudojant DI

Naudojantis „U-Net“ konvoliuciniu neuroniniu tinklu analizuotos III tipo (retikulino) ir I tipo kolageno skaidulos. Analizuota tik rezekuotų HCC pacientų grupė.

- Retikulino lakūnariškumas naviko krašte buvo reikšmingas prognostinis rodiklis (HR – 6,36, p = 0,006).
- I tipo kolageno tekstūros koreliacija ties kepenų parenchimos ir stromos riba buvo antrasis reikšmingas prognostinis rodiklis (HR – 0,21, p = 0,038).

- Modeliai:
  - Modelis A –amžius – ≥ 55 metai (HR 4,05, p = 0,00194), naviko daugiažidiniškumas (HR 1,92, p = 0,01895), retikulino skaidulų vidutinis lakūnariškumas HCC sąveikos zonoje (HR 6,36, p = 0.00615) ir vidutinė kolageno skaidulų tekstūros koreliacija kepenų sąveikos zonoje (HR 0,21, p = 0,03802).
  - Modelis B – analogiškas, tik kolageno tekstūros koreliacija pakeičiama į kolageno skaidulų tiesumą.

Giliu mokymusi pagrįsta audinių „pirštų antspaudų“ analizė

Naudojantis „CTransPath“ modeliu ir nekontroliuojamais klasterizavimo metodais nustatyti audinių tipai, susiję su pacientų išgyvenamumu:

- Bendram išgyvenamumui (OS):
  - Klasteris gm9_c1 buvo nepriklausomas prognostinis rodiklis (HR – 8,67, p = 0,032).
- Išgyvenamumui be recidyvo (RFS):
  - Klasteriai km9_c1 (HR – 3,81, p = 0,024) ir gm6_c0 (HR – 3,20, p = 0,045).

Mašininio mokymosi metodų integravimas

Sujungus klinikinius, laboratorinius ir kompiuterinės audinių analizės duomenis, sukurti prognostiniai modeliai abiem išgyvenamumo rodikliams:

- RFS – geriausias modelis (C indeksas – 0,718) apėmė rezekcijos radikalumą (R1 vs R0), ikioperacinį atitikimą Milano transplantacijos kriterijams ir vidutinį kolageno skaidulų lakūnariškumą naviko krašte;
- OS – į geriausią modelį (C indeksas – 0,782) integruoti septyni veiksniai: vyresnis amžius, intravaskulinė invazija, priešoperacinės AST ir GGT reikšmės, CD8 tankio variacija naviko krašte, retikulino skaidulų tekstūros koreliacija naviko krašte ir retikulino CSD variacija naviko krašte.

Apibendrinimas

Rezultatai, gauti naudojantis skaitmeninių technologijų įrankiais, prisideda prie patologijos tyrimų pažangos. Tyrimas įrodo, kad dirbtiniu intelektu paremtos audinių analizės integravimas su įprastais klinikiniais ir patologijos parametrais gali suteikti tikslesnę rizikos stratifikaciją nei vien tik tradicinių modelių naudojimas. Sukurti metodai turi potencialų klinikinį pritaikymą

planuojant gydymą, ypač priimant sprendimus, kai reikia rinktis tarp kepenų rezekcijos ir transplantacijos. Ateityje šių išvadų validavimas didesnėse, prospektyvinėse grupėse ir jų pritaikomumo priešoperacinių biopsijų mėginiams tyrimas galėtų būti kitas žingsnis siekiant jas įdiegti į klinikinę praktiką. Šis darbas plečia individualizuoto požiūrio į HCC kontrolę svarbą, kas potencialiai gerintų gydymo rezultatus pagrįstai atrenkant ir taikant terapinius sprendimus.

REFERENCES

1. Toh MR, Wong EYT, Wong SH, Ng AWT, Loo LH, Chow PK, et al. Global Epidemiology and Genetics of Hepatocellular Carcinoma. Gastroenterology. 2023;164(5):766-82.
2. Sung H, Ferlay J, Siegel RL, Laversanne M, Soerjomataram I, Jemal A, et al. Global Cancer Statistics 2020: GLOBOCAN Estimates of Incidence and Mortality Worldwide for 36 Cancers in 185 Countries. CA Cancer J Clin. 2021;71(3):209-49.
3. Vogel A, Meyer T, Sapisochin G, Salem R, Saborowski A. Hepatocellular carcinoma. Lancet. 2022;400(10360):1345-62.
4. Singh AK, Kumar R, Pandey AK. Hepatocellular Carcinoma: Causes, Mechanism of Progression and Biomarkers. Curr Chem Genom Transl Med. 2018;12:9-26.
5. Chrysavgis L, Giannakodimos I, Diamantopoulou P, Cholongitas E. Non-alcoholic fatty liver disease and hepatocellular carcinoma: Clinical challenges of an intriguing link. World J Gastroenterol. 2022;28(3):310-31.
6. Nault JC, Galle PR, Marquardt JU. The role of molecular enrichment on future therapies in hepatocellular carcinoma. J Hepatol. 2018;69(1):237-47.
7. Eilard MS, Naredi P, Helmersson M, Hemmingsson O, Isaksson B, Lindell G, et al. Survival and prognostic factors after transplantation, resection and ablation in a national cohort of early hepatocellular carcinoma. HPB (Oxford). 2021;23(3):394-403.
8. Reig M, Forner A, Rimola J, Ferrer-Fabrega J, Burrel M, Garcia-Criado A, et al. BCLC strategy for prognosis prediction and treatment recommendation: The 2022 update. J Hepatol. 2022;76(3):681-93.
9. Mauro E, Forner A. Barcelona Clinic Liver Cancer 2022 update: Linking prognosis prediction and evidence-based treatment recommendation with multidisciplinary clinical decision-making. Liver Int. 2022;42(3):488-91.
10. Chidambaranathan-Reghupaty S, Fisher PB, Sarkar D. Hepatocellular carcinoma (HCC): Epidemiology, etiology and molecular classification. Adv Cancer Res. 2021;149:1-61.
11. Yang JD, Hainaut P, Gores GJ, Amadou A, Plymoth A, Roberts LR. A global view of hepatocellular carcinoma: trends, risk, prevention and management. Nat Rev Gastroenterol Hepatol. 2019;16(10):589-604.
12. Niazi MKK, Parwani AV, Gurcan MN. Digital pathology and artificial intelligence. Lancet Oncol. 2019;20(5):e253-e61.
13. Zarella MD, Bowman D, Aeffner F, Farahani N, Xthona A, Absar SF, et al. A Practical Guide to Whole Slide Imaging: A White Paper From the Digital Pathology Association. Arch Pathol Lab Med. 2019;143(2):222-34.

14. Campanella G, Hanna MG, Geneslaw L, Miraflor A, Werneck Krauss Silva V, Busam KJ, et al. Clinical-grade computational pathology using weakly supervised deep learning on whole slide images. Nat Med. 2019;25(8):1301-9.
15. Bera K, Schalper KA, Rimm DL, Velcheti V, Madabhushi A. Artificial intelligence in digital pathology - new tools for diagnosis and precision oncology. Nat Rev Clin Oncol. 2019;16(11):703-15.
16. Cheng N, Ren Y, Zhou J, Zhang Y, Wang D, Zhang X, et al. Deep Learning-Based Classification of Hepatocellular Nodular Lesions on Whole-Slide Histopathologic Images. Gastroenterology. 2022;162(7):1948-61 e7.
17. Serag A, Ion-Margineanu A, Qureshi H, McMillan R, Saint Martin MJ, Diamond J, et al. Translational AI and Deep Learning in Diagnostic Pathology. Front Med (Lausanne). 2019;6:185.
18. Tabibu S, Vinod PK, Jawahar CV. Pan-Renal Cell Carcinoma classification and survival prediction from histopathology images using deep learning. Sci Rep. 2019;9(1):10509.
19. Saltz J, Gupta R, Hou L, Kurc T, Singh P, Nguyen V, et al. Spatial Organization and Molecular Correlation of Tumor-Infiltrating Lymphocytes Using Deep Learning on Pathology Images. Cell Rep. 2018;23(1):181-93 e7.
20. Mobadersany P, Yousefi S, Amgad M, Gutman DA, Barnholtz-Sloan JS, Velazquez Vega JE, et al. Predicting cancer outcomes from histology and genomics using convolutional networks. Proc Natl Acad Sci U S A. 2018;115(13):E2970-E9.
21. Liao H, Xiong T, Peng J, Xu L, Liao M, Zhang Z, et al. Classification and Prognosis Prediction from Histopathological Images of Hepatocellular Carcinoma by a Fully Automated Pipeline Based on Machine Learning. Ann Surg Oncol. 2020;27(7):2359-69.
22. Abels E, Pantanowitz L, Aeffner F, Zarella MD, van der Laak J, Bui MM, et al. Computational pathology definitions, best practices, and recommendations for regulatory guidance: a white paper from the Digital Pathology Association. J Pathol. 2019;249(3):286-94.
23. Nam D, Chapiro J, Paradis V, Seraphin TP, Kather JN. Artificial intelligence in liver diseases: Improving diagnostics, prognostics and response prediction. JHEP Rep. 2022;4(4):100443.
24. Fridman WH, Pages F, Sautes-Fridman C, Galon J. The immune contexture in human tumours: impact on clinical outcome. Nat Rev Cancer. 2012;12(4):298-306.
25. Xu X, Tan Y, Qian Y, Xue W, Wang Y, Du J, et al. Clinicopathologic and prognostic significance of tumor-infiltrating CD8 T cells in patients with

hepatocellular carcinoma: A meta-analysis. Medicine (Baltimore). 2019;98(2):e13923.
26. Gabrielson A, Wu Y, Wang H, Jiang J, Kallakury B, Gatalica Z, et al. Intratumoral CD3 and CD8 T-cell Densities Associated with Relapse-Free Survival in HCC. Cancer Immunol Res. 2016;4(5):419-30.
27. Stulpinas R, Zilenaite-Petrulaitiene D, Rasmusson A, Gulla A, Grigonyte A, Strupas K, et al. Prognostic Value of CD8Lymphocytes in Hepatocellular Carcinoma and Perineoplastic Parenchyma Assessed by Interface Density Profiles in Liver Resection Samples. Cancers. 2023;15(2).
28. Karsdal MA, Daniels SJ, Holm Nielsen S, Bager C, Rasmussen DGK, Loomba R, et al. Collagen biology and non-invasive biomarkers of liver fibrosis. Liver Int. 2020;40(4):736-50.
29. Renne SL, Sarcognato S, Sacchi D, Guido M, Roncalli M, Terracciano L, et al. Hepatocellular carcinoma: a clinical and pathological overview. Pathologica. 2021;113(3):203-17.
30. Taylor-Weiner A, Pokkalla H, Han L, Jia C, Huss R, Chung C, et al. A Machine Learning Approach Enables Quantitative Measurement of Liver Histology and Disease Monitoring in NASH. Hepatology. 2021;74(1):133-47.
31. Kather JN, Heij LR, Grabsch HI, Loeffler C, Echle A, Muti HS, et al. Pan-cancer image-based detection of clinically actionable genetic alterations. Nat Cancer. 2020;1(8):789-99.
32. Stulpinas R, Morkunas M, Rasmusson A, Drachneris J, Augulis R, Gulla A, et al. Improving HCC Prognostic Models after Liver Resection by AI-Extracted Tissue Fiber Framework Analytics. Cancers (Basel). 2023;16(1).
33. Rasmusson A, Zilenaite D, Nestarenkaite A, Augulis R, Laurinaviciene A, Ostapenko V, et al. Immunogradient Indicators for Antitumor Response Assessment by Automated Tumor-Stroma Interface Zone Detection. Am J Pathol. 2020;190(6):1309-22.
34. Birch CPD, Oom SP, Beecham JA. Rectangular and hexagonal grids used for observation, experiment and simulation in ecology. Ecol Model. 2007;206(3-4):347-59.
35. Budczies J, Klauschen F, Sinn BV, Győrffy B, Schmitt WD, Darb-Esfahani S, et al. Cutoff Finder: A Comprehensive and Straightforward Web Application Enabling Rapid Biomarker Cutoff Optimization. Plos One. 2012;7(12).
36. Stulpinas R, Zilenaite-Petrulaitiene D, Rasmusson A, Gulla A, Grigonyte A, Strupas K, et al. Prognostic Value of CD8 Lymphocytes in Hepatocellular Carcinoma and Perineoplastic Parenchyma Assessed by Interface Density Profiles in Liver Resection Samples. Cancers (Basel). 2023;15(2).

37. Stulpinas R, Jakiunaite I, Sidabraite A, Rasmusson A, Zilenaite-Petrulaitiene D, Strupas K, et al. Low CD8 Density Variation and R1 Surgical Margin as Independent Predictors of Early Post-Resection Recurrence in HCC Patients Meeting Milan Criteria. Curr Oncol. 2024;31(9):5344-53.
38. Morkunas M, Zilenaite D, Laurinaviciene A, Treigys P, Laurinavicius A. Tumor collagen framework from bright-field histology images predicts overall survival of breast carcinoma patients. Sci Rep-Uk. 2021;11(1).
39. Drachneris J, Morkunas M, Fabijonavicius M, Cekauskas A, Jankevicius F, Laurinavicius A. Prediction of Non-Muscle Invasive Papillary Urothelial Carcinoma Relapse from Hematoxylin-Eosin Images Using Deep Multiple Instance Learning in Patients Treated with Bacille Calmette-Guerin Immunotherapy. Biomedicines. 2024;12(2).
40. Wang X, Yang S, Zhang J, Wang M, Zhang J, Yang W, et al. Transformer-based unsupervised contrastive learning for histopathological image classification. Med Image Anal. 2022;81:102559.
41. Krijgsman D, van Leeuwen MB, van der Ven J, Almeida V, Vlutters R, Halter D, et al. Quantitative Whole Slide Assessment of Tumor-Infiltrating CD8-Positive Lymphocytes in ER-Positive Breast Cancer in Relation to Clinical Outcome. Ieee J Biomed Health. 2021;25(2):381-92.
42. Khanam A, Chua JV, Kottilil S. Immunopathology of Chronic Hepatitis B Infection: Role of Innate and Adaptive Immune Response in Disease Progression. Int J Mol Sci. 2021;22(11).
43. Gulla A, Stulpinas R, Grigonyte A, Zilenaite-Petrulaitiene D, Rasmusson A, Laurinavicius A, et al. Overall Survival Prediction by Tumor Microenvironment Lymphocyte Distribution in Hepatocellular Carcinoma After Liver Transplantation. J Surg Res. 2024;295:457-67.
44. Burt ADP, B. C.; Ferrell, L. D. MacSween's Pathology of the Liver: Churchill Livingstone; 2011.

CURRICULUM VITAE

Name and surname: Rokas Stulpinas

Place of birth: Vilnius, Lithuania

Education:

- 2020 – 2024: Doctorate studies, Vilnius University
  HCC Prognostic Modeling Using AI-based Tissue Analysis
- 2020 – 2021: Executive MBA thesis, ISM University of Management and Economics
  Factors Influencing Physicians' Migration Intentions at the National Center of Pathology
- 2011 – 2015: Residency of Pathology, Vilnius University
  Completed training in pathology
- 2008 – 2010: Executive MBA studies, ISM University of Management and Economics
  Completed advanced management courses in Project Management, Human Resource Management, Marketing Strategy and Management, and Business Process Management
- 2000 – 2007: Master's degree in medicine and primary residency (MD), Vilnius University
  Medical Education Encompassing Theoretical Coursework, Clinical Rotations, and Research Activities
- 1988 – 2000: Secondary Education, Vilnius Antakalnio Secondary School
  Secondary education with honors

Professional Experience

- 2017 – currently: Pathologist, Gastrointestinal Pathology Supervisor at the National Center of Pathology, Affiliate of Vilnius University Hospital Santaros Klinikos
  Providing diagnostic services with focus on gastrointestinal pathology and participating in research and training activities
- 2015 – currently: Chief Pathologist at HILA Private Hospital, Vilnius, Lithuania

Overseeing all pathology services and diagnostic operations while implementing quality assurance protocols for accurate and timely diagnosis

- 2015 – 1017: Pathologist at Vilnius City Clinical Hospital
  Specialized in gastrointestinal, urological, and gynecological pathology diagnostics while collaborating with multidisciplinary clinical teams

- 2011 – 2015: Resident of pathology at National Center of Pathology, Affiliate of Vilnius University Hospital Santaros Klinikos
  Completed training in pathology while participating in research projects and regular teaching conferences

- 2006 – 2010: Assistant manager at Hematology, Oncology and Transfusion Medicine Center, Vilnius University Hospital Santaros Klinikos
  Managed clinical trials from inception to publication, coordinating data collection and analysis while preparing publications and presentations

- 2002 – 2004: Project manager at *Vaistų Žinios* publishing house
  Coordinated the development and publication of specialized medical literature, ensuring high-quality content and timely delivery

Complete publication list

1. Stulpinas R, Jakiunaite I, Sidabraite A, Rasmusson A, Zilenaite-Petrulaitiene D, Strupas K, Laurinavicius A, Gulla A. Low CD8+ Density Variation and R1 Surgical Margin as Independent Predictors of Early Post-Resection Recurrence in HCC Patients Meeting Milan Criteria. Curr Oncol. 2024;31:5344-5353. doi:10.3390/curroncol31090394

2. Luksta M, Bausys A, Gendvilaite N, Bickaite K, Rackauskas R, Paskonis M, Luksaite-Lukste R, Ranceva A, Stulpinas R, Brasiuniene B, et al. Pressurized Intraperitoneal Aerosol Chemotherapy (PIPAC) for Gastric Cancer Peritoneal Metastases: Results from the Lithuanian PIPAC Program. Cancers. 2024;16(17):2992. doi:10.3390/cancers16172992

3. Stulpinas R, Morkunas M, Rasmusson A, Drachneris J, Augulis R, Gulla A, Strupas K, Laurinavicius A. Improving HCC Prognostic

Models after Liver Resection by AI-Extracted Tissue Fiber Framework Analytics. Cancers. 2024;16(1):106. doi:10.3390/cancers16010106

4. Rackauskas R, Luksaite-Lukste R, Stulpinas R, Bausys A, Paskonis M, Kvietkauskas M, Sokolovas V, Laurinavicius A, Strupas K. The Impact of Chemotherapy and Transforming Growth Factor-β1 in Liver Regeneration after Hepatectomy among Colorectal Cancer Patients. J Pers Med. 2024;14(2):144. doi:10.3390/jpm14020144

5. Gulla A, Stulpinas R, Grigonyte A, Zilenaite-Petrulaitiene D, Rasmusson A, Laurinavicius A, Strupas K. Overall Survival Prediction by Tumor Microenvironment Lymphocyte Distribution in Hepatocellular Carcinoma After Liver Transplantation. J Surg Res. 2024;295:457-467. doi:10.1016/j.jss.2023.10.011

6. Stulpinas R, Zilenaite-Petrulaitiene D, Rasmusson A, Gulla A, Grigonyte A, Strupas K, Laurinavicius A. Prognostic Value of CD8+ Lymphocytes in Hepatocellular Carcinoma and Perineoplastic Parenchyma Assessed by Interface Density Profiles in Liver Resection Samples. Cancers. 2023;15(2):366. doi:10.3390/cancers15020366

7. Silinskaite U, Gaveliene E, Stulpinas R, Janavicius R, Poskus T. A Novel Mutation of MSH2 Gene in a Patient with Lynch Syndrome Presenting with Thirteen Metachronous Malignancies. J Clin Med. 2023;12(17):5502. doi:10.3390/jcm12175502

8. Luksta M, Bausys A, Bickaite K, et al. Pressurized intraperitoneal aerosol chemotherapy (PIPAC) with cisplatin and doxorubicin in combination with FOLFOX chemotherapy as a first-line treatment for gastric cancer patients with peritoneal metastases: single-arm phase II study. BMC Cancer. 2023;23:1032. doi:10.1186/s12885-023-11549-z

9. Marcinkeviciute K, Jurkeviciute D, Stulpinas R, Stratilatovas E, Dulskas A. Pancreatic Mucinous Cystic Neoplasm with Associated Invasive Carcinoma: A Case Report and Literature Review. Lietuvos Chirurgija. 2023;22(2):99-105. doi:10.15388/LietChirur.2023.22.84

10. Stulpinas R, Zilenaite-Petrulaitiene D, Rasmusson A, Grigonyte A, Kielaite-Gulla A, Strupas K, Laurinavicius A. Computational tissue immune response indicators to predict overall survival in hepatocellular carcinoma. Eur J Surg Oncol. 2023;49(2):e164. doi:10.1016/j.ejso.2022.11.454

11. Cibulskaite G, Stulpinas R, Poskus E, Tulyte S, Mickys U. Colorectal Neoplasm with Predominant Neuroendocrine Immunophenotype: Where does Adenocarcinoma End? Lietuvos Chirurgija. 2022;21(1):56-4. doi:10.15388/lietuvos-chirurgija/article/27421

12. Ranceva A, Stulpinas R, Norvilas R, Mickys U. Hepatoid adenocarcinoma of the stomach with PIK3Ca mutation during pregnancy: A case report with molecular profile. Oxf Med Case Reports. 2021;2021(9):omab078. doi:10.1093/omcr/omab078

13. Dulskas A, Poskus T, Kildusiene I, Patasius A, Stulpinas R, Laurinavicius A, et al. National Colorectal Cancer Screening Program in Lithuania: Description of the 5-Year Performance on Population Level. Cancers. 2021;13(5):1129. doi:10.3390/cancers13051129

14. Anglickis M, Platkevicius G, Stulpinas R, Mikliciute L, Anglickiene G, Keina V, Starolis E, Gradauskas A. Giant prostatic hyperplasia and its causes. Acta Med Litu. 2019;26(4):237-243. doi:10.6001/actamedica.v26i4.4209

15. Anglickis M, Stulpinas R, Anglickiene G, Gabrilevicius J, Jaskevicius A. Case Report of Misleading Features of a Rare Sertoli Cell Testicular Tumor. Medicina (Kaunas). 2019;55(5):170. doi:10.3390/medicina55050170

16. Jonaityte B, Kibarskyte R, Danila E, Miglinas M, Seinin D, Stulpinas R, et al. Fatal pulmonary complication during induction therapy in a patient with ANCA-associated vasculitis. Acta Med Litu. 2016;23(2):142-146. doi:10.6001/actamedica.v23i2.3331

17. Baltruskeviciene E, Mickys U, Zvirblis T, Stulpinas R, Pipiriene Zelviene T, Aleknavicius E. Significance of KRAS, NRAS, BRAF and PIK3CA mutations in metastatic colorectal cancer patients receiving Bevacizumab: a single institution experience. Acta Med Litu. 2016;23(1):24-34. doi:10.6001/actamedica.v23i1.3267

18. Garnelyte A, Samalavicius NE, Stulpinas R, Baltruskeviciene E, Seinin D, Mickys U. Gastric glomus tumor with prominent polytypic plasmacytosis: case report and review of literature. Case Rep Clin Pathol. 2014;1(2):84-89. doi:10.5430/crcp.v1n2p84

19. Samalavicius NE, Stulpinas R, Gasilionis V, Baltruskeviciene E, Aleknavicius E, Mickys U. Rhabdoid carcinoma of the rectum. Ann Coloproctol. 2013;29(6):252-255. doi:10.3393/ac.2013.29.6.252

20. Griskevicius L, Stulpinas R, Vengalyte I, et al. Favorable outcome with chemo-immunotherapy in Burkitt lymphoma and leukemia. Leuk Res. 2009;33(4):587-588. doi:10.1016/j.leukres.2008.07.024

21. Kviliute R, Paskevicius A, Gulbinovic J, Stulpinas R, Griskevicius L. Nonfatal Trichoderma citrinoviride pneumonia in an acute myeloid leukemia patient. Ann Hematol. 2008;87(6):501-502. doi:10.1007/s00277-007-0427-y

LIST OF DOCTORAL PUBLICATIONS AND PRESENTATIONS

Publications

1. **Stulpinas R**, Zilenaite-Petrulaitiene D, Rasmusson A, Gulla A, Grigonyte A, Strupas K, Laurinavicius A. Prognostic Value of CD8 Lymphocytes in Hepatocellular Carcinoma and Perineoplastic Parenchyma Assessed by Interface Density Profiles in Liver Resection Samples. Cancers (Basel). 2023 Jan 5;15(2):366. doi: 10.3390/cancers15020366. PMID: 36672317; PMCID: PMC9857181. https://pubmed.ncbi.nlm.nih.gov/36672317/

2. **Stulpinas R**, Morkunas M, Rasmusson A, Drachneris J, Augulis R, Gulla A, Strupas K, Laurinavicius A. Improving HCC Prognostic Models after Liver Resection by AI-Extracted Tissue Fiber Framework Analytics. Cancers (Basel). 2023 Dec 24;16(1):106. doi: 10.3390/cancers16010106. PMID: 38201532; PMCID: PMC10778366. https://pubmed.ncbi.nlm.nih.gov/38201532/

3. Gulla A, **Stulpinas R**, Grigonyte A, Zilenaite-Petrulaitiene D, Rasmusson A, Laurinavicius A, Strupas K. Overall Survival Prediction by Tumor Microenvironment Lymphocyte Distribution in Hepatocellular Carcinoma After Liver Transplantation. J Surg Res. 2024 Mar;295:457-467. doi: 10.1016/j.jss.2023.10.011. Epub 2023 Dec 8. PMID: 38070260. https://pubmed.ncbi.nlm.nih.gov/38070260/

4. **Stulpinas R**, Jakiunaite I, Sidabraite A, Rasmusson A, Zilenaite-Petrulaitiene D, Strupas K, Laurinavicius A, Gulla A. Low CD8 Density Variation and R1 Surgical Margin as Independent Predictors of Early Post-Resection Recurrence in HCC Patients Meeting Milan Criteria. Curr Oncol. 2024 Sep 10;31(9):5344-5353. doi: 10.3390/curroncol31090394. PMID: 39330022; PMCID: PMC11431076. https://pubmed.ncbi.nlm.nih.gov/39330022/

Presentations

1. EAA - ISGA - ICEM (2022.08.24-27 Vilnius, Lithuania). Oral presentation “Automated Tumor-Host Interface Zone Detection and Immune Response Assessment In HCC”, awarded “Best PhD student e-poster presentation”.

2. ESSO41 (2022.10.19-21 Bordeaux, France). Poster presentation „Computational Tissue Immune Response Indicators to Predict Overall Survival in Hepatocellular Carcinoma“. Published in European journal of surgical oncology: ESSO 41 Abstracts 2022. Oxford : Elsevier Science Ltd. ISSN 0748-7983. 2023, vol. 49, iss. 2, p. e164. DOI: 10.1016/j.ejso.2022.11.454.

3. 18th Annual Academic Surgical Congress (2023.02.7-9 Houston, USA). Oral presentation (co-author dr. Aistė Gulla) „The Value of CD8 and Feasibility of Liver Transplantation for Hepatocellular Carcinoma“.

4. New Technologies in Surgery | International Conference (2023.11.10 Vilnius, Lithuania). Oral presentation „AI-assisted microarchitecture analysis in hepatocellular carcinoma and peritumoral liver“.

5. The Baltic Chapter-E-AHPBA/IHPBA Annual Meeting „Approaching Cancer in Liver: from cell Biology to Personalized Treatment“ (2024.04.26-27). Oral presentation „Where biology meets AI in HCC“.

6. European Congress on Digital Pathology ECDP2024 (2024.06.5-8 Vilnius, Lithuania). Oral presentation „Predicting Survival of HCC Patients after Liver Resection by AI-Driven Fiberomics and Hexagonal Grid Analytics“.

7. Evolutionary Medicine: How evolutionary thinking can contribute to the medical and health sciences (2024.06.18-21, Vilnius, Lithuania). Oral presentation „Images To Insights: AI-Driven Prognostic Modeling in HCC Using CD8 TILs and Fiber Morphometrics“.

1st publication / 1 publikacija

Rokas Stulpinas, Dovile Zilenaite-Petrulaitiene, Allan Rasmusson, Aiste Gulla, Agne Grigonyte, Kestutis Strupas, Arvydas Laurinavicius

Prognostic Value of CD8 Lymphocytes in Hepatocellular Carcinoma and Perineoplastic Parenchyma Assessed by Interface Density Profiles in Liver Resection Samples

Cancers (Basel). 2023 Jan 5;15(2):366.

doi: 10.3390/cancers15020366. PMID: 36672317; PMCID: PMC9857181

https://pubmed.ncbi.nlm.nih.gov/36672317/

cancers

MDPI

Article

Prognostic Value of CD8+ Lymphocytes in Hepatocellular Carcinoma and Perineoplastic Parenchyma Assessed by Interface Density Profiles in Liver Resection Samples

Rokas Stulpinas [1,2,*], Dovile Zilenaite-Petrulaitiene [1,2], Allan Rasmusson [1,2], Aiste Gulla [3,4], Agne Grigonyte [5], Kestutis Strupas [3] and Arvydas Laurinavicius [1,2]

[1] Faculty of Medicine, Institute of Biomedical Sciences, Department of Pathology, Forensic Medicine and Pharmacology, Vilnius University, 03101 Vilnius, Lithuania
[2] National Center of Pathology, Affiliate of Vilnius University Hospital Santaros Clinics, 08406 Vilnius, Lithuania
[3] Faculty of Medicine, Institute of Clinical Medicine, Vilnius University, 03101 Vilnius, Lithuania
[4] Department of Surgery, Memorial Sloan Kettering Cancer Center, New York, NY 10065, USA
[5] Faculty of Medicine, Vilnius University, 03101 Vilnius, Lithuania
* Correspondence: rokas.stulpinas@vpc.lt

Simple Summary: In this study, we present the overall survival and recurrence-free survival models based on CD8 profiles in hepatocellular carcinoma (HCC) and peritumoral liver tissue, including other clinical and pathological variables. We extracted CD8 distribution profiles from the digitized immunohistochemistry slides containing the HCC-stroma interface and the perineoplastic liver parenchyma-stroma interface using the computational method of interface zone immunogradient. The prognostic value of the CD8+ cell spatial distribution indicators from both interfaces as well as clinical, laboratory, and pathology data was assessed. A three-tier prognostic scoring system is proposed to predict overall survival in patients with HCC.

Abstract: Hepatocellular carcinoma (HCC) often emerges in the setting of long-standing inflammatory liver disease. CD8 lymphocytes are involved in both the antitumoral response and hepatocyte damage in the remaining parenchyma. We investigated the dual role of CD8 lymphocytes by assessing density profiles at the interfaces of both HCC and perineoplastic liver parenchyma with surrounding stroma in whole-slide immunohistochemistry images of surgical resection samples. We applied a hexagonal grid-based digital image analysis method to sample the interface zones and compute the CD8 density profiles within them. The prognostic value of the indicators was explored in the context of clinicopathological, peripheral blood testing, and surgery data. Independent predictors of worse OS were a low standard deviation of CD8+ density along the tumor edge, high mean CD8+ density within the epithelial aspect of the perineoplastic liver-stroma interface, longer duration of surgery, a higher level of aspartate transaminase (AST), and a higher basophil count in the peripheral blood. A combined score, derived from these five independent predictors, enabled risk stratification of the patients into three prognostic categories with a 5-year OS probability of 76%, 40%, and 8%. Independent predictors of longer RFS were stage pT1, shorter duration of surgery, larger tumor size, wider tumor-free margin, and higher mean CD8+ density in the epithelial aspect of the tumor-stroma interface. We conclude that (1) our computational models reveal independent and opposite prognostic impacts of CD8+ cell densities at the interfaces of the malignant and non-malignant epithelium interfaces with the surrounding stroma; and (2) together with pathology, surgery, and laboratory data, comprehensive prognostic models can be constructed to predict patient outcomes after liver resection due to HCC.

Citation: Stulpinas, R.; Zilenaite-Petrulaitiene, D.; Rasmusson, A.; Gulla, A.; Grigonyte, A.; Strupas, K.; Laurinavicius, A. Prognostic Value of CD8+ Lymphocytes in Hepatocellular Carcinoma and Perineoplastic Parenchyma Assessed by Interface Density Profiles in Liver Resection Samples. *Cancers* **2023**, *15*, 366. https://doi.org/10.3390/cancers15020366

Academic Editors: Elisabetta Ferretti and Marco Tafani

Received: 24 November 2022
Revised: 28 December 2022
Accepted: 4 January 2023
Published: 5 January 2023

Keywords: CD8; hepatocellular carcinoma; immune response; tumor-infiltrating lymphocytes; liver-infiltrating lymphocytes; digital image analysis; immunohistochemistry; computational pathology

1. Introduction

Primary liver cancer is the third most common cause of cancer-related deaths in the world, with hepatocellular carcinoma (HCC) comprising up to 85% of cases [1]. Although general risk factors for HCC development are well known and surveillance guidelines have been established, the diagnosis of an individual HCC patient is complicated by both the asymptomatic nature of early-stage HCC [2] and the fact that 90% of HCC cases develop in the background of cirrhosis caused by chronic inflammatory liver disease [3]. This persistent inflammatory environment is mostly due to viral infections (HBV or HCV), autoimmune hepatitis, nonalcoholic fatty liver disease, excessive alcohol consumption, or other toxins [3,4]. It has been suggested that a persistent and inefficient immune system response is the cause of both inflammatory liver damage [5] and carcinogenesis [4,5]. In practice, cirrhosis obscures the HCC to the point where therapeutic options become limited [6].

Poor overall survival (OS) and high recurrence rates for patients with HCC emphasize the need for reliable prognostic models to avoid over- or undertreatment [7,8]. Furthermore, the underlying irreversible damage to the liver parenchyma limits established cancer-directed therapies and clinical trials because conventional chemo- and radiotherapy modes are either contraindicated or ineffective in cirrhotic patients [6]. Consequently, the standard potentially curative treatments for HCC are liver transplantation, surgical resection, and local ablative therapy [9]. However, HCC reoccurs in more than 50% of patients in 3 years [10] and in up to 70%, 5 years after surgical resection [11]. New treatment opportunities such as immune checkpoint inhibitors, inhibitory cytokine blockade, oncolytic viruses, adaptive cell therapies, and immunotherapeutic vaccines [12] have emerged; however, the effect of HCC immunotherapy is rather patient-specific, further raising the importance of robust biomarkers of HCC progression.

Assays to estimate the risk of developing and to predict the outcomes of HCC are actively sought. Serum alpha-fetoprotein (AFP) has been used as a biomarker of HCC for over half a century but remains controversial, as many experts consider it nonspecific [13]. Furthermore, most other biomarkers lack informative power if used individually as outcome predictors. Stratification systems based on multiple features, such as the Okuda, Barcelona Clinic Liver Cancer (BCLC), the Italian (CLIP), and French classifications, have been in use for decades [14]. These scoring schemes consider both the tumor properties and the remaining liver function indicators for a comprehensive assessment of liver disease. For example, the BALAD model measures bilirubin, albumin, two forms of alpha-fetoprotein (AFP-L3 and total AFP), and des-γ-carboxyprothrombin from a single blood serum sample [15]. Albumin and bilirubin provide estimates of the remaining liver function, while the combination of other indicators represents the stage and progression of the tumor. The combined results allowed the prediction of HCC patient survival with a hazard ratio of 1.43 per increase of 1 BALAD score [16]. In 2014, a diagnostic iteration of the latter model, named GALAD [13], replaced bilirubin and albumin with the patient's age and sex to predict the presence of HCC; the model score appears to be proportional to the tumor cell mass and performs substantially better than any individual biomarker. Several years later, Sposito et al. proposed a simple scoring scheme based on routine clinical data for a robust stratification of patients with HCC eligible for resection; the model included an end-stage liver disease (MELD) score, HCV infection, the number of tumor lesions, their maximum size, and signs of portal invasion [10].

A novel set of biomarkers for the prognosis of HCC is also gaining the spotlight in the context of advances in immunotherapy. These indicators focus primarily on the distribution and populations of immune cells within the tumor microenvironment (TME) and the non-tumor microenvironment (NTME) [7,17]. However, the assessment of the immune response in liver tissue is complicated by a 'dual' pathology of HCC: a beneficial antitumoral response is conveyed by cytotoxic CD8+ T cells [18], which may have an opposite detrimental effect on the remaining functional liver parenchyma. In particular, in patients with HCC with known HBV or HCV infection, hepatocyte injury is caused by an immune response (involving CD8+ lymphocytes) rather than direct viral damage [4]. One can hypothesize that tumor-infiltrating lymphocytes (TILs) in HCC and non-tumor infiltrating lymphocytes (NILs) in the surrounding liver parenchyma may have independent effects on patient outcomes, hence the precise spatial distribution analysis of immune cells is required.

The role of TILs/NILs in HCC has long been under investigation (mainly based on immunohistochemistry studies); however, their significance in disease progression remains controversial. In 2004, Ikeguchi et al. [19] reported a lower average density of manually counted CD8+ cells in HCC tissue compared to surrounding non-cancerous hepatic lobules. They detected neither a correlation between the individual sample densities of TILs and NILs nor any prognostic significance of CD8+ cell densities. Ramzan et al. demonstrated that high levels of TILs reflect inflammatory conditions and contribute to tumorigenesis and the recurrence of HCC [20]. Abdou et al. found no effect of TILs on patient survival or recurrence [21]. Other studies reported that high levels of TILs were associated with better OS and disease-free survival (DFS) [8,22,23]. In 2013, An et al. [24] published a study of CD4+ and CD8+ cell infiltrates in HCC and perineoplastic liver tissue microarrays with the semiquantitative visual assessment of hotspots. They found an increased number of CD8+ cells in smaller tumors (≤5 cm) and, independently, in the peritumoral liver parenchyma in cases with chronic hepatitis and cirrhosis; unfortunately, the patient outcomes were not assessed in this study. In their meta-analysis, Xu et al. [22] concluded that OS was significantly longer in cases with high CD8+ TIL densities at the edge of the tumor, while patients with low TIL density had a more advanced TNM stage and a larger tumor size; however, no significance of lymphocytes infiltrating peritumoral tissues was established. It was noted that the vast majority of the reviewed studies were conducted in Asia where HBV is still the most prevalent etiological factor; therefore, more evidence needs to be collected from non-Asian populations to assess the significance of TILs in other HCC subgroups [22].

The well-established digital immunohistochemistry-based method Immunoscore assessing the host anti-tumoral response quantifies two (CD3 and CD8) lymphocyte populations at both the invasive margin (IM) and at the core of the tumor (CT) [25,26]. The method was originally proposed to predict a recurrence of stage II/III colon cancer and was later applied to other types of solid cancer [27]. In particular, Gabrielson et al. [28] demonstrated that patients with a high density of CD3+ and CD8+ cells in one or both regions of interest (IM or CT) and their corresponding 'immunoscores' were associated with a lower rate of HCC recurrence and longer relapse-free survival (RFS). Sun et al. [8] argued that although Immunoscore was closely related to the outcome of patients with HCC, it was not an optimal prognostic biomarker, since they observed that CD8+ density in the center of the tumor has the highest prognostic impact for both DFS and OS by Cox multivariate regression analysis. Liu et al. [29] recently reported a comprehensive HCC immunohistochemical study of 14 immune cell subtypes in three representative images captured in the tumor (T) and peritumoral (P) regions to quantify immune cell densities using a computer-automated method. They developed and validated a nine-factor IHC classifier ($CD27_T$, $CD57_T$, $CD57_P$, $CD45RA_P$, $CD45RO_T$, $CD66b_T$, $CD68_P$, $CXCR5_P$, and $PD\text{-}1_T$) to predict recurrence in patients with early-stage HCC, but neither CD3 nor CD8 entered the final model. These findings on the significance of the spatial arrangement of immune cells in HCC warrant the study exploring the CD8+ distribution across the tumor-

stroma interface in both malignant and benign (peritumoral) regions of the resected liver tissue.

Many studies have shown the potential of digital image analysis (DIA) and computational feature extraction tools from pathology images [30,31]. Automated, data-driven, and operator-independent methods can extract subvisual features that represent tissue properties and can be integrated into predictive models along with clinical and pathological parameters [32–35]. In liver pathology, DIA has also been proven to be a useful tool in both neoplastic and non-neoplastic settings [36–38]. Liao et al. used an automated computational deep learning model to extract prognostic characteristics from HCC and surrounding normal tissue from publicly available hematoxylin-eosin (H&E) whole slide images (WSI) [39]. Although this provided quantitative pathology features that were used to successfully diagnose HCC and predict the clinical outcomes of patients, the study was limited by the lack of important clinical information and serum biomarkers in a large proportion of the patients, and by a semiquantitative method of lymphocyte infiltration analysis. Similarly, most research is focused on applying convolutional neural networks (CNNs) to automatically extract features in H&E-stained liver tissue samples [40], while efforts with regard to the IHC-based computational assessment of TILs and NILs are lacking.

In this study, we present the OS and RFS models based on CD8 profiles in the tumor and peritumoral liver tissue, including other variables. We extracted CD8 distribution profiles from the HCC-stroma interface and from the perineoplastic liver parenchyma-stroma interface using the computational method of interface zone immunogradient [41]. The prognostic value of the CD8+ cell spatial distribution indicators from both interfaces as well as clinical, laboratory, and pathology data was assessed. A three-tier prognostic scoring system is proposed to predict OS in patients with HCC.

2. Materials and Methods

2.1. Study Population

The retrospective cohort used in this study included 106 patients (24 females and 82 males) who underwent liver resection for HCC in Vilnius University Hospital Santaros Clinics (Vilnius, Lithuania) from 2007 to 2020; the resection samples were analyzed at the National Center of Pathology (Vilnius, Lithuania). Clinical, laboratory, and pathology data were retrospectively collected according to the approval of the Vilnius Regional Biomedical Research Ethics Committee (permit number 2021/6-1354-843), which waived the requirement of individual informed consent according to the International Ethical Guidelines for Health-related Research Involving Humans [42].

The median time of OS was 39 (range 1–152) months calculated from the date of the first pathologically proven diagnosis of HCC, and for RFS it was 25 (range 1–174) months to the date of the first documented statement of HCC relapse. A summary of patient and tumor characteristics is presented in Table 1, and the results of preoperative blood tests are listed in Table 2.

Table 1. Clinical, pathological, and follow-up characteristics of the patient cohort.

Characteristic	Value
Patients	106 (100%)
Age, years	
Mean (range)	65 (13–82)
Median	64
Gender	
Male	82 (77.4%)
Female	24 (22.6%)
OS time, months	

Mean (range)	46 (1–152)
Median	39
Deceased	63 (59.4%)
RFS time, months	
Mean (range)	41 (1–174)
Median	25
Recurrences	56 (52.8%)
HCC grade	
G1	8 (7.5%)
G2	79 (74.5%)
G3	19 (18.0%)
pT stage	
T1	38 (35.9%)
T2	60 (56.6%)
T3	7 (6.6%)
T4	1 (0.9%)
Resection margin	
R0	86 (81.1%)
R1	20 (18.9%)
Largest tumor dimension, mm	
Mean (range)	48 (8–190)
Median	40
Surgical margin in R0 resections, mm	
Mean (range)	3.1 (0.1–25.0)
Median	3.1
History of viral infection	
HBV	9 (8.5%)
HCV	53 (50.0%)
None or unknown	44 (41.5%)
Hospitalization time, days	
Mean (range)	16 (4–70)
Median	13
Duration of surgery, min	
Mean (range)	170 (70–350)
Median	160

Table 2. Summary of the results of the preoperative blood test.

Variable	Mean	Median	Min	Max	N	No Data
LEU, $\times 10^9$/L	6.00	5.65	1.99	15.35	91	15
LYM, $\times 10^9$/L	2.94	1.62	0.22	106.00	90	16
MON, $\times 10^9$/L	0.56	0.50	0.12	1.38	90	16
EOS, $\times 10^9$/L	0.17	0.10	0.00	1.47	90	16
BAS, $\times 10^9$/L	0.03	0.02	0.00	0.20	90	16
RBC, $\times 10^{12}$/L	4.43	4.32	3.15	6.42	90	16
Albumin, g/L	40.25	40.30	24.80	51.10	64	42
Creatinine, μmol/L	74.05	71.00	42.00	144.00	82	24
Total bilirubin, μmol/L	17.75	14.45	5.10	52.80	82	24
Alanine transaminase (ALT), U/L	69.07	53.00	11.00	249.00	89	17
Aspartate transaminase (AST), U/L	69.35	56.00	19.00	209.00	86	20
Alkaline phosphatase (ALP), U/L	117.29	100.00	34.00	690.00	75	31
Gamma-glutamyl transferase (GGT), U/L	135.40	80.00	16.00	817.00	80	26
Alpha-fetoprotein (AFP), kU/L	669.54	10.65	0.50	30,000.00	94	12

2.2. Immunohistochemistry

All available archived slides stained with hematoxylin and eosin were reviewed by a pathologist (RS) to select the most informative formalin-fixed paraffin-embedded (FFPE) block that contains both non-necrotic HCC tissue (N = 106) and the surrounding liver parenchyma if present (N = 100, 94.3%) (Figure 1A). The samples were cut to a thickness of 3 µm and mounted on positively charged slides and stained for CD8 antibody (Dako, clone C8/144B, dilution 1:100, Denmark) on a Roche Ventana BenchMark ULTRA automated stainer (Ventana Medical Systems, Oro Valley, AZ, USA), using the ultraView Universal DAB Detection kit (Ventana Medical Systems, Oro Valley, AZ, USA).

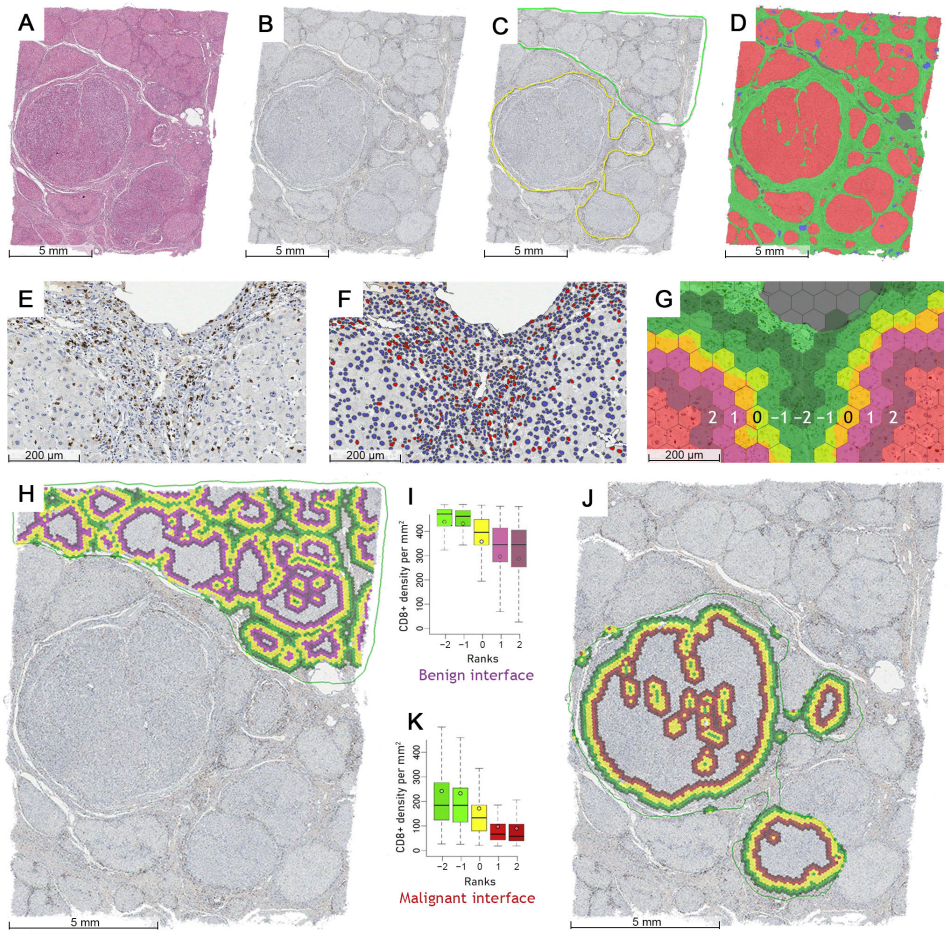

Figure 1. Study workflow (stroma interfaces with neoplastic (HCC) tissue and non-malignant liver parenchyma sampled to assess CD8+ cell density profiles): (**A**) low magnification view of the whole H&E stained tissue sample containing HCC nodules and the surrounding cirrhotic liver parenchyma; (**B**) a matching CD8 immunohistochemistry slide that was further used for analysis (see

panel E and Supplementary Figure S1A and S1B for higher magnification); (**C**) a sample of manually annotated HCC and non-neoplastic liver areas, avoiding ambiguous or artifact-containing zones; (**D**) HALO®AI epithelium versus stroma segmentation: both malignant and non-malignant hepatocytes—red, stroma—green, debris and artifacts—blue, background—gray; (**E**) magnified detection zone on a CD8 slide, positive cytotoxic T lymphocytes—brown cytoplasmic staining; (**F**) Multiplex IHC® nuclei segmentation masks, CD8 positive cells—red, CD8 negative cells—blue; (**G**) identification of the epithelial edge (yellow hexagons, rank 0), epithelial aspect (red hexagons, ranks 1–2) and stromal aspect (green hexagons, ranks −1 and −2) of the interface zone (ranks from −2 to 2) based on a hexagonal grid; (**H**) the benign (liver) interface zone, epithelial aspect (i.e., liver parenchyma)—purple, epithelial edge—yellow, stromal aspect—green; (**I**) an example boxplot showing a decrease of average CD8+ cell density per rank towards the epithelial aspect of the benign interface zone; (**J**) the malignant (HCC) interface zone, epithelial aspect (i.e., HCC)—red, epithelial edge—yellow, stromal aspect—green; (**K**) an example boxplot showing the decrease of average CD8+ cell density per rank towards the epithelial aspect of the malignant interface zone.

2.3. Digital Image Analysis and Indicator Extraction

All slides stained with H&E and CD8 were digitized (Figure 1A,B) at 20× magnification (0.5 μm per pixel) using an Aperio® AT2 DX scanner (Leica Aperio Technologies, Vista, CA, USA). A pathologist (RS) then manually annotated the largest available continuous malignant and non-malignant area on each slide while avoiding ambiguous or artifact-containing zones (Figure 1C), as the HALO® AI (Indica Labs, Albuquerque, NM, USA) classifier was not sufficient to fully discriminate between the well-differentiated HCC and reactive or dysplastic epithelium in some of the hematoxylin counterstained IHC slides. Thus, the AI system was trained to segment the tissue into hepatocytes (both malignant and non-malignant), stroma (fibrous tissue including the vasculature and bile ducts), and background/debris classes (Figure 1D), with subsequent segmentation (Figure 1E,F) of CD8+ cells via HALO® Multiplex IHC algorithm (Indica Labs, USA).

We further processed the DIA outputs using a computational method based on hexagonal grid tiling as described by Rasmusson et al. [41] to extract CD8 spatial distribution indicators for malignant (HCC-stroma) and non-malignant (liver parenchyma-stroma) interfaces. In this study, we used a grid with hexagons that have a side length of 65 μm (Figure 1G) and aggregated the number of CD8+ cells and the area of tissue classes in each hexagon. Based on the abrupt change in the proportion of tissue class area across the grid, the hexagons that make up the edge between the stroma and the epithelium (which is either composed of benign hepatocytes or neoplastic HCC cells, depending on the annotation used) are identified (Figure 1G, yellow hexagons). The tiles are then ranked so that the hexagons on the extracted edge have rank 0 (Figure 1G, rank 0), the epithelial hexagons (HCC or liver) are assigned a positive rank equal to their distance from the nearest edge (Figure 1G, ranks 1 and 2), while the hexagons on the stromal side are assigned a negative rank equal to their distance from the edge (Figure 1G, ranks −1 and −2). Multiple combinations of the width of the central edge (TE) and analysis depth (number of ranks on both sides of TE) can be generated to provide different density characteristics. A five-hexagon wide interface zone having a three-rank wide central edge (Figure 1I,K) was used for further calculations in this study.

Indicators were extracted from the interface zones of the non-neoplastic liver (Figure 1H) and HCC (Figure 1J) to reflect the density profiles of CD8+ cells in both tissue compartments: the mean density (m) and standard deviation (sd) of CD8+ cells were calculated for the epithelial (T), stroma (S) and edge (TE) compartments, and indicators (center of mass (CM) and immunodrop (ID)) representing the whole IZ were also calculated. CM can represent either an increase in CD8+ density (when calculated using means) toward the epithelial aspect or a higher CD8+ variance (when using standard deviation) along the IZ. The ID indicator is a ratio between the mean CD8+ density in ranks −1 (stromal aspect) and 1 (epithelial aspect) and reflects an abrupt decrease in CD8 density across the TE, hence the 'Immuno drop'.

2.4. Statistical Analysis and Modeling

Statistical analyses were performed using SAS software (version 9.4; SAS Institute Inc., Cary, NC, USA). A two-sided Welch t-test was applied for homogeneity of variance comparison. χ^2 and Fisher's exact test was used to examine the significant associations between categorical clinicopathological parameters. The nominal statistical significance level was set at $p < 0.05$. Since immune cell density distributions revealed left asymmetry, indicators were logarithm transformed for parametric statistics; however, for better readability, the prefix 'log' is not used in the text.

Cutoff Finder [43] was used to obtain an optimal cutoff value for each continuous indicator to test univariate OS predictions. The OS was estimated using the Kaplan–Meier method followed by log-rank testing to compare the statistical significance of the OS distributions. Multiple Cox regression was performed to further assess the independent prognostic value of the statistically significant biomarkers identified in the univariate analysis. Cox regression proportional hazards models were obtained using a stepwise likelihood ratio (LR) test to establish the independent prognostic significance of immunogradient indicators in the context of clinicopathological variables. Due to a limited cohort size, overfitting was minimized by leave-one-out cross-validation [44], and the most frequently selected variables were further tested in survival prediction models.

3. Results

3.1. Univariate Predictors of Overall Survival and Recurrence-Free Survival

Table 3 contains the statistically significant results of the univariate regression analysis with the hazard ratio (HR) and log-rank test of the impact of clinicopathological characteristics and CD8+ cell spatial distribution indicators on OS and RFS. The OS and RFS probability plots for variables that also provided an independent prognostic impact (see Section 3.2) are presented in Figures 2 and 3, respectively. Variables can be broadly grouped into three sets: conventional clinical and pathological parameters reported in daily practice, laboratory data obtained from blood analysis, and computed immunogradient indicators.

Table 3. Univariate predictors of overall survival and recurrence-free survival.

Variable	OS			RFS		
	HR	95% CI	*p*-Value	HR	95% CI	*p*-Value
Conventional clinicopathological parameters						
Stage pT1	0.42	0.24–0.73	0.0023	0.54	0.30–0.98	0.0425
Age	3.14	1.33–7.42	0.0061	2.09	0.95–3.02	0.0697
Intravascular invasion present	2.13	1.28–3.54	0.0034	1.40	0.82–2.37	0.2137
Max tumor size	1.54	0.88–2.70	0.1300	0.45	0.24–0.86	0.0124
Ishak's HAI score > 5	2.88	1.11–7.45	0.0292	1.96	0.86–4.45	0.1085
R1 resection	1.18	0.63–2.22	0.6073	3.52	1.95–6.38	<0.0001
Tumor-free margin width	0.79	0.43–1.46	0.4500	0.28	0.16–0.50	<0.0001
Blood loss during surgery	2.02	1.20–3.43	0.0074	0.45	0.14–1.43	0.1627
Duration of surgery	2.03	1.16–3.54	0.0112	1.87	1.07–3.29	0.0276
Duration of hospital stay	5.08	2.50–10.30	<0.0001	1.66	0.96–2.84	0.0647
Blood laboratory data						
Alanine transaminase (ALT)	4.29	1.33–7.74	<0.0001	2.92	1.05–8.10	0.0313
Aspartate transaminase (AST)	4.81	2.40–9.64	<0.0001	2.10	1.08–4.09	0.0263
Gamma-glutamyl transferase (GGT)	3.06	1.51–6.22	0.0012	1.69	0.79–3.62	0.1751
Alkaline phosphatase (ALP)	1.81	0.95–3.42	0.0660	3.69	1.14–11.94	0.0196
Total bilirubin	2.73	1.43–5.22	0.0015	1.65	0.93–2.91	0.0813
LEU count	2.50	1.11–5.63	0.0218	1.81	1.03–3.20	0.0376
NEU count	1.89	1.12–3.18	0.0145	2.27	1.29–4.01	0.0035

BAS count	3.67	1.86–7.23	0.0001	2.02	1.10–3.72	0.0206
Interface zone immunogradient indicators						
Malignant (HCC–stroma) interface *						
HCC_CM_m	0.49	0.26–0.95	0.0307	0.42	0.19–0.94	0.0291
HCC_m_T	0.34	0.18–0.64	0.0005	0.40	0.22–0.73	0.0021
HCC_m_TE	0.53	0.29–0.98	0.0397	0.55	0.32–0.93	0.0230
HCC_sd_T	0.60	0.37–1.00	0.0464	0.56	0.32–0.96	0.0328
HCC_sd_TE	0.39	0.24–0.65	0.0002	0.51	0.30–0.87	0.0113
Benign (liver–stroma) interface *						
Liver_CM_m	3.06	0.96–9.78	0.0475	1.73	0.62–4.78	0.2869
Liver_CM_sd	2.26	1.35–3.78	0.0016	0.38	0.12–1.21	0.0886
Liver_ID	0.57	0.34–0.96	0.0338	1.55	0.73–3.29	0.2486
Liver_m_T	3.65	1.54–8.67	0.0019	0.63	0.33–1.17	0.1374
Liver_sd_T	2.04	1.17–3.55	0.0104	0.71	0.42–1.22	0.2159

* Suffixes for immunogradient indicators (values are logarithm transformed for parametric statistics; for better readability, the prefix 'log' is not used): CM_m—the center of mass calculated from the mean CD8 density, CM_sd—center of mass calculated from the standard deviation of the CD8 density, m_T—mean CD8 density in the epithelial aspect of the interface zone, m_TE—mean CD8 density at the epithelial edge, sd_T—standard deviation of the CD8 density at the epithelial aspect of the interface zone, sd_TE—standard deviation of the CD8 density at the epithelial edge, ID—immunodrop.

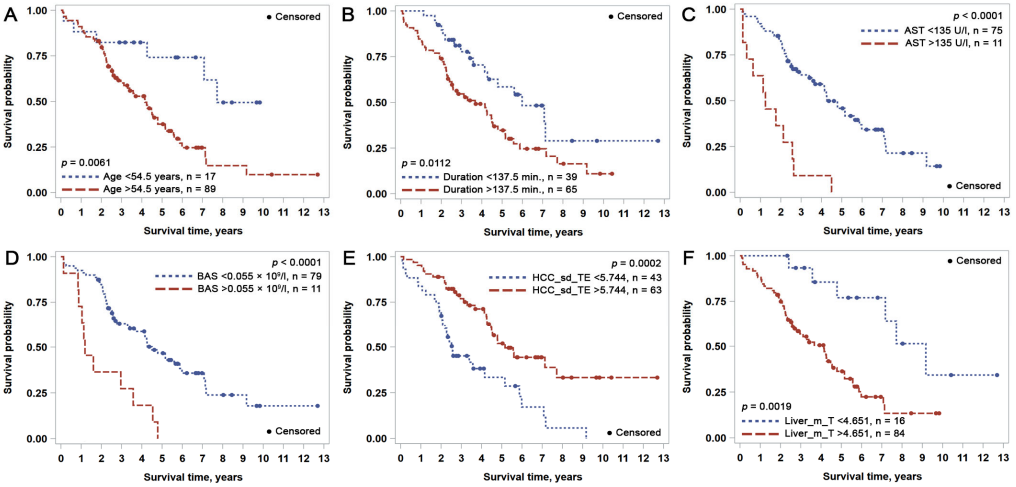

Figure 2. Kaplan-Meier overall survival (OS) plots for independent prognostic indicators identified by multiple Cox regression analysis: (**A**) patient age; (**B**) duration of surgery; (**C**) aspartate transaminase (AST); (**D**) peripheral blood basophil count; (**E**) standard deviation of CD8 density at the tumor edge (HCC_sd_TE); (**F**) mean CD8+ density within the epithelial aspect of the perineoplastic liver-stroma interface (Liver_m_T).

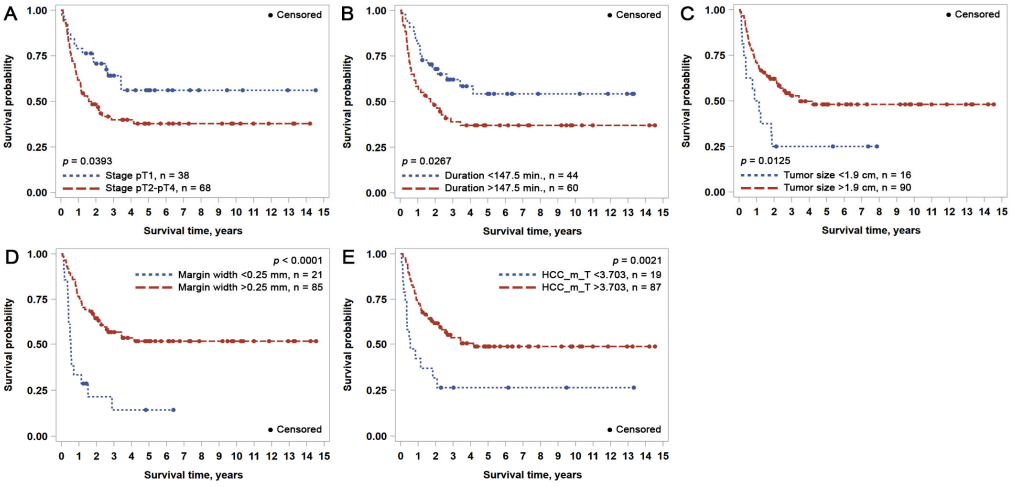

Figure 3. Kaplan-Meier recurrence-free survival (RFS) plots for independent prognostic indicators identified by multiple Cox regression analysis: (**A**) pT tumor stage; (**B**) duration of surgery; (**C**) tumor size; (**D**) tumor-free resection margin width; (**E**) mean CD8+ density in the epithelial aspect of tumor-stroma interface.

The statistically significant univariate predictors of worse OS were patient age > 54.5 years, stage pT2-pT4 (as opposed to pT1), any type of intravascular invasion, Ishak (modified Knodell) hepatitis activity index score > 5, >450 mL blood loss during liver surgery, longer (>137.5 min) duration of surgery, and longer (>30.5 days) hospital stay after surgery. Markedly elevated liver enzymes (ALT and AST > 135 U/L, GGT > 55 U/L), total bilirubin > 28.3 μmol/L and higher values of blood count variables (LEU > 8.89, NEU > 3.28, BAS > 0.055 × 10^9/L) also had a negative impact on OS. Interface zone immunogradient indicators from both the malignant (HCC_CM_m, HCC_m_T, HCC_m_TE, HCC_sd_T, HCC_sd_TE—see Table 3) and non-malignant (Liver_CM_m, Liver_CM_sd, Liver_ID, Liver_m_T, Liver_sd_T—see Table 3) compartments demonstrated either a positive or negative effect on OS.

Statistically significant univariate predictors of shorter RFS were the advanced stage (pT2–pT4), longer (>147.5 min) duration of surgery, either R1 resection or a tumor-free margin < 0.25 mm, and, paradoxically, a smaller tumor size (<1.9 cm). Higher levels of liver enzymes (ALT > 22.5 U/L, AST > 36.5 U/L, ALP > 69 U/L), blood count variables (LEU > 6.585, NEU > 3.595, BAS > 0.0365 × 10^9/L) and immunogradient indicators of the malignant compartment were also associated with a shorter RFS time in univariate analysis. None of the immunogradient indicators from non-malignant liver parenchyma was statistically significant for RFS.

3.2. Independent Predictors of Overall Survival and Recurrence-Free Survival

Independent prognostic features were explored using Cox regression models for OS and RFS using different sets of variables, starting from standard clinical and pathology data, and then supplementing them with laboratory and interface zone CD8+ cell profile data (Table 4).

Table 4. Independent predictors of OS and RFS based on multivariate Cox regression.

Variable	HR	95% CI	*p*-Value	χ^2
OS Model 1: demographic and pathology data. LR: 22.30, $p < 0.0001$, N = 106				
Age > 54.5 years	3.93	1.59–9.69	0.0030	8.8142
Stage pT1 (versus T2–T4)	0.35	0.20–0.64	0.0007	11.6134
OS Model 2: demographic, pathology, and surgery data. LR: 29.60, $p < 0.0001$, N = 101				
Age > 54.5 years	4.46	1.76–11.33	0.0017	9.9012
Stage pT1 (versus T2–T4)	0.37	0.20–0.68	0.0013	10.2742
Blood loss during surgery > 450 mL	2.05	1.20–3.50	0.0090	6.8239
OS Model 3: demographic, pathology, surgery, and laboratory data. LR: 46.18, $p < 0.0001$, N = 81				
Age > 54.5 years	4.20	1.52–11.57	0.0055	7.7057
Duration of surgery > 137.5 min	2.61	1.42–4.81	0.0021	9.4252
Intravascular invasion present	3.10	1.71–5.61	0.0002	14.0066
Aspartate transaminase (AST) > 135 U/L	4.59	2.20–9.57	<0.0001	16.5728
Blood basophil (BAS) count > 0.055 × 10^9/L	6.03	2.62–13.91	<0.0001	17.7860
OS Model 4: demographic, pathology, surgery, laboratory, and HCC (malignant) interface zone data. LR: 61.47, $p < 0.0001$, N = 81				
Age > 54.5 years	3.35	1.23–9.10	0.0177	5.6270
Duration of surgery > 137.5 min	2.07	1.09–3.92	0.0261	4.9488
Intravascular invasion present	3.00	1.65–5.43	0.0003	13.1234
Aspartate transaminase (AST) > 135 U/L	5.33	2.51–11.30	<0.0001	18.9716
Blood basophil (BAS) count > 0.055 × 10^9/L	6.91	2.99–15.99	<0.0001	20.3752
HCC_sd_TE * > 5.744	0.41	0.23–0.73	0.0026	9.0769
OS Model 5: demographic, pathology, surgery, laboratory parameters, and data from both interface zones. LR: 54.61, $p < 0.0001$, N = 76				
Duration of surgery > 137.5 min	2.64	1.41–4.95	0.0023	9.2615
Aspartate transaminase (AST) > 135 U/L	4.50	2.01–10.11	0.0003	25.0296
Blood basophil (BAS) count > 0.055 × 10^9/L	8.67	3.72–20.21	<0.0001	13.2883
HCC_sd_TE * > 5.744	0.33	0.18–0.59	0.0002	13.5590
Liver_m_T * > 4.651	4.81	1.73–13.28	0.0024	9.1963
RFS Model 6: demographic, pathology, and surgery data LR: 32.61, $p < 0.0001$, N = 104				
Stage pT1 (versus T2–T4)	0.40	0.20–0.82	0.0119	6.3248
Duration of surgery > 147.5 min	1.99	1.10–3.58	0.0224	5.2120
Max tumor size > 1.9 cm	0.20	0.09–0.44	<0.0001	15.6909
Tumor-free margin width > 0.25 mm	0.33	0.18–0.60	0.0003	12.8879
RFS Model 7: from demographic, pathology, surgery, and HCC (malignant) interface zone. LR: 40.50, $p < 0.0001$, N = 104				
Stage pT1 (versus T2–T4)	0.41	0.21–0.82	0.0108	6.4998
Duration of surgery > 147.5 min	2.07	1.13–3.80	0.0184	5.5614
Max tumor size > 1.9 cm	0.21	0.10–0.47	0.0001	14.7466
Tumor-free margin width > 0.25 mm	0.31	0.17–0.58	0.0002	13.5868
HCC_m_T * > 3.703	0.38	0.20–0.71	0.0024	9.2482

* Suffixes for immunogradient indicators (values are logarithm transformed for parametric statistics; for better readability, the prefix 'log' is not used): sd_TE—standard deviation of CD8 density at the epithelial edge, m_T—mean CD8 density at the epithelial aspect of IZ.

Although Model 1 (LR: 22.3) revealed that older patients' age and stage pT2–pT4 were the only independent predictors of worse OS, the addition of surgical data (Model 2) increased the prognostic power (LR: 29.6) by including the amount of blood lost during surgery. The addition of laboratory data (Model 3) further improved the prognostic value (LR: 46.18) taking into account the longer duration of surgery, intravascular invasion of the tumor, aspartate transaminase (AST) level > 135 U/L, and blood BAS count > 0.055 ×

10^9/L. Model 4 (LR: 61.5) was achieved by adding CD8+ cell density profiles at the HCC interface to model 3: a higher standard deviation of CD8+ density within the tumor edge improved OS (HR: 0.41, $p = 0.0026$). Adding CD8+ cell profile indicators from the non-malignant interface (Model 5, LR: 54.6) revealed mean CD8+ density in the epithelial aspect (i.e., remaining liver parenchyma) to be an independent predictor of worse survival.

Longer RFS could be predicted from a set of conventional independent features (Model 6, LR: 32.6): stage pT1, shorter duration of surgery (<147.5 min), a larger tumor size (>1.9 cm), wider resection margin around the tumor (>0.25 mm). Including CD8+ cell profiles at the malignant interface (Model 7, LR: 40.5) revealed the higher mean CD8+ density in the epithelial aspect (HCC) as an independent predictor of longer RFS.

3.3. Combined OS Prognostic Score

Based on Model 5, a combined prognostic OS score was constructed by adding the contributions to OS from each independent variable (duration of surgery, aspartate transaminase (AST), blood basophil count (BAS), HCC_sd_TE, Liver_m_T): 1 for poor, 0 for good prognosis. Patients were assigned a prognostic category according to the combined score: scores 0–1 have low risk, score 2 has intermediate risk, and scores 3–5 make up the high-risk group, with a corresponding 5-year OS probability of 76%, 40%, and 8% (Figure 4A), respectively. The differences in OS probability between the groups were statistically significant: $p < 0.0001$ for low vs. high, $p = 0.0045$ for low vs. intermediate, and $p < 0.0001$ for intermediate vs. high risk. The prognostic power of the combined score is further illustrated by the probability of OS 4 years after liver resection at 100%, 51%, and 12% in the low, intermediate, and high-risk groups, respectively (Figure 4A). Of note, similar but less informative risk stratification could be achieved by combining only the impact of TILs and NILs (Figure 4B).

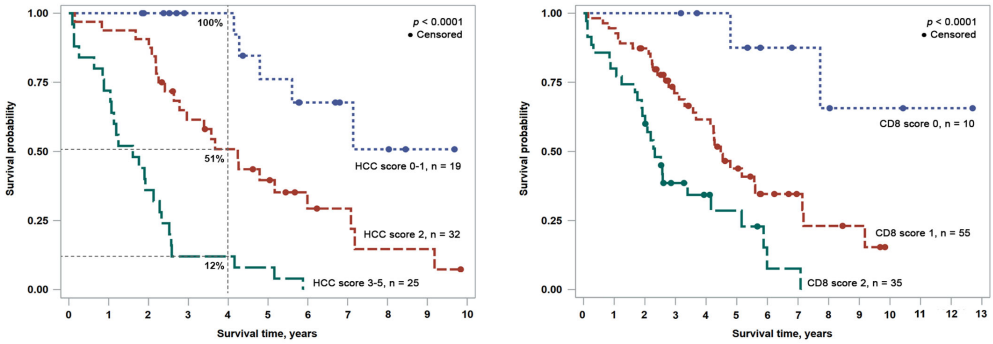

Figure 4. OS risk stratification based on combined prognostic scores: (**A**) comprehensive HCC OS score derived from five independent predictors from Model 5; (**B**) combined CD8 OS score derived from two independent predictors (CD8 density profiles at malignant and non-malignant interfaces).

4. Discussion

Our study reveals that computational assessment of CD8+ cell density profiles at the interfaces of malignant and non-malignant epithelium with the surrounding stroma provides independent prognostic information for HCC patients after surgical liver resection. We also observed an independent impact of clinical (duration and/or blood loss during surgery) and laboratory (blood AST, basophils) parameters on the OS of HCC patients, which can further be combined into a comprehensive prognostic score. Meanwhile, only

limited prognostic models could be obtained from conventional demographic (patient's age) and pathology data (pT stage).

We applied hexagonal grid-based spatial analyses to assess CD8+ density profiles across automatically detected HCC-stroma and liver-stroma interfaces in surgical excision liver samples. The method enables the sampling of the interface zone ranks from which cell density-based indicators can be computed, including standard deviation (SD), as a measure of spatial heterogeneity of the densities along the interface. We found that a higher variance (SD) of mean CD8+ T lymphocyte density at the tumor edge of HCC is an independent predictor of longer OS. Recently, Krijgsman et al. [45] similarly reported that the high SD of the CD8+ T lymphocyte density distribution was the only DIA-derived parameter that provided an independent prediction of longer OS in a cohort of 236 Dutch patients with ER-positive breast cancer. The authors hypothesized that this phenomenon could be due to the positive contribution of local high-density CD8 infiltrates. Similar findings were recently published by Li et al. [46]: the presence of organized lymphoid aggregates (named tertiary lymphoid structures, which could be interpreted as a manifestation of local TIL density variance) in HCC was significantly associated with longer RFS, yet no effect on OS was observed. It is worthy of note that the precise location of the tertiary lymphoid structures in the tissue was not indicated in this study. Radziuviene et al. [33] also reported that the variance in CD8 density along the tumor edge is an independent predictor of OS in IHC HER2-borderline breast cancer without HER2 amplification; however, high CD8+ SD was associated with shorter OS in this patient cohort. The pathobiological and prognostic significance of irregular CD8 cell infiltrates along the tumor edge requires further elucidation; nevertheless, this adds to the accumulating evidence that intratumoral heterogeneity of a feature expression may be more informative than a general quantification of a feature per se [6,33,38,47,48].

On the other hand, we found that the high mean density of CD8+ cells in the epithelial aspect of the interface zone of the non-neoplastic liver parenchyma was an independent predictor of worse OS. The infiltration of cytotoxic CD8+ lymphocytes could reflect an active inflammatory process in the remaining liver. It is possible that in chronic HBV infection, virus-specific CD8+ cells acquire an exhaustive phenotype and produce fewer inflammatory cytokines [49], so a high CD8+ density may indicate ongoing liver damage driven by the immune system. No sufficient data on the current state of viral hepatitis was available in our cohort to test this hypothesis. In contrast, we demonstrate that higher mean CD8 density in the HCC tumor edge, most likely representing the host's anti-tumoral immune response, is an independent predictor of longer RFS. Of note, this indicator was also significant for OS stratification in a univariate analysis (HCC_m_T with HR = 0.34, $p = 0.0005$), although it was not established as an independent predictor in multiple regression models for OS. Importantly, our computational assessment of CD8+ cell density profiles within the interfaces of malignant and non-malignant liver parenchyma with stroma revealed opposing prognostic effects of TILs and NILs, measurable in a surgical resection sample. Although a direct comparison cannot be made, contrary to Sun et al., who observed CD8+ density > 97 cells/mm^2 in the center of the tumor to be an independent predictor of longer DFS and OS [8], in our study CD8+ cell densities obtained by DIA within the entire malignant, non-malignant, and stroma compartments did not reveal an independent prognostic impact on OS or RFS[REF].

Some features of the surgical procedure (duration and blood loss) revealed an independent prognostic value in our dataset. A longer duration of surgery was associated with worse OS (>137.5 min) and RFS (>147.5 min). An interpretation of this finding is not straightforward. One could speculate that multiple characteristics such as tumor size, multifocality, proximity to critical structures such as large intrahepatic vessels, etc. converge into a complex surgical setting that reflects the severity of liver disease in general. Lee et al. found that a longer duration (>210 min) of the liver resection procedure was associated with a higher proportion of patients with relapsed (RFS) and deceased (OS) HCC in 1-, 3- and 5-year periods [50]. Similarly, the duration of surgery was also found to

be independently associated with an increased risk of severe complications after liver resection for colorectal cancer metastases [51]. However, in a recent study, He et al. [52] found no significant effect of the duration of surgery on OS in patients with HCC.

A negative effect of intraoperative blood loss has previously been reported on both RFS and OS in HCC patients [53,54]. Xiaocui Lv et al. [55] found that the extent of intraoperative blood loss during laparoscopic hepatectomy was directly associated with tumor size, surgery time, and type. Furthermore, increased intraoperative blood loss during the operation was found to be an independent predictor of HCC recurrence. Similarly, a longer hospital stay, which could reflect postoperative complications, was an independent predictor of hepatic decompensation after liver resection [56].

In our study, laboratory blood test data before surgery also contributed to the prognostic models. We found a negative impact of elevated alanine transaminase (ALT) and aspartate transaminase (AST) on OS, as previously reported [57]. Higher white blood cell, neutrophil, and basophil counts (Table 3) were associated with worse OS and RFS in our univariate analyses; these associations are less established in previous studies, in particular regarding RFS. A basophil count above 0.055×10^9/L served as an independent predictor of worse OS in our cohort; Wu et al. [58] reported a similar finding in a subgroup of gastric cancer patients. In Wu's study, a basophil count above 0.020×10^9/L was an independent predictor of a lower overall response rate to anti-PD-1 immunotherapy plus chemotherapy combination as well as worse progression-free survival and OS. More studies are needed to clarify the role of increased basophil counts in the context of persistent viral infection and/or in tumor-host interaction [59].

Based on the independent prognostic features established in our study, we propose a comprehensive scoring system to stratify patients into three risk groups after HCC resection. In this model, aspartate transaminase (AST) and mean CD8 cell density in the epithelial aspect of the non-malignant interface zone reflect an active inflammatory process in the remaining liver, while the duration of surgery and the variance (SD) of the mean CD8+ T lymphocyte density at the tumor edge are tumor related. The peripheral blood basophil count is potentially a feature of the patient's immune contexture, which could be affected by both antiviral and anti-tumoral responses. Similarly, the Barcelona Clinic Liver Cancer System (BCLC), which is the most widely used and validated staging system for HCC [60], incorporates the tumor parameters, residual liver function, and the general condition of the patient. BCLC classifies the patients into five groups: 0 (very early), A (early), B (intermediate), C (advanced), and D (terminal state).

The median OS time in the low (scores 0–1) risk group of our cohort was not reached, while it was approximately 50 months in the intermediate (score 2) group, and approximately 19 months in the high (scores 3–5) risk group. In a study by Wu et al. [61], the median survival time of the patients who underwent surgical resection in the BCLC 0-A (corresponding to low-risk) group was 52 months, it was 45 months in the BCLC B (intermediate risk) group, and it was 42 months in the BCLC C (high-risk) group, showing only marginal stratification.

Two years after the surgery, the low (scores 0–1), intermediate (score 2), and high (scores 3–5) risk groups of our cohort presented with OS rates of 100%, 91%, and 36%, respectively. In a validation study by Chan et al. [62], the 2-year probability of survival after curative treatment was 84% in BLCL group 0-A, 73% in BLCL group B, and 73% in BLCL group C. Two other staging systems were validated, the Cancer of the Liver Italian Program, CLIP (with a 2-year survival probability of 82% in the low-risk CLIP 0 group, 69% in intermediate-risk CLIP 1–3 group, and no patients in the high-risk CLIP 4–6 group) and the Chinese University Prognostic Index, CUPI (78% in low risk, 62% in the intermediate, and 100% in the high-risk group). The authors concluded that the performance of all three systems was suboptimal for the prediction of OS among patients who underwent curative HCC treatment [62]. Results of our study could help identify suitable indicators for a more precise prognostication system, although it is based on a retrospective single-

center patient cohort of 106 patients and serves as a proof-of-concept that requires further validation studies

Our study has some additional limitations. First, we did not have sufficient data in our patient cohort to investigate prognostic models for disease specific survival, which would be relevant to further discriminate the impact of both neoplastic and non-neoplastic components of the liver disease. Second, although most of our analysis steps are automated, in some cases we could not achieve the satisfactory AI segmentation of malignant and non-malignant hepatocytes. The well-differentiated HCC, reactive atypia and dysplastic nodules were not properly distinguished in the WSI of IHC slides and, therefore, a pathologist manually annotated the neoplastic and nonneoplastic areas of interest in all resection samples.

5. Conclusions

In conclusion, we present computational models to assess CD8 density profiles in the interfaces of both malignant and non-malignant liver parenchyma with the surrounding stroma. In conjunction with clinical, pathological, and laboratory data, they enable comprehensive prognostic stratification of OS and RFS in patients with HCC after liver resection.

Supplementary Materials: The following supporting information can be downloaded at: https://www.mdpi.com/article/10.3390/cancers15020366/s1, Figure S1. (**A**) CD8 Slide HIGH. (**B**) CD8 Slide LOW.

Author Contributions: Conceptualization, R.S., A.L., K.S. and A.R.; methodology, R.S., A.L., A.R.; software, R.S., D.Z.-P., A.R.; validation, D.Z.-P., R.S.; formal analysis, R.S., D.Z.-P., A.L.; investigation, R.S., A.G. (Aiste Gulla), A.G. (Agne Grigonyte), A.L.; resources, R.S., A.G. (Aiste Gulla), A.G. (Agne Grigonyte), K.S.; data curation, R.S.; writing—original draft preparation, R.S.; writing—review and editing, R.S., A.L., A.R., D.Z.-P., A.G. (Aiste Gulla), A.G. (Agne Grigonyte), K.S.; visualization, R.S., A.R.; supervision, A.L.; project administration, R.S.; funding acquisition, A.L., R.S. All authors have read and agreed to the published version of the manuscript.

Funding: This research is in part funded by the European Social Fund resources allocated for the project "Development of Doctoral Studies " implemented by Research Council of Lithuania, project No. 09.3.3-ESFA-V-711-01-0001, under the Specific objective "Strengthen the Skills and Capacities of Public Sector Researchers for Engaging in High Level R & D Activities" of Priority Axis 9 "Educating the Society and Strengthening the Potential of Human Resources" within the framework of the Operational Programme for the European Union Funds' Investments in 2014–2020.

Institutional Review Board Statement: The Lithuanian Bioethics Committee approved (permit number 2021/6-1354-843, issued 29 June 2021) the study design.

Informed Consent Statement: Patient consent was waived by the Vilnius Regional Biomedical Research Ethics Committee according to the International Ethical Guidelines for Health-related Research Involving Humans [42].

Data Availability Statement: The data presented in this study are available on request from the corresponding author. The data are not publicly available due to permit restrictions.

Acknowledgments: The authors would like to thank their colleagues from the National Center of Pathology for their valuable help in producing IHC slides, diagnostic work on the cases, IT support and significantly contributing to many other technical tasks that enabled the publication of these results.

Conflicts of Interest: The authors declare that they have no conflicts of interest.

References

1. Sung, H.; Ferlay, J.; Siegel, R.L.; Laversanne, M.; Soerjomataram, I.; Jemal, A.; Bray, F. Global cancer statistics 2020: GLOBOCAN estimates of incidence and mortality worldwide for 36 cancers in 185 countries. *CA Cancer J. Clin.* **2021**, *71*, 209–249.
2. Paradis, V. Histopathology of hepatocellular carcinoma. *World J. Gastroenterol.* **2012**, *20*, 15955–15964. https://doi.org/10.3748/wjg.v20.i43.15955.

3. Kim, E.; Viatour, P. Hepatocellular carcinoma: Old friends and new tricks. *Exp. Mol. Med.* **2020**, *52*, 1898–1907. https://doi.org/10.1038/s12276-020-00527-1.
4. Singh, A.K.; Kumar, R.; Pandey, A.K. Hepatocellular Carcinoma: Causes, Mechanism of Progression and Biomarkers. *Curr. Chem. Genom. Transl. Med.* **2018**, *12*, 9–26. https://doi.org/10.2174/2213988501812010009.
5. Roehlen, N.; Crouchet, E.; Baumert, T.F. Liver Fibrosis: Mechanistic Concepts and Therapeutic Perspectives. *Cells* **2020**, *9*, 875. https://doi.org/10.3390/cells9040875.
6. Nault, J.C.; Galle, P.R.; Marquardt, J.U. The role of molecular enrichment on future therapies in hepatocellular carcinoma. *J. Hepatol.* **2018**, *69*, 237–247. https://doi.org/10.1016/j.jhep.2018.02.016.
7. Zheng, X.; Jin, W.; Wang, S.; Ding, H. Progression on the Roles and Mechanisms of Tumor-Infiltrating T Lymphocytes in Patients With Hepatocellular Carcinoma. *Front. Immunol.* **2021**, *12*, 729705. https://doi.org/10.3389/fimmu.2021.729705.
8. Sun, C.; Xu, J.; Song, J.; Liu, C.Q.; Wang, J.; Weng, C.; Sun, H.; Wei, H.; Xiao, W.; Sun, R.; et al. The predictive value of centre tumour CD8+ T cells in patients with hepatocellular carcinoma: Comparison with Immunoscore. *Oncotarget* **2015**, *6*, 35602–35615. https://doi.org/10.18632/oncotarget.5801.
9. Lin, S.; Hoffmann, K.; Schemmer, P. Treatment of Hepatocellular Carcinoma: A Systematic Review. *Liver Cancer* **2012**, *1*, 144–158. https://doi.org/10.1159/000343828.
10. Sposito, C.; Di Sandro, S.; Brunero, F.; Buscemi, V.; Battiston, C.; Lauterio, A.; Bongini, M.; De Carlis, L.; Mazzaferro, V. Development of a prognostic scoring system for resectable hepatocellular carcinoma. *World J. Gastroenterol.* **2016**, *22*, 8194–8202. https://doi.org/10.3748/wjg.v22.i36.8194.
11. Renne, S.L.; Sarcognato, S.; Sacchi, D.; Guido, M.; Roncalli, M.; Terracciano, L.; Di Tommaso, L. Hepatocellular carcinoma: A clinical and pathological overview. *Pathologica* **2021**, *113*, 203. https://doi.org/10.32074/1591-951X-295.
12. Johnston, M.P.; Khakoo, S.I. Immunotherapy for hepatocellular carcinoma: Current and future. *World J. Gastroenterol.* **2019**, *25*, 2977–2989. https://doi.org/10.3748/wjg.v25.i24.2977.
13. Johnson, P.J. HCC in Focus. *Clin. Adv. Hematol. Oncol.* **2017**, *15*, 452–454.
14. Villa, B.E.; Colantoni, A.; Camma, C.; Grottola, A.; Buttafoco, P.; Gelmini, R.; Ferretti, I. Estrogen Receptor Classification for Hepatocellular Carcinoma : Comparison With Clinical Staging Systems. *J. Clin. Oncol.* **2003**, *21*, 441–446. https://doi.org/10.1200/JCO.2003.11.051.
15. Toyoda, H.; Kumada, T.; Osaki, Y.; Oka, H.; Urano, F.; Kudo, M.; Matsunaga, T. Staging Hepatocellular Carcinoma by a Novel Scoring System (BALAD Score) Based on Serum Markers. *Clin. Gastroenterol. Hepatol.* **2006**, *4*, 1528–1536. https://doi.org/10.1016/j.cgh.2006.09.021.
16. Wongjarupong, N.; Negron-Ocasio, G.M.; Mara, K.C.; Prasai, K.; Abdallah, M.A.; Ahn, K.S.; Yang, J.D.; Addissie, B.D.; Giama, N.H.; Harmsen, W.S.; et al. BALAD and BALAD-2 predict survival of hepatocellular carcinoma patients: A North American cohort study. *HPB Off. J. Int. Hepato Pancreato Biliary Assoc.* **2021**, *23*, 762–769. https://doi.org/10.1016/j.hpb.2020.09.014.
17. Chew, V.; Lai, L.; Pan, L.; Lim, C.J.; Li, J.; Ong, R.; Chua, C.; Leong, J.Y.; Lim, K.H.; Toh, H.C.; et al. Delineation of an immunosuppressive gradient in hepatocellular carcinoma using high-dimensional proteomic and transcriptomic analyses. *Proc. Natl. Acad. Sci. USA* **2017**, *114*, E5900–E5909. https://doi.org/10.1073/pnas.1706559114.
18. Raskov, H.; Orhan, A.; Christensen, J.P.; Gögenur, I. Cytotoxic CD8+ T cells in cancer and cancer immunotherapy. *Br. J. Cancer* **2021**, *124*, 359–367. https://doi.org/10.1038/s41416-020-01048-4.
19. Ikeguchi, M.; Oi, K.; Hirooka, Y.; Kaibara, N. CD8+ lymphocyte infiltration and apoptosis in hepatocellular carcinoma. *Eur. J. Surg. Oncol.* **2004**, *30*, 53–57. https://doi.org/10.1016/j.ejso.2003.10.001.
20. Ramzan, M.; Sturm, N.; Decaens, T.; Bioulac-Sage, P.; Bancel, B.; Merle, P.; Tran Van Nhieu, J.; Slama, R.; Letoublon, C.; Zarski, J.P.; et al. Liver-infiltrating CD8+ lymphocytes as prognostic factor for tumour recurrence in hepatitis C virus-related hepatocellular carcinoma. *Liver Int.* **2016**, *36*, 434–444. https://doi.org/10.1111/liv.12927.
21. Hala, S.; Asmaa, G.A.; Mervat, S.S.; Nanis, S.H.; Shymaa, H. Role of CD8 Cytotoxic T Lymphocytes in Hepatocellular Carcinoma: An Immunohistochemical Study. *Med. J. Cairo Univ.* **2019**, *87*, 4061–4069. https://doi.org/10.21608/mjcu.2019.76624. Available online: https://mjcu.journals.ekb.eg/article_76624.html (accessed on 9 September 2022).
22. Xu, X.; Tan, Y.; Qian, Y.; Xue, W.; Wang, Y.; Du, J.; Jin, L.; Ding, W. Clinicopathologic and prognostic significance of tumor-infiltrating CD8+ T cells in patients with hepatocellular carcinoma: A meta-analysis. *Medicine* **2019**, *98*, e13923. https://doi.org/10.1097/MD.0000000000013923.
23. Ding, W.; Xu, X.; Qian, Y.; Xue, W.; Wang, Y.; Du, J.; Jin, L.; Tan, Y. Prognostic value of tumor-infiltrating lymphocytes in hepatocellular carcinoma: A meta-analysis. *Medicine* **2018**, *97*, e13301. https://doi.org/10.1097/MD.0000000000013301.
24. An, J.L.; Ji, Q.H.; An, J.J.; Masuda, S.; Tsuneyama, K. Clinicopathological analysis of CD8-positive lymphocytes in the tumor parenchyma and stroma of hepatocellular carcinoma. *Oncol. Lett.* **2014**, *8*, 2284–2290. https://doi.org/10.3892/ol.2014.2516.
25. Portland, F.; Toronto, G.; Madrid, C.; Nijmegen, U.K.; Medicine, T. Cancer classification using the Immunoscore : A worldwide task force Cancer classification using the Immunoscore: A worldwide task force. *J. Transl. Med.* **2012**, *10*, 205. https://doi.org/10.1186/1479-5876-10-205.
26. Galon, J.; Lanzi, A. Immunoscore and its introduction in clinical practice. *Q. J. Nucl. Med. Mol. Imaging* **2020**, *64*, 152–161. https://doi.org/10.23736/S1824-4785.20.03249-5.
27. Angell, H.K.; Bruni, D.; Barrett, J.C.; Herbst, R. The Immunoscore : Colon Cancer and Beyond. *Clin. Cancer Res.* **2020**, *26*, 332–339. https://doi.org/10.1158/1078-0432.CCR-18-1851.

28. Gabrielson, A.; Wu, Y.; Wang, H.; Jiang, J.; Kallakury, B.; Gatalica, Z.; Reddy, S.; Kleiner, D.; Fishbein, T.; Johnson, L.; et al. Intratumoral CD3 and CD8 T-cell Densities Associated with Relapse-Free Survival in HCC. *Cancer Immunol. Res.* **2016**, *4*, 419–430. https://doi.org/10.1158/2326-6066.CIR-15-0110.
29. Liu, W.-R.; Tian, M.-X.; Tang, Z.; Fang, Y.; Zhou, Y.-F.; Song, S.-S.; Jiang, X.-F.; Wang, H.; Tao, C.-Y.; Zhou, P.-Y.; et al. Nine-factor-based immunohistochemistry classifier predicts recurrence for early-stage hepatocellular carcinoma after curative resection. *Br. J. Cancer* **2020**, *123*, 92–100. https://doi.org/10.1038/s41416-020-0864-0.
30. Steele, K.E.; Tan, T.H.; Korn, R.; Dacosta, K.; Brown, C.; Kuziora, M.; Zimmermann, J.; Laffin, B.; Widmaier, M.; Rognoni, L.; et al. Measuring multiple parameters of CD8+ tumor-infiltrating lymphocytes in human cancers by image analysis. *J. Immunother. Cancer* **2018**, *6*, 1–14. https://doi.org/10.1186/s40425-018-0326-x.
31. Koelzer, V.H.; Sirinukunwattana, K.; Rittscher, J.; Mertz, K.D. Precision immunoprofiling by image analysis and artificial intelligence. *Virchows Arch.* **2019**, *474*, 511–522. https://doi.org/10.1007/s00428-018-2485-z.
32. Laurinavicius, A.; Rasmusson, A.; Plancoulaine, B.; Shribak, M.; Levenson, R. Machine-Learning–Based Evaluation of Intratumoral Heterogeneity and Tumor-Stroma Interface for Clinical Guidance. *Am. J. Pathol.* **2021**, *191*, 1724–1731. https://doi.org/10.1016/j.ajpath.2021.04.008.
33. Radziuviene, G.; Rasmusson, A.; Augulis, R.; Grineviciute, R.B.; Zilenaite, D.; Laurinaviciene, A.; Ostapenko, V.; Laurinavicius, A. Intratumoral Heterogeneity and Immune Response Indicators to Predict Overall Survival in a Retrospective Study of HER2-Borderline (IHC 2+) Breast Cancer Patients. *Front. Oncol.* **2021**, *11*, 774088. https://doi.org/10.3389/fonc.2021.774088.
34. Zilenaite, D.; Rasmusson, A.; Augulis, R.; Besusparis, J.; Laurinaviciene, A.; Plancoulaine, B.; Ostapenko, V.; Laurinavicius, A. Independent Prognostic Value of Intratumoral Heterogeneity and Immune Response Features by Automated Digital Immunohistochemistry Analysis in Early Hormone Receptor-Positive Breast Carcinoma. *Front. Oncol.* **2020**, *10*, 950. https://doi.org/10.3389/fonc.2020.00950.
35. Nestarenkaite, A.; Fadhil, W.; Rasmusson, A.; Susanti, S.; Hadjimichael, E.; Laurinaviciene, A.; Ilyas, M.; Laurinavicius, A. Immuno-interface score to predict outcome in colorectal cancer independent of microsatellite instability status. *Cancers* **2020**, *12*, 2902. https://doi.org/10.3390/cancers12102902.
36. Cheng, N.; Ren, Y.; Zhou, J.; Zhang, Y.; Wang, D.; Zhang, X.; Chen, B.; Liu, F.; Lv, J.; Cao, Q.; et al. Deep Learning-Based Classification of Hepatocellular Nodular Lesions on Whole-Slide Histopathologic Images. *Gastroenterology* **2022**, *162*, 1948-1961.e7. https://doi.org/10.1053/j.gastro.2022.02.025.
37. Naoumov, N.V.; Brees, D.; Loeffler, J.; Chng, E.; Ren, Y.; Lopez, P.; Tai, D.; Lamle, S.; Sanyal, A.J. Digital pathology with artificial intelligence analyses provides greater insights into treatment-induced fibrosis regression in NASH. *J. Hepatol.* **2022**, *77*, 1399–1409. https://doi.org/10.1016/j.jhep.2022.06.018.
38. Taylor-Weiner, A.; Pokkalla, H.; Han, L.; Jia, C.; Huss, R.; Chung, C.; Elliott, H.; Glass, B.; Pethia, K.; Carrasco-Zevallos, O.; et al. A Machine Learning Approach Enables Quantitative Measurement of Liver Histology and Disease Monitoring in NASH. *Hepatology* **2021**, *74*, 133–147. https://doi.org/10.1002/hep.31750.
39. Liao, H.; Xiong, T.; Peng, J.; Xu, L.; Liao, M. Classification and Prognosis Prediction from Histopathological Images of Hepatocellular Carcinoma by a Fully Automated Pipeline Based on Machine Learning. *Ann. Surg. Oncol.* **2020**, *27*, 2359–2369. https://doi.org/10.1245/s10434-019-08190-1.
40. Nam, D.; Chapiro, J.; Paradis, V.; Seraphin, T.P.; Kather, J.N. Artificial intelligence in liver diseases: Improving diagnostics, prognostics and response prediction. *JHEP Rep.* **2022**, *4*, 100443. https://doi.org/10.1016/j.jhepr.2022.100443.
41. Rasmusson, A.; Zilenaite, D.; Nestarenkaite, A.; Augulis, R.; Laurinaviciene, A.; Ostapenko, V.; Poskus, T.; Laurinavicius, A. Immunogradient Indicators for Antitumor Response Assessment by Automated Tumor-Stroma Interface Zone Detection. *Am. J. Pathol.* **2020**, *190*, 1309–1322. https://doi.org/10.1016/j.ajpath.2020.01.018.
42. WHO C for IO of MS (CIOMS) in Collaboration with the WH. International Ethical Guidelines for Health-Related Research Involving Humans [Internet]. Biomedical Research. 2016. pp. 1921–1931. Available online: http://www.sciencedirect.com/science/article/B6VC6-45F5X02-9C/2/e44bc37a6e392634b1cf436105978f01 (accessed on 2 September 2022).
43. Budczies, J.; Klauschen, F.; Sinn, B.V.; Gyorffy, B.; Schmitt, W.D.; Darb-Esfahani, S.; Denkert, C. Cutoff Finder: A Comprehensive and Straightforward Web Application Enabling Rapid Biomarker Cutoff Optimization. *PLoS ONE* **2012**, *7*, e51862. https://doi.org/10.1371/journal.pone.0051862.
44. Rushing, C.; Bulusu, A.; Hurwitz, H.I.; Nixon, A.B.; Pang, H. A leave-one-out cross-validation SAS macro for the identi fi cation of markers associated with survival. *Comput. Biol. Med.* **2015**, *57*, 123–129. https://doi.org/10.1016/j.compbiomed.2014.11.015.
45. Krijgsman, D.; Van Leeuwen, M.B.; Van Der Ven, J.; Almeida, V.; Vlutters, R.; Halter, D.; Kuppen, P.J.K.; Van De Velde, C.J.H.; Wimberger-Friedl, R. Quantitative Whole Slide Assessment of Tumor-Infiltrating CD8-Positive Lymphocytes in ER-Positive Breast Cancer in Relation to Clinical Outcome. *IEEE J. Biomed. Health Inform.* **2021**, *25*, 381–392. https://doi.org/10.1109/JBHI.2020.3003475.
46. Li, J.; Nie, Y.; Jia, W.; Wu, W.; Song, W.; Li, Y. Effect of Tertiary Lymphoid Structures on Prognosis of Patients with Hepatocellular Carcinoma and Preliminary Exploration of Its Formation Mechanism. *Cancers* **2022**, *14*, 5157. https://doi.org/10.3390/cancers14205157.
47. Chidambaranathan-Reghupaty, S.; Fisher, P.B.; Sarkar, D. Hepatocellular carcinoma (HCC): Epidemiology, etiology and molecular classification. *Adv. Cancer Res.* **2021**, *149*, 1–61. https://doi.org/10.1016/bs.acr.2020.10.001.

48. Heindl, A.; Nawaz, S.; Yuan, Y. Mapping spatial heterogeneity in the tumor microenvironment: A new era for digital pathology. *Lab. Investig.* **2015**, *95*, 377–384. https://doi.org/10.1038/labinvest.2014.155.
49. Khanam, A.; Chua, J.V.; Kottilil, S. Immunopathology of Chronic Hepatitis B Infection: Role of Innate and Adaptive Immune Response in Disease Progression. *Int. J. Mol. Sci.* **2021**, *22*, 5497. https://doi.org/10.3390/ijms22115497.
50. Lee, E.C.; Kim, S.H.; Park, H.; Lee, S.D.; Lee, S.; Park, S. Survival analysis after liver resection for hepatocellular carcinoma : A consecutive cohort of 1002 patients. *J. Gastroenterol. Hepatol.* **2016**, *32*, 1055–1063. https://doi.org/10.1111/jgh.13632.
51. Egeland, C.; Rostved, A.A.; Schultz, N.A.; Pommergaard, H.C.; Daugaard, T.R.; Thøfner, L.B.; Rasmussen, A.; Hillingsø, J.G. Morbidity and mortality after liver surgery for colorectal liver metastases: A cohort study in a high - volume fast - track programme. *BMC Surg.* **2021**, *21*, 1–9. https://doi.org/10.1186/s12893-021-01301-4.
52. He, Y.; Liang, T.; Mo, S.; Chen, Z.; Zhao, S.; Zhou, X.; Yan, L.; Wang, X.; Su, H. Effect of timing of surgical resection of primary hepatocellular carcinoma on survival outcomes in elderly patients and prediction of clinical models. *BMC Gastroenterol.* **2021**, *21*, 1–8. https://doi.org/10.1186/s12876-021-01815-4.
53. Hanazaki, K.; Kajikawa, S.; Koide, N.; Adachi, W.; Amano, J. Prognostic factors after hepatic resection for hepatocellular carcinoma with hepatitis C viral infection: Univariate and multivariate analysis. *Am. J. Gastroenterol.* **2001**, *96*, 1243–1250. https://doi.org/10.1016/S0002-9270(00)02427-8.
54. Katz, S.C.; Shia, J.; Liau, K.H.; Gonen, M.; Ruo, L.; Jarnagin, W.R.; Fong, Y.; D'Angelica, M.I.; Blumgart, L.H.; Dematteo, R.P. Operative blood loss independently predicts recurrence and survival after resection of hepatocellular carcinoma. *Ann. Surg.* **2009**, *249*, 617–623. https://doi.org/10.1097/SLA.0b013e31819ed22f.
55. Lv, X.; Zhang, L.; Yu, H.; Yu, X. Laparoscopic hepatectomy for hepatocellular carcinoma: Short- And long-term outcomes with blood loss. *Transl. Cancer Res.* **2021**, *10*, 4303–4315. https://doi.org/10.21037/tcr-21-463.
56. Elshaarawy, O.; Aman, A.; Zakaria, H.M.; Zakareya, T.; Gomaa, A.; Elshimi, E.; Abdelsameea, E. Outcomes of curative liver resection for hepatocellular carcinoma in patients with cirrhosis. *World J. Gastrointest. Oncol.* **2021**, *13*, 424–439. https://doi.org/10.4251/wjgo.v13.i5.424.
57. Sempokuya, T.; Wong, L.L. Ten-year survival and recurrence of hepatocellular cancer. *Hepatoma Res.* **2019**, *5*, 38. https://doi.org/10.20517/2394-5079.2019.013.
58. Wu, C.; Qiu, Y.; Zhang, R.; Li, X.; Liang, H.; Wang, M.; Li, F. Association of peripheral basophils with tumor M2 macrophage infiltration and outcomes of the anti - PD - 1 inhibitor plus chemotherapy combination in advanced gastric cancer. *J. Transl. Med.* **2022**, *20*, 1–15. https://doi.org/10.1186/s12967-022-03598-y.
59. Chauhan, J.; Stavraka, C.; Grandits, M.; Palhares, L.C.G.F.; Josephs, D.H.; Lacy, K.E.; Spicer, J.; Bax, H.J.; Karagiannis, S.N. Clinical and Translational Significance of Basophils in Patients with Cancer. *Cells* **2022**, *11*, 438. https://doi.org/10.3390/cells11030438.
60. Forner, A.; Reig, M.; Bruix, J. Hepatocellular carcinoma. *Lancet* **2018**, *391*, 1301–1314. https://doi.org/10.1016/S0140-6736(18)30010-2.
61. Wu, T.; Wu, Z. Surgical resection improves long-term survival of patients with hepatocellular carcinoma across diff. *Cancer Manag. Res.* **2018**, *10*, 361–369. https://doi.org/10.2147/CMAR.S152707.
62. Chan, S.L.; Johnson, P.J.; Mo, F.; Berhane, S.; Teng, M.; Chan, A.W.H.; Poon, M.C.; Lai, P.B.S.; Yu, S.; Chan, A.T.C.; et al. International validation of the Chinese university prognostic index for staging of hepatocellular carcinoma: A joint United Kingdom and Hong Kong study. *Chin. J. Cancer* **2014**, *33*, 481–491. https://doi.org/10.5732/cjc.014.10133.

2nd publication / 2 publikacija

Rokas Stulpinas, Mindaugas Morkunas, Allan Rasmusson, Julius Drachneris, Renaldas Augulis Aiste Gulla, Kestutis Strupas, Arvydas Laurinavicius

Improving HCC Prognostic Models after Liver Resection by AI-Extracted Tissue Fiber Framework Analytics

Cancers (Basel). 2023 Dec 24;16(1):106.

doi: 10.3390/cancers16010106. PMID: 38201532; PMCID: PMC10778366

https://pubmed.ncbi.nlm.nih.gov/38201532/

cancers

MDPI

Article

Improving HCC Prognostic Models after Liver Resection by AI-Extracted Tissue Fiber Framework Analytics

Rokas Stulpinas [1,2,*], Mindaugas Morkunas [2,3], Allan Rasmusson [1,2], Julius Drachneris [1,2], Renaldas Augulis [1,2], Aiste Gulla [4,5,6], Kestutis Strupas [4,5,6] and Arvydas Laurinavicius [1,2]

1 Faculty of Medicine, Institute of Biomedical Sciences, Department of Pathology and Forensic Medicine, Vilnius University, 03101 Vilnius, Lithuania; arvydas.laurinavicius@vpc.lt (A.L.)
2 National Center of Pathology, Affiliate of Vilnius University Hospital Santaros Klinikos, 08406 Vilnius, Lithuania; mindaugas.morkunas@santa.lt
3 Vilnius Santaros Klinikos Biobank, Vilnius University Hospital Santaros Klinikos, 08661 Vilnius, Lithuania
4 Faculty of Medicine, Institute of Clinical Medicine, Vilnius University, 03101 Vilnius, Lithuania
5 Faculty of Medicine, Centre for Visceral Medicine and Translational Research, Vilnius University, 03101 Vilnius, Lithuania
6 Center of Abdominal Surgery, Vilnius University Hospital Santaros Klinikos, 08410 Vilnius, Lithuania
* Correspondence: rokas.stulpinas@vpc.lt

Simple Summary: Prognosis of patients after surgical resection for hepatocellular carcinoma (HCC) is often obscured by the variable impact of the tumor and remaining liver properties. We applied a convolutional neural network and hexagonal grid analytics to extract prognostic indicators from collagen microarchitecture within the tumor and adjacent liver tissue. By associating the extracted features from two distinct fiber types with clinical outcomes, we have developed two computational models to predict the overall survival of the patients. We report the independent prognostic roles for reticulin in HCC and fibrillary collagen in the peritumoral liver, highlighting the significance of assessing region-specific and type-specific fiber features. Our study provides evidence that the predictive power of prognostic models of HCC can be enhanced by artificial intelligence solutions generating computational image-based biomarkers.

Abstract: Despite advances in diagnostic and treatment technologies, predicting outcomes of patients with hepatocellular carcinoma (HCC) remains a challenge. Prognostic models are further obscured by the variable impact of the tumor properties and the remaining liver parenchyma, often affected by cirrhosis or non-alcoholic fatty liver disease that tend to precede HCC. This study investigated the prognostic value of reticulin and collagen microarchitecture in liver resection samples. We analyzed 105 scanned tissue sections that were stained using a Gordon and Sweet's silver impregnation protocol combined with Picric Acid–Sirius Red. A convolutional neural network was utilized to segment the red-staining collagen and black linear reticulin strands, generating a detailed map of the fiber structure within the HCC and adjacent liver tissue. Subsequent hexagonal grid subsampling coupled with automated epithelial edge detection and computational fiber morphometry provided the foundation for region-specific tissue analysis. Two penalized Cox regression models using LASSO achieved a concordance index (C-index) greater than 0.7. These models incorporated variables such as patient age, tumor multifocality, and fiber-derived features from the epithelial edge in both the tumor and liver compartments. The prognostic value at the tumor edge was derived from the reticulin structure, while collagen characteristics were significant at the epithelial edge of peritumoral liver. The prognostic performance of these models was superior to models solely reliant on conventional clinicopathologic parameters, highlighting the utility of AI-extracted microarchitectural features for the management of HCC.

Keywords: hepatocellular carcinoma; liver; hexagonal grid; artificial intelligence; CNN; prognostic modelling; digital pathology; overall survival

check for updates

Citation: Stulpinas, R.; Morkunas, M.; Rasmusson, A.; Drachneris, J.; Augulis, R.; Gulla, A.; Strupas, K.; Laurinavicius, A. Improving HCC Prognostic Models after Liver Resection by AI-Extracted Tissue Fiber Framework Analytics. *Cancers* **2024**, *16*, 106. https://doi.org/10.3390/cancers16010106

Academic Editor: Claudio Tiribelli

Received: 31 October 2023
Revised: 11 December 2023
Accepted: 21 December 2023
Published: 24 December 2023

1. Introduction

Hepatocellular carcinomas (HCC) constitute up to 80% of all primary liver cancers [1]. Liver cirrhosis—often induced by viral hepatitis B and C, alcohol consumption, chemical toxins, or metabolic liver diseases—precedes HCC in at least 80% of cases [2]. Furthermore, the global rise of obesity and type 2 diabetes leads to the increased incidence of non-alcoholic fatty liver disease (NAFLD), a primary cause of HCC in the absence of cirrhosis [3]. In recent decades, the impact of HCC has grown significantly, now ranking as the third leading cause of cancer-related mortality worldwide [4]. From 1990 to 2019, there was a staggering 70% increase in HCC incidence, resulting in 480,000 attributable deaths, exacerbated by late diagnoses and advanced disease stages [1,5]. While early detection leads to a five-year survival rate of over 70%, the rate plummets to a mere 18% in later stages [4,6]. These trends highlight the necessity for research into surgical techniques, pharmaceutical options, and prognostic factors to meet the challenge posed by HCC.

Unlike many other cancers, post-resection clinical outcomes of HCC patients do not rely solely on tumor properties and success of its therapy. An important additional determinant is the pathology and functional capacity of the residual liver tissue, underscoring the need for comprehensive assessment of both tumor and non-tumor components [7]. This aspect was taken into account by the Barcelona Clinic Liver Cancer (BCLC) staging and treatment strategy. BLCL points to the limitations of scoring systems for liver failure, like the Child–Pugh system and the model for end-stage liver disease (MELD), which fail to accurately predict the loss of liver function specifically in the context of HCC [8]. To address this, BCLC staging incorporates multiple parameters of tumor burden, liver function, and cancer-related symptoms, as well as alpha-fetoprotein (AFP) levels and the albumin–bilirubin score for liver function assessment [9].

Surgical liver resection provides samples containing HCC and liver parenchyma, as well as their interface. This opens multiple opportunities of tissue pathology methods to assess cellular, molecular, and architectural properties of the disease in the spatial context of the tissue microenvironment. A particular aspect that unifies both tumor and non-tumor tissues is represented by properties of the extracellular matrix (ECM), which has been shown to provide rich and quantifiable data of clinical significance. Tumor associated collagen signatures (TACS) have been conceptualized as computational biomarkers to reflect changes in the organization, alignment, and composition of fibers in the stroma that surround and interact with cancer cells [10]. Originally proposed and demonstrated to have prognostic significance in breast cancer tissue by Keely et al., collagen-derived features were subsequently refined and described in oral, gastric, salivary gland, skin neoplasms and benign fibrous lesions [11–14]. On the other hand, microarchitectural transformations of liver tissue represent progression of chronic liver disease.

At the molecular level, the ECM is represented by co-polymers comprising various types of collagen, non-collagenous glycoproteins, proteoglycans, and other molecules. These composite biological materials have distinct characteristics, and thus bear similarities with metal alloys, as noted by Bruckner [15]. Arranged into fibrillary structures of the interstitial matrix and the basement membrane—the main components of the ECM—they provide a structural foundation for the liver parenchyma [10]. The molecular complexity of ECM became evident in the 1970s with the discovery that normal liver tissue primarily contains three types of collagen: Type I, Type III, and basement membrane collagens. Type III collagen is the main constituent of reticulin fibers [16]. However, persistent liver injury leads to significant alterations of the composition, orientation, and quantity of all collagen types [17]. As fibrosis progresses, Type I collagen accumulates, eventually becoming predominant in the cirrhotic liver [18]. Despite well-established association between cirrhosis and hepatocarcinogenesis, the exact role of Type I collagen remains unclear: some studies associate it with HCC progression [19], whereas others propose that Type I collagen accumulation may have a beneficial effect by mechanically restraining tumor spread [20]. Conversely, the role of Type III collagen is more established, given that the progressive distortion and dissolution of reticulin framework are histopathological

hallmarks of HCC [21]. Therefore, a comprehensive analysis of Type I and Type III (reticulin) collagen properties could provide insights for clinical assessment of patients with HCC.

Currently, histochemical or immunohistochemical methods are used to highlight the different types of collagen [22]. Assessment of the fiber microarchitecture can be performed by visual inspection of the patterns; however, rapid development of computational methods in digital pathology brings novel opportunities for high-capacity quantification of the structural patterns [23]. It has been shown that AI solutions are capable of extracting subvisual features with prognostic relevance from liver tissue [24]. Recently, Patil et al. developed a deep learning model for quantifying reticulin (represented by black, silver-impregnated fibers) in HCC tissue after liver resection [25]. They found that a decreased reticulin proportionate area (RPA) was an independent predictor of metastasis, shorter disease-free survival, and worse overall survival in this study. Similarly, Taylor-Weiner et al. demonstrated the utility of a convolutional neural network (CNN) for Ishak and NASH Clinical Research Network fibrosis scoring in trichrome-stained slides [26]. A recent study suggests that liver pathologists are eager for further development of digital pathology and AI integration [27].

Morkunas et al. proposed a more detailed method for extracting collagen-derived prognostic features; they used a CNN to segment collagen from images of tissue microarrays (TMA) containing Picrosirius Red stained samples of ductal breast carcinoma [28]. From 37 features of fiber morphometry, density, orientation, texture, and fractal characteristics, they found an independent prognostic value of observed heterogeneity of distances between collagen fibers, fiber straightness, and variance of fiber orientation angles to predict patient survival, even though their method was limited to samples of small amount of tumor tissue (TMA cores). On the other hand, full-face surgical resection samples contain large amount of data that are also affected by intratissue heterogeneity, including the malignant and non-malignant components and their interfaces. Therefore, it is essential to properly assess the spatial aspects of pathology features extracted. To tackle this complexity, Plancoulaine et al. proposed a hexagonal tiling approach that allowed quantification of intratumoral heterogeneity of biomarker expression in breast cancer [29]. Building upon this method, a tool for automatic detection of the tumor-stroma interface was further developed by Rasmusson et al. [30].

In this study, we explored the predictive value of linear reticulin and thick septal collagen fibers in both HCC and adjacent liver. Utilizing AI for fiber segmentation and tissue classification, followed by hexagonal grid subsampling of the data, we extracted fiber-specific features in the spatial context of the tissue components and their interfaces. Our findings indicate the potential utility of these features to predict overall survival of patients undergoing liver resection for HCC.

2. Materials and Methods

2.1. Study Design

An overview of the study design is presented in Figure 1. Archived formalin-fixed paraffin-embedded (FFPE) samples from 105 patients were used in this retrospective study. Patients met the following inclusion criteria: (1) they underwent surgical liver resection due to HCC at the Vilnius University hospital Santaros Clinics (Vilnius, Lithuania) with the specimens tested at the National Center of Pathology, an affiliate of the Vilnius University Hospital Santaros Clinics (Vilnius, Lithuania) between 2007 and 2020; and (2) they had at least one archived FFPE block containing both non-necrotic HCC and peritumoral liver tissues. Overall survival (OS) data were obtained with a median OS duration of 938 days and 60% of the individuals deceased as of 2022. The study was approved by the Vilnius Regional Biomedical Research Ethics Committee (permit number 2021/6-1354-843), who waived the requirement of individual informed consent.

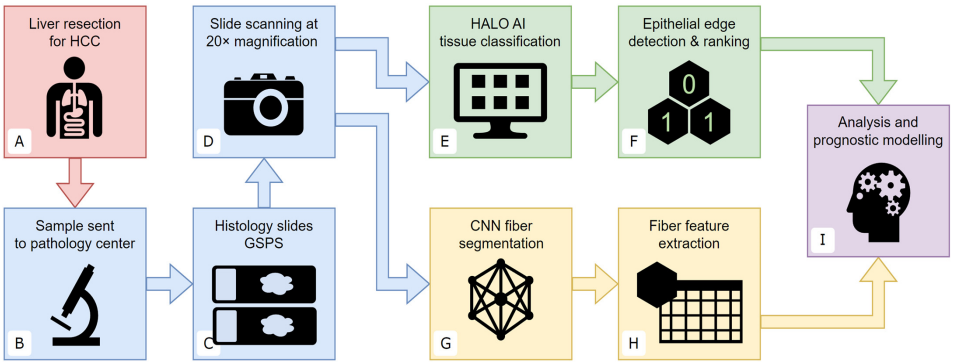

Figure 1. Study design: (**A**) surgical liver resection due to HCC at the Vilnius University hospital Santaros Klinikos (Vilnius, Lithuania); (**B**) specimens tested at the National Center of Pathology (Vilnius, Lithuania); (**C**) samples stained using a modified Gordon and Sweet's silver impregnation protocol, combined with Picric Acid–Sirius Red; (**D**) slides scanned at 20× magnification (0.5 µm per pixel) using an Aperio® AT2 DX scanner; (**E**) tissue segmentation using HALO® AI on the manual annotations; (**F**) epithelial edge detection and ranking of the hexagonal grid tiles according to tissue class proportions; (**G**) segmentation of reticulin and collagen fibers using a pretrained convolutional neural network, producing an image of red and green fibers against the black background for viewing and analysis; (**H**) calculating pixel-level, fiber-level, and image-level features describing the microarchitecture of the fibers within each hexagon; (**I**) data from individual hexagons are aggregated across predetermined tissue regions to provide case-level features for prognostic modeling.

Clinicopathologic parameters were retrospectively collected from the medical records and are presented in Table 1. Briefly, in this cohort of 105 individuals with a median age of 65 years, there is a predominance of male patients (77.1%) and grade 2 HCC (74.3%), while the extent of the primary tumor is mostly pT2 (56.2%) and pT1 (36.2%).

Table 1. Patient and tumor characteristics of the study cohort.

Characteristic	Value (Range or Percent)
Patients	105 (100%)
Age, years	
Mean (range)	63.7 (13–82)
Median	65
≥55 years	88 (83.8)
Gender	
Male	81 (77.1%)
Female	24 (22.9%)
Metavir fibrosis stage	
F0 (no fibrosis)	12 (11.4%)
F1 (portal fibrosis without septa)	5 (4.8%)
F2 (portal fibrosis with rare septa)	11 (10.4%)
F3 (numerous septa without cirrhosis)	16 (15.3%)
F4 (cirrhosis)	61 (58.1%)
Largest tumor dimension, cm	
Mean (range)	4.76 (0.8–19.0)
Median	40
Tumor multinodularity	
Single HCC nodule	74 (70.5%)
Multiple HCC nodules	31 (29.5%)

Table 1. *Cont.*

Characteristic	Value (Range or Percent)
HCC grade	
G1	8 (7.6%)
G2	78 (74.3%)
G3	19 (18.1%)
pT stage	
T1	38 (36.2%)
T2	59 (56.2%)
T3	7 (6.7%)
T4	1 (0.9%)
Intravascular invasion	
Present	52 (49.5%)
Absent	53 (50.5%)
Lymph nodes present	
Yes	19 (18.1%)
No	86 (81.9%)
Lymph nodes per patient if present, mean (median)	2.7 (2)
Metastatic spread confirmed	1/19 (5.3%)
Resection margin	
R0	85 (80.9%)
R1	20 (19.1%)
History of viral infection	
HBV	9 (8.6%)
HCV	52 (49.5%)
None or unknown	44 (41.9%)
Other treatment prior to current resection	
Yes	13 (12.4%)
No	92 (87.6%)
HCC recurrence after resection	
Yes	56 (53.3%)
No	49 (46.7%)
OS time, days	
Mean (range)	1108.7 (20–3160)
Median	938

2.2. Sample Preparation and Segmentation

A pathologist (RS) reviewed all archived slides to identify the most representative formalin-fixed paraffin-embedded (FFPE) block. The selected block includes non-necrotic HCC tissue, and, whenever possible (in 103 samples, accounting for 98.1% of the cases), the surrounding peritumoral liver parenchyma. The 3 µm sections were stained using a modified Gordon and Sweet's silver impregnation protocol combined with Picric Acid–Sirius Red, referred to as GSPS (see Figure 2E–H, supplementary Table S1). This method is standard for liver and bone marrow samples at the National Center of Pathology. Throughout this paper, we define the red-staining fibers in the thick fibrous septae as 'collagen', and the delicate black linear strands mostly located in the epithelial areas as 'reticulin'.

All slides were subsequently digitized at 20× magnification (0.5 µm per pixel) using an Aperio® AT2 DX scanner (Leica Aperio Technologies, Vista, CA, USA). A pathologist (RS) reviewed the images to mark the malignant (HCC) and non-malignant (peritumoral liver) areas on each slide by placing manual annotations (see Figure 3A,D). A HALO® AI (Indica Labs, Albuquerque, NM, USA) classifier was used to categorize the tissue into hepatocytes (indiscriminately malignant and non-malignant), stroma, and background classes.

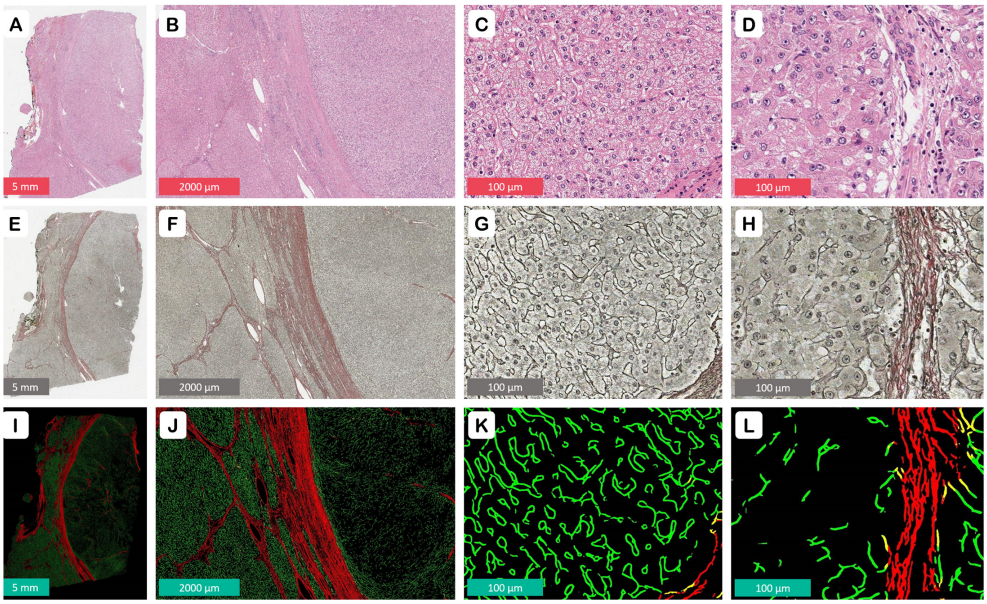

Figure 2. Staining and segmentation: (**A**–**D**) hematoxylin–eosin (H&E) staining is inferior to GSPS in the frame of this study due to its limited capacity to highlight the fibrous structures, such as the tumor capsule and septation of cirrhotic liver parenchyma; (**E**–**H**) a modified Gordon and Sweet's silver impregnation protocol combined with Picric Acid–Sirius Red (GSPS). The nodularity of the cirrhotic liver and the encapsulation of the tumor are highlighted by red-stained bands of collagen (**F**); note the regular black linear reticulin network of the liver (**G**) in contrast to the loss of reticulin in HCC (**H**); (**I**–**L**) the CNN-generated pixel-precise mask of red (collagen) and green (reticulin) fibers set against a contrasting black background, optimized for viewing and morphometric feature extraction.

2.3. CNN-Based Fiber Framework Extraction

We used a modified version of a U-Net model architecture proposed by Morkunas et al. in 2021 [28] to analyze the images of GSPS-stained samples. The model was designed to produce three output channels, representing collagen (red), reticulin (green), and an empty channel (black). This produces an RGB image, which is easy to view and analyze (see Figure 2I–L).

To produce the ground truth for model training, we selected 85 large (2048 × 2048 pixel-sized) regions of interest (ROIs) in 31 whole slide images (WSIs). We manually annotated fibrous structures of both collagen and reticulin in all ROIs by freeform annotation to produce RGB annotation masks of the fibers. Each region of interest (ROI) and its corresponding mask was then partitioned into 256 × 256-pixel image patches to match the model's input size, resulting in a total of 5440 patches ($N = 85 \times (2048/256)^2$). To increase the training set, we augmented the dataset with 90° rotations, vertical and horizontal flips, blurring, zooming, and annotation erosion or dilation. Examples of annotated image patches are shown in Supplementary Figure S1. The final augmented dataset contained 54,400 image patches. The dataset was randomly divided into an 80% training subset and a 20% validation subset for model training.

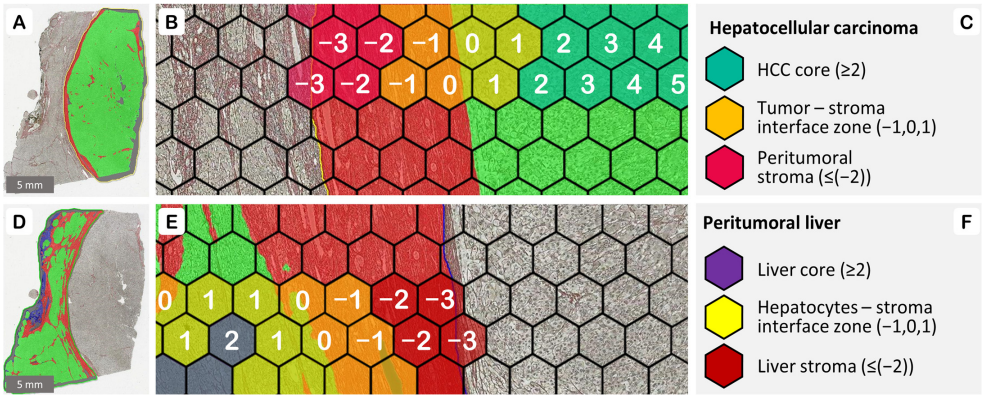

Figure 3. Hexagonal tiling, ranking, and zones of interest: (**A**) HALO® AI (Indica Labs, Albuquerque, NM, USA) classifier result on the manually placed HCC annotation; (**B**) ranking of the hexagonal tiles according to their shortest distance from the tumor edge (rank 0 hexagon); (**C**) regions of interest within the HCC annotation; (**D**) classifier result for the manually annotated non-malignant liver parenchyma; (**E**) ranking of the hexagons on the sides of non-malignant epithelial edge; (**F**) regions of interest within the peritumoral liver annotation.

During inference, the target WSI is divided into overlapping patches of size 256 × 256 pixels, with a step-size of 128 pixels in both vertical and horizontal directions on the image plane. Pixels in both red and green layers of the predicted fiber mask undergo separate thresholding processes. A pixel in the predicted collagen mask is assigned a value of 1.0 if the probability of collagen detection in that pixel exceeds 0.5; otherwise, it is assigned a value of 0.0. No rules were implemented to prevent a single target pixel from being attributed to more than one output layer. This lack of constraint allows for model uncertainty, manifesting as yellow pixels in the predicted RGB images where red and green fibers overlap, despite the absence of overlapping red and green fiber annotations in the ground truth.

The model was trained with adaptive moment estimation optimizer (using default parameters provided in the original method [31]) minimizing the binary cross-entropy loss function. We trained the model on single patch batches. Model weights were saved after each improvement in validation loss. The training phase was terminated after validation loss did not improve for 20 consecutive epochs. We used a suite of software tools including h5py (2013, Collete A., Boulder, CO, USA), numpy (version 1.20.0), and tensorflow with tensorboard (version 2.7.0).

2.4. Hexagonal Grid Tiling

Grid subsampling was utilized to sample the whole slide images (WSI) into hexagonal tiles (in this study having a long diagonal of 780 pixels) and rank them according to the distance to the automatically detected edge between the epithelium and stroma tissue classes, as described previously [30], see Figure 3. The tiling offers a number of advantages over processing the entire slide at once, with two of them being crucial. First, tiles allow a localized analysis of the tumor features, thus helping us identify the gradual changes and heterogeneity within different regions of the tissue, which might be overlooked in a whole-image analysis. Secondly, the spatially ranked tiles enable the extraction of specific regions of interest within the tumor, thereby providing more targeted insights. Briefly, during the ranking step, the hexagons at the stroma–epithelium (either benign hepatocytes or neoplastic HCC cells) boundary are identified and assigned a rank 0. Subsequently, the

epithelial-side hexagons are attributed a positive rank, and stromal hexagons a negative rank, according to their shortest distance from the edge (rank 0 hexagon).

2.5. Calculation of Fiber Texture Descriptors

Morkunas et al. [28] originally proposed a set of 37 pixel-level, fiber-level, and image-level features to describe the CNN-derived fibrous matrix of breast cancer tissue. Drawing on past experience, we have reduced the number of features by removing the ones that were previously found to be the most correlated, dependent upon tissue placement on the glass slide, or difficult to interpret. In this study, for each tissue type marked by a pathologist, we calculated 11 features (see Table 2) including fiber orientation, morphometrics, fractal characteristics, and Haralick's texture descriptors. Since these features are calculated per channel, separate descriptor sets were obtained for the green (reticulin) and the red (collagen) fibers, and the final number of calculated tissue characteristics is 22. Features were extracted for each hexagon, thus enabling analysis of fiber features according to hexagonal rank.

Table 2. List of features used to characterize the fibrous matrix, calculated twice per each hexagon: for the green (reticulin or Type 3 collagen) and the red (Type 1 collagen) fibers separately.

Feature	Description
Orientation:	
Circular standard deviation (CSD)	Dispersion of circular angles of the individual fibers
Magnitude, mean (mMag)	Average strength or intensity of vectors (e.g., gradients) in the fiber mask
Morphometry:	
Fiber length, mean (mFL)	Average Euclidean distance between the endpoints of each skeletonized fiber
Fiber path, mean (mFP)	Average pixel length of a line dividing a fiber into two equal parts along its longer axis
Fiber straightness, mean (mFS)	A ratio of fiber length over fiber path
Density:	
Fiber density (FD)	Number of pixels in the mask
Endpoints (nENDP)	Number of fiber endpoints in the hexagon mask
Texture (Haralick's):	
Homogeneity (hom)	The closeness of the distribution of elements in the gray-level co-occurrence matrix to the matrix diagonal
Entropy (ent)	Amount of information or randomness in the texture
Correlation (cor)	Linear dependency of gray levels on those of neighboring pixels
Fractal:	
Lacunarity (lac)	A measure of both gaps and heterogeneity: the variation in space around objects in the image and their irregular distribution

2.6. Statistical Analysis

The main goal of this study was to determine the impact of reticulin and collagen patterns in the tumor microenvironment on overall survival. Both the HCC and the peritumoral liver areas (as determined by a pathologist's annotation), were further subdivided into three regions of interest each (see Figure 3): the three hexagon-wide 'interface zone' (IZ3), consisting of ranks [−1, 0, 1]; the epithelial 'core', incorporating ranks [≥2]; and the 'stroma', with the remaining ranks [≤(−2)]. For survival analysis, the data from individual hexagons across each of the six regions had to be aggregated on a per-case basis. During this aggregation, the mean and standard deviation of every feature measurement (across all hexagons, in each region of interest) are calculated for every case. The compiled case-level dataset contains 264 potential fiber-derived predictors, representing 2 annotations × 3 regions per annotation × 2 summary metrics (mean and standard deviation) × 2 types of fibers (green and red) × 11 fiber features. Twelve clinicopathological variables such as patient age, gender, tumor grade, size, stage, intravascular invasion, etc. were added to the set.

The data were analyzed using SAS software (version 9.4; SAS Institute Inc., Cary, NC, USA) and Python libraries (Pandas version 1.3.4, Scikit-learn version 1.0.2 and Lifelines

version 0.27.0). Descriptive statistics were computed to summarize the main features of the data, with means, medians and ranges reported for continuous variables, and frequencies and percentages for categorical variables. Min–max scaling (or min–max normalization) was used to transform the metrics of the features to be on a similar scale in a fixed range between 0 and 1. Univariate Cox regression analysis with LASSO (least absolute shrinkage and selection operator) regularization was used to assess the performance of individual variables. Features with a $p < 0.1$ were used to construct the survival prediction models that underwent further evaluation using multivariate LASSO Cox analysis. After running LASSO Cox regression, only the models where all variables had $p < 0.05$ were retained. The C-index on the five-fold cross-validation test set was used to measure performance and rank the models accordingly. The individual features included in these models were ranked based on the frequency of their combined occurrence across all the models. Given the extensive list of significant predictors, we used the factor analysis as an additional step to identify underlying relationships among the variables, aiding interpretation.

3. Results

3.1. Descriptive Statistics

A total of 162,435 hexagonal tiles comprised the complete hexagon-level dataset. The range of measurements of reticulin and collagen fiber features in the individual hexagons prior to min–max scaling is presented in Table 3.

Table 3. Range of the reticulin (green, prefix 'g_') and collagen (red, prefix 'r_') fiber features as measured per individual hexagonal tiles prior to scaling.

Feature	Min	Max	Mean	Median
g_CSD	0.327599	1.551254	0.874630	0.872546
g_mMag	2.731371	25,599.785804	7410.622809	6869.993232
g_mFL	0.000000	1059.079906	61.729315	52.348669
g_mFP	2.500000	1246.933333	90.089874	78.200000
g_mFS	0.000000	0.956133	0.497333	0.507360
g_FD	1.000000	151,375.000000	34,755.695386	30,771.000000
g_nENDP	0.000000	1394.000000	322.604360	312.000000
g_hom	0.947687	0.999997	0.984834	0.985913
g_ent	0.000068	1.092885	0.380083	0.378187
g_cor	−0.000008	0.944431	0.843028	0.851353
g_lac	0.000000	1.206979	0.589991	0.579632
r_CSD	0.282147	1.583950	0.842409	0.824565
r_mMag	2.630596	34,292.920449	6742.703072	3761.257993
r_mFL	0.000000	28,507.246022	132.393359	51.126263
r_mFP	2.500000	14,861.500000	133.552675	72.366667
r_mFS	0.000000	3.478550	0.470136	0.482461
r_FD	1.000000	386,398.000000	45,713.265522	19,491.000000
r_nENDP	0.000000	2221.000000	360.981139	206.000000
r_hom	0.929537	0.999998	0.986157	0.992241
r_ent	0.000044	1.315616	0.380543	0.259431
r_cor	−0.000008	0.988216	0.839329	0.858877
r_lac	0.000000	1.295812	0.594719	0.602250

3.2. Univariate Predictors of Overall Survival

After scaling to standardize feature metrics, the impact of individual variables on the overall survival (OS) was evaluated using univariate Cox regression with LASSO regularization. Fifteen variables were determined to be statistically significant univariate predictors of OS. Higher stage (pT2-4, $p = 0.0026$), older patient age at the time of diagnosis ($\geq$55 years, $p = 0.0074$), and the presence of intravascular invasion ($p = 0.0089$) were the strongest predictors of shorter OS in this cohort. Twelve fiber-derived features, all derived from the HCC 'interface zone' or 'core' regions, had $p < 0.05$, while showing either a positive or negative effect on OS. For a more inclusive approach, allowing for a comprehensive

assessment in the subsequent multivariate Cox regression analysis, 36 features with $p < 0.1$ were selected for further modelling (see Table 4). The expanded list included multiple tumor nodules in the resected liver, alongside the addition of fiber-derived features from the peritumoral stroma, and the non-neoplastic liver parenchyma.

Table 4. Univariate predictors of overall survival ranked by the *p*-value (Cox regression with LASSO regularization).

Feature	*p*-Value	Hazard Ratio (HR)
Stage pT2-4	0.0026	2.3719
Age $\geq$ 55 years	0.0074	3.1990
Intravascular invasion	0.0089	1.9564
g_mn_mFL_HCC_IZ3	0.0095	0.0897
g_mn_mFP_HCC_IZ3	0.0095	0.1078
g_mn_cor_HCC_IZ3	0.0199	0.1114
g_sd_mFL_HCC_IZ3	0.0285	0.2203
g_mn_ent_HCC_IZ3	0.0294	0.2987
g_mn_FD_HCC_IZ3	0.0340	0.3049
g_mn_lac_HCC_IZ3	0.0343	4.1651
g_mn_mMag_HCC_IZ3	0.0356	0.3049
g_mn_hom_HCC_IZ3	0.0361	3.2656
g_mn_cor_HCC_CORE	0.0394	0.1385
g_sd_mFP_HCC_IZ3	0.0397	0.2500
g_mn_cor_HCC_STROMA	0.0482	0.1466
g_mn_mFS_HCC_IZ3	0.0514	0.1900
r_sd_mFS_LVR_IZ3	0.0532	0.0417
g_mn_nENDP_HCC_IZ3	0.0553	0.3200
g_mn_ent_HCC_CORE	0.0589	0.3644
g_sd_FD_HCC_STROMA	0.0595	0.3406
g_mn_mFP_HCC_STROMA	0.0702	0.1600
Multiple tumors	0.0717	1.6175
g_sd_mFS_HCC_STROMA	0.0733	2.6564
r_sd_FD_LVR_IZ3	0.0745	0.2762
g_mn_mFL_HCC_STROMA	0.0784	0.1616
r_mn_cor_LVR_IZ3	0.0858	0.2579
g_mn_FD_HCC_CORE	0.0865	0.3792
g_sd_mFS_HCC_IZ3	0.0902	3.0509
r_mn_mFS_HCC_IZ3	0.0935	4.2304
g_sd_ent_HCC_STROMA	0.0941	0.3704
g_sd_mMag_HCC_STROMA	0.0954	0.3911
g_sd_hom_HCC_STROMA	0.0963	0.3912
g_mn_hom_HCC_CORE	0.0986	2.5157
g_mn_mMag_HCC_CORE	0.0988	0.3972
g_mn_ent_HCC_STROMA	0.0995	0.2707
g_sd_lac_HCC_CORE	0.0995	3.1310

3.3. Multivariate Analysis

In adherence with the 'rule of ten' guideline, which suggests at least 10 events per variable in constructing a regression model, and given the presence of 56 events in our dataset, we systematically generated and listed all the possible regression models (N = 2,835,199) containing 1, 2, 3, 4, 5 or 6 components from the previously defined set of features. After applying LASSO Cox regression, only those models (N = 139) in which all variables exhibited a *p*-value of less than 0.05 were retained (the complete list is presented in the Supplementary Table S2). The concordance index (C-index) on a five-fold cross-validation test set was chosen as the metric of performance, and the models were ranked accordingly. A C-index above 0.7 indicates good discriminative ability, and two similar models in our study have shown values above this threshold (see Table 5). Both models include a demographic variable (patient age), a pathological parameter (HCC multifocality), a reticulin-derived feature at the tumor edge, and the collagen-derived feature at the epithelial edge of peritumoral

liver. The Kaplan–Meier OS plots (the cutoff values for groups here are the median values) for the individual components of these two models are presented in Figure 4.

Table 5. Cox regression models with a C-index above 0.7.

Features	HR	95% CI	*p*-Value
Model A, test set C-index 0.7094, AIC 359.3840			
Age ≥ 55 years	4.05	1.67–9.80	0.00194
Multiple_tumors	1.92	1.11–3.31	0.01895
g_mn_lac_HCC_IZ3	6.36	1.69–23.87	0.00615
r_mn_cor_LVR_IZ3	0.21	0.05–0.92	0.03802
Model B, test set C-index 0.7061, AIC 359.2425			
Age ≥ 55 years	4.33	1.73–10.81	0.0017
Multiple_tumors	2.24	1.30–3.83	0.0035
g_mn_lac_HCC_IZ3	5.58	1.48–21.06	0.0113
r_sd_mFS_LVR_IZ3	0.02	0.00–0.84	0.0396

The models in which every component had a *p*-value less than 0.05, were further analyzed by counting the number of times each variable appeared. Of the 139 models considered, all were composed of just 30 unique components in different combinations. The variables (features) were ranked based on the number of occurrences, and are presented in Table 6.

Table 6. List of the variables comprising statistically significant ($p < 0.05$) OS models ranked by the number of occurrences in the models.

Feature	Number of Occurrences
Age_55plus	57
r_mn_cor_LVR_IZ3	39
r_sd_mFS_LVR_IZ3	28
LVI	27
r_sd_FD_LVR_IZ3	23
Multiple_tumors	23
g_mn_lac_HCC_IZ3	16
g_sd_lac_HCC_CORE	13
pT2-3	12
g_mn_cor_HCC_IZ3	11
g_mn_mMag_HCC_IZ3	10
g_mn_hom_HCC_IZ3	10
g_mn_ent_HCC_IZ3	8
g_mn_FD_HCC_IZ3	7
g_mn_cor_HCC_STROMA	7
g_mn_mFL_HCC_IZ3	7
g_mn_ent_HCC_CORE	6
g_mn_mFP_HCC_IZ3	6
g_mn_hom_HCC_CORE	6
g_mn_mMag_HCC_CORE	6
g_mn_nENDP_HCC_IZ3	6
g_sd_mFS_HCC_STROMA	5
g_sd_mFL_HCC_IZ3	3
g_mn_mFS_HCC_IZ3	2
g_mn_FD_HCC_CORE	2
r_mn_mFS_HCC_IZ3	2
g_mn_cor_HCC_CORE	2
g_sd_mFP_HCC_IZ3	2
g_sd_mMag_HCC_STROMA	1
g_sd_hom_HCC_STROMA	1

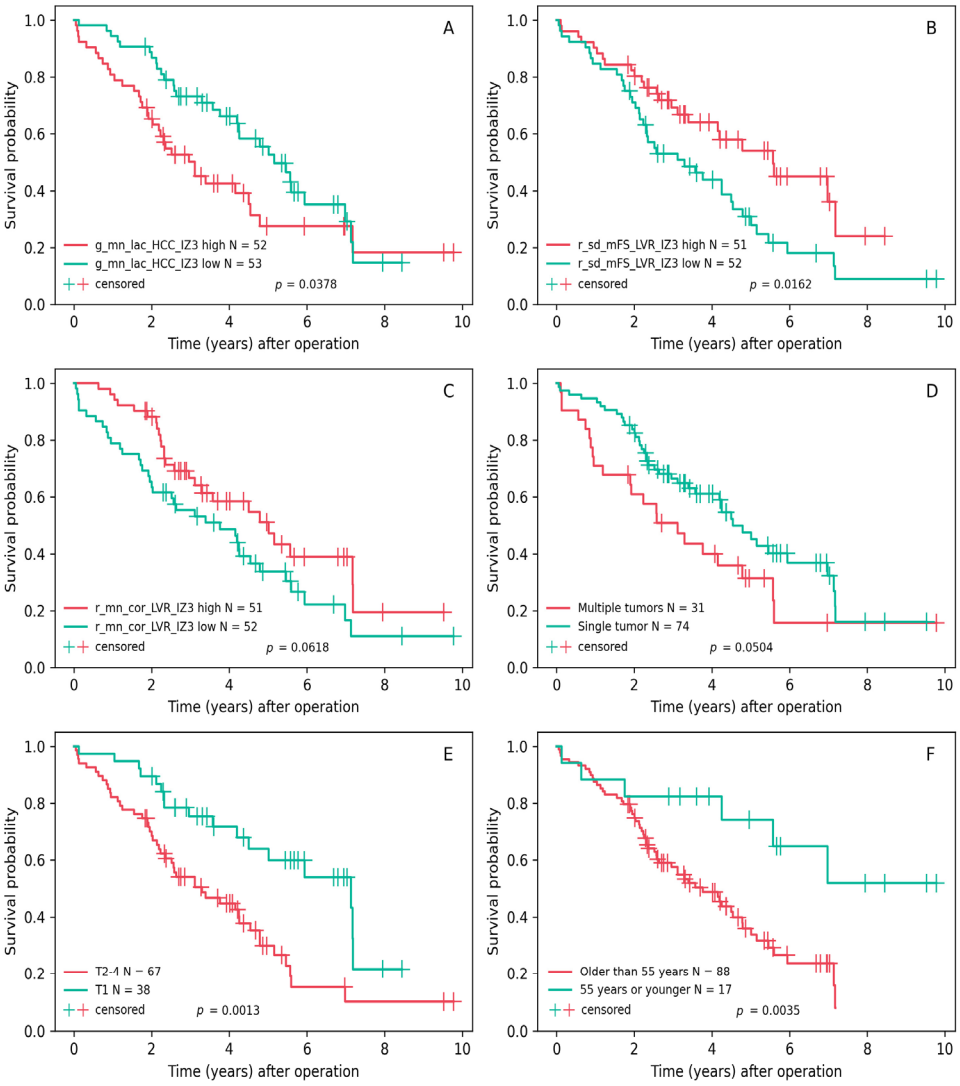

Figure 4. (**A**–**F**) Kaplan–Meier overall survival plots and the cutoff values for the components of models with good discriminative ability (C-index > 0.7); the best univariate predictor is also added.

3.4. Factor Analysis

We have further applied a factor analysis to investigate the underlying relationships of the fiber-derived features (N = 26) after removing the conventional clinicopathologic variables from the list of significant predictors. Six factors explaining 85.12% of the variance in the data were kept, using an eigenvalue of 1 as the criterion. Orthogonal varimax rotation was used to maximize the variance of the loadings within factors (the results are presented in Figure 5).

Feature	Factor1	Factor2	Factor3	Factor4	Factor5	Factor6
g_mn_nENDP_HCC_IZ3	0.94773	0.10036	−0.05121	0.16403	−0.00628	0.06156
g_mn_mMag_HCC_IZ3	0.93981	0.20883	−0.04795	0.14834	0.10887	0.0344
g_mn_ent_HCC_IZ3	0.92941	0.22806	−0.02563	0.15822	0.11101	0.07623
g_mn_FD_HCC_IZ3	0.92271	0.27999	−0.00784	0.1591	0.07985	0.09032
g_mn_mMag_HCC_CORE	0.86283	0.23747	0.0052	0.20692	0.00278	0.03374
g_mn_FD_HCC_CORE	0.84686	0.29006	0.03427	0.21055	−0.02641	0.06987
g_mn_ent_HCC_CORE	0.84435	0.25703	0.01367	0.20808	0.01141	0.06455
g_mn_mFP_HCC_IZ3	0.66879	0.65105	0.04369	0.13945	0.15138	0.18189
g_mn_mFL_HCC_IZ3	0.65465	0.66181	0.06318	0.14	0.12075	0.19207
g_sd_mFL_HCC_IZ3	0.48998	0.8429	0.07264	0.11847	−0.00616	0.1104
g_sd_mFP_HCC_IZ3	0.48386	0.84866	0.05612	0.11783	0.01193	0.08454
g_sd_mMag_HCC_STROMA	0.48089	0.1491	0.073	0.85148	0.01272	0.02513
g_sd_hom_HCC_STROMA	0.48035	0.14801	0.07334	0.85223	0.01008	0.02487
g_mn_cor_HCC_CORE	0.28905	0.36481	0.14022	0.0537	0.09471	0.32009
g_mn_mFS_HCC_IZ3	0.20433	0.05334	0.10008	0.00595	0.95706	0.1307
g_mn_cor_HCC_IZ3	0.12828	0.25347	0.22098	0.03485	0.1635	0.87085
r_sd_mFS_LVR_IZ3	−0.0139	0.00568	0.24617	−0.04347	0.03284	0.04839
r_mn_cor_LVR_IZ3	−0.02628	0.03934	0.9317	0.02386	0.09006	0.13865
r_sd_FD_LVR_IZ3	−0.07918	0.0805	0.92717	0.09005	0.02329	0.05877
g_mn_cor_HCC_STROMA	−0.08075	0.05255	0.08409	0.02572	0.0195	0.14305
g_sd_mFS_HCC_STROMA	−0.085	0.05502	−0.00142	−0.13163	−0.08492	0.06053
r_mn_mFS_HCC_IZ3	−0.40508	−0.03649	0.06498	−0.01958	0.02606	−0.03992
g_sd_lac_HCC_CORE	−0.54988	−0.09544	0.05536	−0.08286	−0.0678	−0.11139
g_mn_lac_HCC_IZ3	−0.83271	−0.24683	0.05698	−0.15718	−0.31933	0.1236
g_mn_hom_HCC_CORE	−0.8632	−0.23658	−0.00485	−0.20711	−0.00141	−0.03397
g_mn_hom_HCC_IZ3	−0.94044	−0.20717	0.04841	−0.14824	−0.10603	−0.03462

Figure 5. The heatmap of factor loadings (sorted by the loadings in Factor 1). Positive loadings in dark green boxes, negative loadings in red. Color intensity indicates magnitude, with dark green for high positive loadings and light green for low positive loadings.

Factor 1 explains 53.73% of data variance and is characterized by the irregularity of reticulin fibers within the tumor–stroma interface and, to the lesser extent, the tumor core. Factor 1 has high loadings for variables like density, entropy, magnitude, and the number of endpoints of the reticulin fibers. Conversely, it displays negative loadings for parameters such as lacunarity and homogeneity. Factor 2 covers 11.08% of variance and highlights the heterogeneity of the reticulin fiber measurements, also within the same tumor–stroma interface. It is primarily influenced by variables corresponding to reticulin fiber length and fiber path, with emphasis on both mean values and standard deviations (SD) at the tumor edge. Factor 3 (6.56% of variance) captures the irregularity of the collagen network within the peritumoral liver–stroma interface, representing fibrosis around the functioning hepatocytes. It is mostly associated with the standard deviation of red pixel density per hexagon, and mean texture correlation of the collagen fibers.

Each of the other three factors covers less than 5% of the data variance. Factor 4 represents the heterogeneity of reticulin fibers in the peritumoral stroma, particularly in the standard deviation of homogeneity and magnitude. The pronounced straightness of reticulin fibers in the tumor–stroma interface forms the most of Factor 5. Lastly, Factor 6 emphasizes the correlation of reticulin fibers in all of the HCC tissue, represented by both the tumor–stroma interface, and the tumor core.

The first five factors exhibited cutoff values that divided the cohort into groups with statistically significant differences in overall survival duration, as indicated by a *p*-value of less than 0.05 in univariate analysis. However, after applying the LASSO Cox regression, none of these factors were found to be significant in the models, and therefore, they did not outperform the individual features.

4. Discussion

This study demonstrates the prognostic value of convolutional neural network-based mapping of reticulin and collagen fiber architecture in the HCC microenvironment. The integration of computational features describing the reticulin and collagen texture with the clinical parameters resulted in two multivariate overall survival models with a test cohort C-index > 0.7 after penalized LASSO Cox regression. Both models reveal the independent prognostic impact of patient age, tumor multifocality and fiber-derived features at the interfaces of HCC and the remaining functional hepatocytes with the surrounding stroma. Also, the reticulin structure provided the prognostic value at the tumor edge, while at the border of liver parenchyma, the collagen structure was relevant. Meanwhile, none of the models consisting of conventional clinicopathologic metrics only were able to surpass the 0.7 C-index threshold.

We have discovered that among the HCC-derived features in our cohort, the mean lacunarity of the reticulin framework at the tumor margin was the best-performing metric. Following closely, as indicated by its recurrent appearances in the models (Table 6), is the variance (SD) of the reticulin lacunarity at the core of the tumor. This observation aligns with the established significance of reticulin which is a key element in the structure of a normal liver, providing the framework of its lobular architecture. The alteration, disruption or dissipation of reticulin fibers is a well-documented diagnostic sign of HCC, first reported nearly 50 years ago [32]. Lacunarity is a fractal parameter that captures both gaps (Lat. lacuna) and heterogeneity in a pattern. In the context of our study, higher lacunarity would suggest the reduction and distortion of the reticulin framework, possibly indicating a more aggressive tumor phenotype. The high variance of lacunarity at the central part of the tumor—the core—might suggest the existence of areas with different degrees of aggressiveness. This insight finds parallels with a recent study by Patil A. et al., which confirmed a reduction in the AI-identified reticulin proportionate area (RPA) in HCC as a strong predictor of adverse patient outcomes [25]. However, our work revealed a potential superiority of spatial variations in the reticulin framework, as captured by lacunarity. The underperformance of the mean fiber density (FD, derived from the number of pixels in the mask and comparable to RPA) in our study, in contrast to lacunarity, suggests that the spatial heterogeneity in reticulin arrangement may provide more insight than merely the proportion of reticulin in the HCC tissue.

In cancer diagnostics, the non-neoplastic component of the tissue often receives somewhat lesser attention. However, our findings also underscore the independent prognostic significance of the peritumoral liver parenchyma. The extent of fibrosis, a well-documented predictor of chronic liver disease outcomes, can be assessed using a variety of invasive or non-invasive methods [33,34]. We have demonstrated that collagen in the peritumoral liver serves as a significant source of prognostic information, in contrast to the role of reticulin in HCC, as previously discussed. This aligns with the known role of Type I collagen as the primary component of fibrous tissue that accumulates during persistent liver damage. In our study, two features associated with peritumoral liver collagen were included in the most predictive models of overall survival (Table 5): the mean texture correlation of collagen fibers, and the high variance of collagen fiber straightness. Additionally, the high variance in fiber density emerged as the third collagen-derived feature, listed among the ten most recurrent components in the prognostic models (Table 6). Importantly, all these indicators were measured at the interface between remaining functional hepatocytes and the fibrous tissue (hexagon ranks −1, 0, 1). The standard deviation of individual measurements serves as an indicator of variability or heterogeneity between hexagons.

In this case, it can highlight regions of dense, compact fibrosis in contrast to areas of the liver that remain somewhat intact, characterized by sparsely deposited and less organized collagen fibers. On the other hand, a more consistent overall tissue structure (reflected by the high mean correlation), might indicate a less advanced liver disease with higher residual functional capacity. Combined, the high variability of collagen deposition in the individual hexagons and the maintenance of general parenchymal integrity might indicate the presence of ongoing successful tissue repair. As sufficient residual liver function is crucial for the survival of patients [35], its assessment alongside tumor parameters on the same tissue slide offers a streamlined and practical approach in HCC resection samples.

A factor analysis was used to investigate the inherent relations between the 26 fiber-derived features that, when combined in certain ways (see Supplementary Table S2), showed statistically significant predictive power ($p < 0.05$) in regression models. Six factors were identified, capturing the majority of the information in the original data. The heatmap in Figure 5 highlights the strong negative association between the mean reticulin lacunarity at the tumor edge (g_mn_lac_HCC_IZ3) and the dominant Factor 1, positioning it as a key determinant. Notably, this variable also exhibits the most negative loadings for both Factor 2 and Factor 5, and ranks second to last in terms of negative loadings for Factor 4. These consistent negative loadings across four of the six factors suggest that g_mn_lac_HCC_IZ3 captures multidimensional information about the reticulin framework at the tumor edge, making it the most prominent HCC-derived feature. Furthermore, the predominant features defining peritumoral liver-derived Factor 3 reflect the consistency in collagen fiber orientation (r_mn_cor_LVR_IZ3), variability in density (r_sd_FD_LVR_IZ3), and variability in fiber straightness (r_sd_mFS_LVR_IZ3). Consequently, the pairing of a tumor-based g_mn_lac_HCC_IZ3 indicator with either r_mn_cor_LVR_IZ3 or r_sd_mFS_LVR_IZ3, both liver-based features, collectively covers Factors 1–5, which represent 81.04% of the variance. This unique combination demonstrates remarkable performance in Cox regression models and outperforms the factor values, emphasizing the synergistic role of tumor and liver characteristics in HCC prognostication.

Our study contains some limitations. The lack of complete data on HBV and HCV infections restricts a thorough examination of their potential impact on the overall survival in our HCC patients. Secondly, the lack of the information on the cause of death limits our options for predicting disease-specific survival, which would be relevant for our focus on impact of malignant and non-malignant components. Thirdly, the cohort of 105 patients is rather limited and serves as a proof-of-concept study. Validation studies on independent cohorts would be needed to assess generalizability of our findings.

5. Conclusions

We have focused on using a convolutional neural network to segment the two types of fibers from the histopathology images containing HCC and the adjacent liver tissue, which were then used to calculate the predictive biomarkers of overall survival. These biomarkers are based on the structure of reticulin and collagen fibers both in the tumor microenvironment and the adjacent residual non-neoplastic liver tissue. We underscore the critical importance of precise tissue zoning due to the concentration of prognostic information at the edges of both benign and malignant epithelial tissue. The dual-type fiber extraction method allowed us to confirm the central role of reticulin in HCC, while collagen emerged as a more predictive component in the peritumoral liver. Moreover, our findings show that fiber-derived features provide independent prognostic value, augmenting conventional clinicopathologic parameters such as patient age, tumor multifocality, intravascular invasion, and pT stage.

Supplementary Materials: The following supporting information can be downloaded at: https://www.mdpi.com/article/10.3390/cancers16010106/s1, Table S1: GSPS staining protocol; Table S2: Models (N = 139) in which all variables exhibited a p-value of less than 0.05; Figure S1: Applied augmentations: rotation, flipping, blurring, zooming, and different amounts of annotation erosion and dilation applied to one image patch.

Author Contributions: Conceptualization, R.S., M.M., A.R., K.S. and A.L.; methodology, R.S., M.M., A.R., J.D. and A.L.; software, R.S., M.M., A.R. and R.A.; validation, J.D.; formal analysis, R.S., J.D. and R.A.; investigation, R.S., A.G. and M.M.; resources, R.S., A.G. and K.S.; data curation, R.S. and J.D.; writing—original draft preparation, R.S.; writing—review and editing, A.L., A.R., M.M., J.D., R.A., A.G. and K.S.; visualization, R.S. and M.M.; supervision, A.L.; project administration, R.S.; funding acquisition, A.L. and R.S. All authors have read and agreed to the published version of the manuscript.

Funding: This research was in part funded by the European Social Fund resources allocated to the project "Development of Doctoral Studies " implemented by the Research Council of Lithuania, project No. 09.3.3-ESFA-V-711-01-0001, under the specific objective to "Strengthen the Skills and Capacities of Public Sector Researchers for Engaging in High Level R & D Activities" of Priority Axis 9, "Educating the Society and Strengthening the Potential of Human Resources", within the framework of the Operational Program for the European Union Funds' Investments in 2014–2020.

Institutional Review Board Statement: The Lithuanian Bioethics Committee approved (permit number 2021/6-1354-843, issued 29 June 2021) the study design.

Informed Consent Statement: Patient consent was waived by the Vilnius Regional Biomedical Research Ethics Committee according to the International Ethical Guidelines for Health-related Research Involving Humans [36].

Data Availability Statement: The datasets generated during the study are not publicly available due to permit restrictions. However, they can be made available for collaborative work upon reasonable request, subject to the approval of our team regarding the intended use of the data. Interested parties should reach out with specific collaboration proposals for consideration.

Acknowledgments: The authors would like to thank their colleagues from the National Center of Pathology for their diagnostic work on the cases and the production of required material, IT support, and significantly contributions to other technical tasks that enabled the publication of these results. We would like to extend our gratitude to the entire team at the Center of Abdominal Surgery, Vilnius University Hospital Santaros Klinikos, for their work with HCC patients. Their efforts are central to our research and our main goal: better patient care. Finally, we would like to thank Vilnius University for their continuous commitment to advancing scientific research, and for providing the necessary foundation and support for our initiatives.

Conflicts of Interest: The authors declare no conflicts of interest.

References

1. Toh, M.R.; Wong, E.Y.T.; Wong, S.H.; Ng, A.W.T.; Loo, L.H.; Chow, P.K.H.; Ngeow, J. Global Epidemiology and Genetics of Hepatocellular Carcinoma. *Gastroenterology* **2023**, *164*, 766–782. [CrossRef] [PubMed]
2. Eswaran, S.L.; Reau, N.S. Hepatocellular Carcinoma: 5 Things to Know. Available online: https://www.medscape.com/viewarticle/925146?form=fpf (accessed on 15 September 2023).
3. Chrysavgis, L.; Giannakodimos, I.; Diamantopoulou, P.; Cholongitas, E. Non-alcoholic fatty liver disease and hepatocellular carcinoma: Clinical challenges of an intriguing link. *World J. Gastroenterol.* **2022**, *28*, 310–331. [CrossRef] [PubMed]
4. Vogel, A.; Meyer, T.; Sapisochin, G.; Salem, R.; Saborowski, A. Hepatocellular carcinoma. *Lancet* **2022**, *400*, 1345–1362. [CrossRef] [PubMed]
5. Younossi, Z.M.; Wong, G.; Anstee, Q.M.; Henry, L. The Global Burden of Liver Disease. *Clin. Gastroenterol. Hepatol.* **2023**, *21*, 1978–1991. [CrossRef] [PubMed]
6. Calderon-Martinez, E.; Landazuri-Navas, S.; Vilchez, E.; Cantu-Hernandez, R.; Mosquera-Moscoso, J.; Encalada, S.; Zevallos-Delgado, C.; Cinicola, J. Prognostic Scores and Survival Rates by Etiology of Hepatocellular Carcinoma: A Review. *J. Clin. Med. Res.* **2023**, *15*, 200–207. [CrossRef] [PubMed]
7. Eilard, M.S.; Naredi, P.; Helmersson, M.; Hemmingsson, O.; Isaksson, B.; Lindell, G.; Sandström, P.; Strömberg, C.; Rizell, M. Survival and prognostic factors after transplantation, resection and ablation in a national cohort of early hepatocellular carcinoma. *HPB* **2021**, *23*, 394–403. [CrossRef] [PubMed]
8. Reig, M.; Forner, A.; Rimola, J.; Ferrer-Fàbrega, J.; Burrel, M.; Garcia-Criado, Á.; Kelley, R.K.; Galle, P.R.; Mazzaferro, V.; Salem, R.; et al. BCLC strategy for prognosis prediction and treatment recommendation: The 2022 update. *J. Hepatol.* **2022**, *76*, 681–693. [CrossRef]
9. Mauro, E.; Forner, A. Barcelona Clinic Liver Cancer 2022 update: Linking prognosis prediction and evidence-based treatment recommendation with multidisciplinary clinical decision-making. *Liver Int.* **2022**, *42*, 488–491. [CrossRef]

10. Karsdal, M.A.; Daniels, S.J.; Holm Nielsen, S.; Bager, C.; Rasmussen, D.G.K.; Loomba, R.; Surabattula, R.; Villesen, I.F.; Luo, Y.; Shevell, D.; et al. Collagen biology and non-invasive biomarkers of liver fibrosis. *Liver Int.* **2020**, *40*, 736–750. [CrossRef]
11. Chen, D.; Liu, Z.; Liu, W.; Fu, M.; Jiang, W.; Xu, S.; Wang, G.; Chen, F.; Lu, J.; Chen, H.; et al. Predicting postoperative peritoneal metastasis in gastric cancer with serosal invasion using a collagen nomogram. *Nat. Commun.* **2021**, *12*, 179. [CrossRef]
12. Brett, E.A.; Sauter, M.A.; Machens, H.G.; Duscher, D. Tumor-associated collagen signatures: Pushing tumor boundaries. *Cancer Metab.* **2020**, *8*, 4. [CrossRef] [PubMed]
13. Pavithra, V.; Sowmya, S.V.; Rao, R.S.; Patil, S.; Augustine, D.; Haragannavar, V.C.; Nambiar, S. Tumor-associated collagen signatures: An insight. *World J. Dent.* **2017**, *8*, 224–230. [CrossRef]
14. Xi, G.; Guo, W.; Kang, D.; Ma, J.; Fu, F.; Qiu, L.; Zheng, L.; He, J.; Fang, N.; Chen, J.; et al. Large-scale tumor-associated collagen signatures identify high-risk breast cancer patients. *Theranostics* **2021**, *11*, 3229–3243. [CrossRef] [PubMed]
15. Bruckner, P. Suprastructures of extracellular matrices: Paradigms of functions controlled by aggregates rather than molecules. *Cell Tissue Res.* **2010**, *339*, 7–18. [CrossRef] [PubMed]
16. Rojkind, M.; Giambrone, M.A.; Biempica, L. Collagen Types in Normal and Cirrhotic Liver. *Gastroenterology* **1979**, *76*, 710–719. [CrossRef] [PubMed]
17. Karsdal, M.A.; Nielsen, S.H.; Leeming, D.J.; Langholm, L.L.; Nielsen, M.J.; Manon-Jensen, T.; Siebuhr, A.; Gudmann, N.S.; Rønnow, S.; Sand, J.M.; et al. The good and the bad collagens of fibrosis—Their role in signaling and organ function. *Adv. Drug Deliv. Rev.* **2017**, *121*, 43–56. [CrossRef] [PubMed]
18. Abrutyn, S.; Mueller, A.S. The role of CAFs and fibrosis in liver cancer. *Annu. Rev. Pathol.* **2015**, *79*, 211–227.
19. Zhang, R.; Ma, M.; Lin, X.H.; Liu, H.H.; Chen, J.; Chen, J.; Gao, D.M.; Cui, J.F.; Ren, Z.G.; Chen, R.X. Extracellular matrix collagen i promotes the tumor progression of residual hepatocellular carcinoma after heat treatment. *BMC Cancer* **2018**, *18*, 901. [CrossRef]
20. Bhattacharjee, S.; Hamberger, F.; Ravichandra, A.; Miller, M.; Nair, A.; Affo, S.; Filliol, A.; Chin, L.; Savage, T.M.; Yin, D.; et al. Tumor restriction by type I collagen opposes tumor-promoting effects of cancer-associated fibroblasts. *J. Clin. Investig.* **2021**, *131*, e146987. [CrossRef]
21. Burt, A.D.; Portmann, B.; Ferrell, L.D. *MacSween's Pathology of the Liver*, 6th ed.; Churchill Livingstone/Elsevier: Edinburgh, Scotland, 2012; 784p.
22. Hall, A.; Cotoi, C.; Luong, T.V.; Watkins, J.; Bhathal, P.; Quaglia, A. Collagen and elastic fibres in acute and chronic liver injury. *Sci. Rep.* **2021**, *11*, 14569. [CrossRef]
23. Allaume, P.; Turlin, B.; Bardou-Jacquet, E.; Lor, O.; Calderaro, J.; Khene, Z.e.; Acosta, O.; De Crevoisier, R.; Rioux-Leclercq, N.; Pecot, T. Artificial Intelligence-Based Opportunities in Liver Pathology—A Systematic Review. *Diagnostics* **2023**, *13*, 1799. [CrossRef]
24. Burt, A.D. Augmented liver pathology: Artificial intelligence and the assessment of hepatocellular neoplasms. *Histopathology* **2023**, *83*, 509–511. [CrossRef] [PubMed]
25. Patil, A.; Salvatori, R.; Smith, L.; Jenkins, S.M.; Cannon, A.; Hartley, C.P.; Graham, R.P.; Moreira, R.K. Artificial intelligence-based reticulin proportionate area—A novel histological outcome predictor in hepatocellular carcinoma. *Histopathology* **2023**, *83*, 512–525. [CrossRef] [PubMed]
26. Taylor-Weiner, A.; Pokkalla, H.; Han, L.; Jia, C.; Huss, R.; Chung, C.; Elliott, H.; Glass, B.; Pethia, K.; Carrasco-Zevallos, O.; et al. A Machine Learning Approach Enables Quantitative Measurement of Liver Histology and Disease Monitoring in NASH. *Hepatology* **2021**, *74*, 133–147. [CrossRef] [PubMed]
27. McGenity, C.; Randell, R.; Bellamy, C.; Burt, A.; Cratchley, A.; Goldin, R.; Hubscher, S.G.; Neil, D.A.; Quaglia, A.; Tiniakos, D.; et al. Survey of liver pathologists to assess attitudes towards digital pathology and artificial intelligence. *J. Clin. Pathol.* **2023**, *77*, 27–33. [CrossRef] [PubMed]
28. Morkunas, M.; Zilenaite, D.; Laurinaviciene, A.; Treigys, P.; Laurinavicius, A. Tumor collagen framework from bright-field histology images predicts overall survival of breast carcinoma patients. *Sci. Rep.* **2021**, *11*, 15474. [CrossRef] [PubMed]
29. Plancoulaine, B.; Laurinaviciene, A.; Herlin, P.; Besusparis, J.; Meskauskas, R.; Baltrusaityte, I.; Iqbal, Y.; Laurinavicius, A. A methodology for comprehensive breast cancer Ki67 labeling index with intra-tumor heterogeneity appraisal based on hexagonal tiling of digital image analysis data. *Virchows Arch.* **2015**, *467*, 711–722. [CrossRef]
30. Rasmusson, A.; Zilenaite, D.; Nestarenkaite, A.; Augulis, R.; Laurinaviciene, A.; Ostapenko, V.; Poskus, T.; Laurinavicius, A. Immunogradient Indicators for Antitumor Response Assessment by Automated Tumor-Stroma Interface Zone Detection. *Am. J. Pathol.* **2020**, *190*, 1309–1322. [CrossRef]
31. Kingma, D.P.; Ba, J. Adam: A Method for Stochastic Optimization. *arXiv* **2014**, arXiv:1412.6980. Available online: https://arxiv.org/abs/1412.6980 (accessed on 31 October 2023).
32. Nørredam, K. Primary Carcinoma of the Liver: Histological Study of 27 Cases of Primary Carcinoma of the Liver from Malawi. *Acta Pathol. Microbiol. Scand. A* **1977**, *85*, 461–469. [CrossRef]
33. Mózes, F.E.; Lee, J.A.; Vali, Y.; Alzoubi, O.; Staufer, K.; Trauner, M.; Paternostro, R.; Stauber, R.E.; Holleboom, A.G.; van Dijk, A.M.; et al. Performance of non-invasive tests and histology for the prediction of clinical outcomes in patients with non-alcoholic fatty liver disease: An individual participant data meta-analysis. *Lancet Gastroenterol. Hepatol.* **2023**, *8*, 704–713. [CrossRef] [PubMed]

34. Abeysekera, K.W.M.; Srivastava, A.; Rowe, I.; Jarvis, H.; Ryder, S.D.; Yeoman, A.; Dillon, J.F.; Rosenberg, W. Exploring changing attitudes to non-invasive liver fibrosis tests in secondary care pathways: Comparison of two national surveys. *Frontline Gastroenterol.* **2023**, *14*, 483–490. [CrossRef] [PubMed]
35. Johnson, P.J.; Berhane, S.; Kagebayashi, C.; Satomura, S.; Teng, M.; Reeves, H.L.; O'Beirne, J.; Fox, R.; Skowronska, A.; Palmer, D.; et al. Assessment of liver function in patients with hepatocellular carcinoma: A new evidence-based approach—The ALBI grade. *J. Clin. Oncol.* **2015**, *33*, 550–558. [CrossRef] [PubMed]
36. Council for International Organizations of Medical Sciences (CIOMS) in Collaboration with the World Health Organization (WHO). *International Ethical Guidelines for Health-Related Research Involving Humans*, 4th ed.; Biomedical Research: Geneva, Switzerland, 2016; pp. 1921–1931. Available online: https://cioms.ch/wp-content/uploads/2017/01/WEB-CIOMS-EthicalGuidelines.pdf (accessed on 31 October 2023).

3rd publication / 3 publikacija

Aiste Gulla, **Rokas Stulpinas**, Agne Grigonyte, Dovile Zilenaite-Petrulaitiene, Allan Rasmusson, Arvydas Laurinavicius, Kestutis Strupas

Overall Survival Prediction by Tumor Microenvironment Lymphocyte Distribution
in Hepatocellular Carcinoma After Liver Transplantation

J Surg Res. 2024 Mar;295:457-467

doi: 10.1016/j.jss.2023.10.011. Epub 2023 Dec 8. PMID: 38070260.

https://pubmed.ncbi.nlm.nih.gov/38070260/

Available online at www.sciencedirect.com

ScienceDirect

journal homepage: www.JournalofSurgicalResearch.com

Association for Academic Surgery

Overall Survival Prediction by Tumor Microenvironment Lymphocyte Distribution in Hepatocellular Carcinoma After Liver Transplantation

Aiste Gulla, MD, PhD,[a,1,*] *Rokas Stulpinas, MD,*[b,c,1] *Agne Grigonyte, MS,*[d] *Dovile Zilenaite-Petrulaitiene, PhD,*[b,c] *Allan Rasmusson, PhD,*[b,c] *Arvydas Laurinavicius, MD, PhD,*[b,c] *and Kestutis Strupas, MD, PhD*[a]

[a] *Faculty of Medicine, Institute of Clinical Medicine, Vilnius University, Vilnius, Lithuania*
[b] *Department of Pathology, Forensic Medicine and Pharmacology, Faculty of Medicine, Institute of Biomedical Sciences, Vilnius University, Vilnius, Lithuania*
[c] *National Center of Pathology, Affiliate of Vilnius University Hospital Santaros Clinics, Vilnius, Lithuania*
[d] *Faculty of Medicine, Vilnius University, Vilnius, Lithuania*

ARTICLE INFO

Article history:
Received 7 March 2023
Received in revised form
16 September 2023
Accepted 28 October 2023
Available online xxx

Keywords:
CD8+
Digital image analysis
Hepatocellular carcinoma
Immunohistochemistry
Transplantation

ABSTRACT

Introduction: Our previous research demonstrated that CD8+ cell density profiling using a hexagonal grid-based digital image analysis method provides predictors of patient outcomes after liver resection due to hepatocellular carcinoma (HCC). Continuing our study, we have further investigated the applicability of the methodology to patients receiving a liver transplant for HCC.

Methods: The retrospective study enrolled patients with HCC who underwent liver transplantation (LT) at the Vilnius University Hospital Santaros Clinics between 2007 and 2020. We determined the density profiles of CD8+ lymphocytes at the interface between HCC and stroma and the interface between the perineoplastic liver parenchyma and stroma. Both digital image analysis and the hexagonal grid-based immunogradient method were applied to CD8+ immunohistochemistry images. Survival statistics based on clinicopathological, peripheral blood analysis, and surgical data determined the prognostic value of these indicators.

Results: Univariate clinicopathological predictors of worse OS after LT included: patient's age at the time of the transplantation, a higher number of HCC nodules, lower platelet count, longer activated thromboplastin time, lower serum albumin, higher serum total bilirubin, and lower serum creatinine levels. The two independent predictors of overall survival were mean CD8+ cell density at the epithelial edge of the explanted liver parenchyma-stroma interface and peripheral blood platelet count.

* *Corresponding author*. Institute of Clinical Medicine, Faculty of Medicine, Vilnius University, Vilnius LT-01513, Lithuania.
E-mail address: aiste.kielaite-gulla@mf.vu.lt (A. Gulla).
[1] AiG and RS contributed equally to this paper and share first authorship.
0022-4804/$ – see front matter
https://doi.org/10.1016/j.jss.2023.10.011

Conclusions: Our model discloses that preoperative peripheral blood platelet count and mean CD8+ cell density at the epithelial edge of nonmalignant interface in the explanted liver parenchyma are independent predictors of OS for HCC after LT.

Introduction

Hepatocellular carcinoma (HCC) accounts for ~75% of all liver cancers and is the fourth leading cause of cancer mortality worldwide.[1,2] Despite scientific progress in the field of HCC, the prognosis of HCC patients remains poor and cancer-related mortality continues to increase in many countries.[3,4] In most cases, risk factors for HCC are liver cirrhosis, viral hepatitis B and C, nonalcoholic fatty liver disease, diabetes, and alcohol consumption.[4] Partial liver resection or liver transplantation (LT) continue to be the main options of curative therapy for early-stage HCC. Both surgical options may result in similar survival rates; however, HCC recurrence rates are significantly different. According to the literature, the 5-y survival rate after partial liver resection for HCC is 50%-68%, unfortunately, the 5-y recurrence rate is around 50%-70%.[5] A 4- to 5-y survival rate varies from 75% to 61%, and a recurrence rate of 17% for patients who meet the Milan criteria for LT.[5] While model for end-stage liver disease (MELD) score is used, preoperative laboratory data could predict posttreatment survival and influence the surgical decision of patients who undergo liver resection or transplantation for early HCC. Detailed preoperative evaluation of the liver function and use of the Child-Pugh scoring system could influence treatment decisions, as reduced liver function (Child-Pugh 6 and >7, albumin <36 g/L) could be associated with a decreased risk in the transplantation group, but increased risk in resected patients.[6] The improved outcomes among resected patients are plausible due to advances in the surgical field, perioperative management, and the development of multimodal treatment strategies. Salehi *et al.* reported that HCC differentiation and liver fibrosis could synergistically determine the efficacy of liver resection *versus* transplantation.[7] According to the authors, while transplantation confers survival benefits for well and moderately differentiated tumors, resection is equivalent to transplantation in patients with poorly differentiated HCC, and low liver fibrosis.[8] Pathological analysis of the tumor offers insights into the microenvironment of the cancer-host interaction and its impact on the prognosis of HCC patients.

While tumor immune microenvironment in HCC includes cancer cells, subsets of innate and adaptive immune cells, stromal, endothelial cells, and the extracellular matrix and is a crucial factor in the cancerogenesis of HCC,[9] digital pathology is gaining momentum, image analysis and artificial intelligence systems are constantly proven to be useful in both inflammatory and neoplastic liver diseases, yet their everyday clinical utility remains very limited.[10]

Host immune cells, such as tumor-infiltrating lymphocytes (TILs), play a pivotal role in the antitumoral response. TILs are a group of lymphocytes located around tumor cells and constitute a prognostic factor in HCC. A retrospective study by Min Du *et al.* concluded that patients having a high number of infiltrating lymphocytes tend to have a lower recurrence rate and fewer microvascular invasion.[11] The most common subsets of TILs are CD3+, CD4+, CD8+, and FoxP3+ T lymphocytes. Specifically, CD8+ lymphocytes belong to cytotoxic T cells, which are responsible for the elimination of target cells and work as key effectors of antitumor immunity.[12]

A meta-analysis analyzing the prognostic value of TILs in HCC concluded that patients with high levels of CD8+ TILs had longer overall survival (OS) and recurrence-free survival, compared to patients with lower levels of TILs.[12] Furthermore, precise spatial mapping of CD8+ lymphocyte infiltration in the tissue is crucial, as patients with high density of CD8+ cells in the center of HCC or at the margin of the tumor may have a better OS.[13] We have recently published results of a study investigating the prognostic role of CD8+ lymphocytes after liver resection due to HCC.[14] A hexagonal grid-based digital image analysis method[15] was used to determine the CD8+ lymphocytes density profiles in whole-slide immunohistochemistry images. CD8+ lymphocytes were independently analyzed in two areas of the same tissue section. One area included HCC with the surrounding fibrovascular stroma, with CD8+ lymphocytes representing the anti-tumoral response that is beneficial to the host. The second area contained the peritumoral liver parenchyma, with CD8+ cytotoxic cells representing an opposite detrimental effect on the remaining functional liver parenchyma. The results showed that five independent factors, including standard deviation of CD8+ density along the tumor edge, mean CD8+ density in the perineoplastic liver, duration of surgery, aspartate transaminase levels and preoperative blood basophil count, can be combined to predict patient outcomes after liver resection. Furthermore, a comprehensive OS score combining the five independent predictors provided statistically significant prognostic stratification: patients with scores 0-1 had a low risk (5-y OS 76%), score 2 had an intermediate risk (5-y OS 40%), and scores 3-5 had a high risk (5-y OS 8%).

In this study we have explored the applicability of CD8+ lymphocyte density profiling using a hexagonal grid-based method in HCC and surrounding liver parenchyma regions in a new cohort of patients who underwent LT. The generated CD8+ distribution indicators were tested using the OS analysis along the conventional clinical variables. Cause-of-death analysis and results of previously published prognostic OS score is also provided.

Materials and Methods

Study population

Approval from the Vilnius Regional Bioethics Committee (Permit #2021/6-1354-843, issued June 29, 2021) defined the study timeframe between 2007 and 2020, and waived the requirement of individual informed consent according to the

International Ethical Guidelines for Health-related Research Involving Humans.[16] During this period, a total of 28 patients received a liver transplant for HCC at the Vilnius University Hospital Santaros Clinics and had archived tissue stored at the National Center of Pathology (Vilnius, Lithuania). Clinical, pathological, and laboratory data were retrospectively collected.

The gender ratio of the transplanted cohort was close to 2:1 with male predominance (19 men and nine women). All patients were caucasians with the median age of 54 y (range 18-64). The median follow-up time after transplantation was 61 mo (range 0-175). During the follow-up period, seven transplanted patients have died, five patients <30 d, and two >30 d after transplantation. Most of the explanted livers had 1 HCC nodule ($n = 19$, 68%). All patients met the Milan criteria for transplantation.[17] The majority of patients had a history of viral hepatitis C ($n = 21$, 75%). A single case of HCC recurrence after LT with disease free-survival of 340 d was recorded. In most cases, the HCC was grade G2 ($n = 22$, 79%) and more than half of the patients had stage T1 cancer ($n = 15$, 54%). Tumor size varied from 0.9 to 4.2 cm, and the median tumor size was 2.6 cm. The median duration of LT was 453 min (range 315-720 min) and median blood loss during the operation was 1750 mL (range 100-9000 mL). The median hospitalization time was 23 d (range 2-169 d). A summary of patient and tumor characteristics is presented in Table 1.

Preoperative blood tests were performed before the transplantation. Summary of preoperative laboratory findings are listed in Table 2.

Study workflow

Following the workflow of previous study on the resected HCC patients[14] a pathologist (R.S.) reviewed all available archived hematoxylin and eosin slides to select an formalin-fixed paraffin-embedded block including both HCC tissue and liver parenchyma. 3 μm samples were cut, mounted on positively charged slides and stained for CD8 (Dako, C8/144B, 1:100) using Ventana BenchMark ULTRA and ultraView Universal DAB Detection kit (Ventana Medical Systems, USA). The prepared immunohistochemical (IHC) slides were digitized at 20× (0.5 μm/pixel) using a ScanScope XT scanner (Leica Aperio Technologies, USA). We have used the same HALO artificial intelligence (Indica Labs, USA) digital image analysis system that was previously trained to segment the tissue into hepatocytes, fibrovascular stroma, glass, and debris classes (Fig. 1E and F). CD8 positive lymphocytes (cells with brown cytoplasmic staining on IHC) were identified using the Multiplex IHC algorithm (Indica Labs, USA) (Fig. 1H).

A pathologist placed manual annotations marking two areas of interest on each of the slides: one area included viable cancer tissue with its capsule, the second included nonneoplastic peritumoral liver parenchyma (Fig. 1D). Tissue with staining or coagulation artifacts, poor visual quality, or ambiguous atypia were excluded. These two areas were further analyzed separately using digital microscopy image analytics based on hexagonal grid tiling as described by Rasmusson *et al.*[15] Briefly, a hexagonal grid is overlayed on the immunohistochemistry image with a tissue classifier map generated in a previous step. The composition of each

Table 1 – Demographics, clinicopathological, and follow-up characteristics of the patients who underwent LT for HCC at the Vilnius University Hospital Santaros Clinics between 2007 and 2020.

Characteristic	Value
Patients	28 (100%)
Age, years	
Mean (range)	52.5 (18-64)
Median	54
Gender	
Male	19 (68%)
Female	9 (32%)
Race	
White	28 (100%)
Black	0 (0%)
Asian	0 (0%)
Latin	0 (0%)
Other	0 (0%)
Follow up time, months	
Median (range)	61 (0-175)
Deceased	7 (25%)
Posttransplant recurrence and RFS time, days	
Recurrences	1 (3.6%)
Time	340
Milan criteria for transplantation	
Within	28 (100%)
Exceeded	0
Tumor nodules	
1	19 (67.9%)
2	6 (21.4%)
3	3 (10.7%)
HCC grade	
G1	5
G2	22
G3	1
pT stage	
T1	15 (53.6%)
T2	13 (46.4%)
T3	0
T4	0
Largest tumor dimension, mm	
Mean (range)	25 (9-42)
Median	26
History of viral infection	
HBV	3 (10.7%)
HCV	21 (75%)
None or unknown	4 (14.3%)
Hospitalization time, days	
Mean (range)	34 (2-169)
Median	23
Duration of surgery, min	
Mean (range)	469 (315-720)

(*continued*)

Table 1 – (*continued*)

Characteristic	Value
Median	453
Blood loss during surgery, mL	$n = 26$*
Mean (range)	2497 (100-9000)
Median	1750

RFS = relapse-free survival; HCC = hepatocellular carcinoma; pT = pathological T stage; HBV = hepatitis B virus; HCV = hepatitis C virus.
* The exact amount of lost blood was not reported in one of the cases (stating "a lot"), in the second case the amount was reported to be "1.5 mL", what probably is a mistake. These cases are excluded.

hexagon having a 65 μm side length is assessed by measuring the proportion of every tissue class in the covered area. The boundary of interest, which is this study is named epithelial edge (TE) since it exists between the hepatocytes (both benign and malignant) and fibrous tissue (stoma) is then detected based upon the abrupt changes in fractions of the two tissue classes. Hexagons on the TE, (as named in the original paper by Rasmusson *et al.*[15]) are given a rank of 0 (zero) and the hexagons on both sides of TE are assigned either positive (if overlaying hepatocytes) or negative (if overlaying stroma) number with its value being the shortest distance to the nearest rank 0 hexagon (Fig. 1I). As each hexagon has a known number of positive CD8+ lymphocytes within its limits (identified using a Multiplex IHC algorithm), multiple indicators can be calculated (Fig. 1K) to reflect the spatial distribution of immune cells in relation to the edge of the tumor or liver parenchyma (Fig. 1J). Width of the interface zone (IZ), being the number of hexagons between the largest positive and negative rank used for analysis, was chosen to be five and include hexagons with ranks −2, −1, 0, 1, and 2.

Indicators, statistical analysis and modeling

Indicators reflecting the spatial CD8+ cell distribution were independently calculated for the HCC (IZ between tumor and stroma) and peritumoral liver (IZ between nonneoplastic hepatocytes and the fibrous tissue in the remaining parenchyma) compartments to reflect the two separate processes driven by CD8+ lymphocytes as discussed previously.[14] The mean density and standard deviation of CD8+ cells are calculated for the epithelial (i.e., either benign or malignant, depending on the annotation used, positive ranks 1-2), stroma (negative ranks −2, −1) and TE (rank 0) aspects of the IZ. Combined indicators—center of mass (CM, briefly CD8+ cell density differences on either side of rank 0) and immunodrop (ID, a measure of abrupt change in CD8+ density between rank 1 and −1) – representing the whole IZ are also computed as described by Rasmusson *et al.*[15]

As expected from previous studies[14,15,18] the density distributions of CD8+ lymphocytes showed a left asymmetry, so values were logarithm-transformed for further analysis using parametric statistics. A freely available application "Cutoff Finder" was used to dichotomize the continuous indicators with respect to survival outcome.[19] Kaplan–Meier method followed by log-rank testing was used to compare the

Table 2 – Summary of preoperative blood test of the patients who underwent LT for HCC at the Vilnius University Hospital Santaros Clinics between 2007 and 2020.

Variable	Mean	Median	Min	Max	N
LEU, $\times 10^9$/L	5.87	5.05	1.78	15.39	28
LYM, $\times 10^9$/L	1.47	1.38	0.28	2.88	28
Mon, $\times 10^9$/L	0.71	0.61	0.14	1.67	28
EOS, $\times 10^9$/L	0.35	0.16	0.00	4.90	28
BAS, $\times 10^9$/L	0.07	0.03	0.00	0.80	28
NEU, $\times 10^9$/L	4.49	2.94	1.10	30.60	28
RBC, $\times 10^{12}$/L	3.84	3.85	1.56	5.28	28
Hemoglobin g/L	125.62	129.00	56.00	168.00	28
Hematocrit %	0.37	0.36	0.20	0.50	28
Albumin, g/L	30.16	28.50	15.70	48.50	28
Creatinine, μmol/l	69.54	63.00	46.00	129.00	28
INR	1.56	1.45	1.00	3.15	28
CRP, mg/l	8.11	8.00	0.90	30.60	28
Total bilirubin, μmol/l	57.19	37.30	6.20	269.90	28
Alanine transaminase (ALT), U/l	80.54	51.00	15.00	432.00	28
Aspartate transaminase (AST), U/l	98.64	84.00	22.00	286.00	28
Alkaline phosphatase (ALP), U/l	163.32	157.50	85.00	346.00	28
Gamma-glutamyl transferase (GGT), U/l	76.96	73.00	19.00	264.00	28
Alpha fetoprotein (AFP), kU/l	52.92	7.38	2.23	474.00	28

LEU = leukocytes; LYM = lymphocytes; MON = monocytes; EOS = eosinophils; BAS = basophils; NEU = neutrophils; RBC = red blood cell; INR = international normalised ratio; CRP = C-reactive protein.

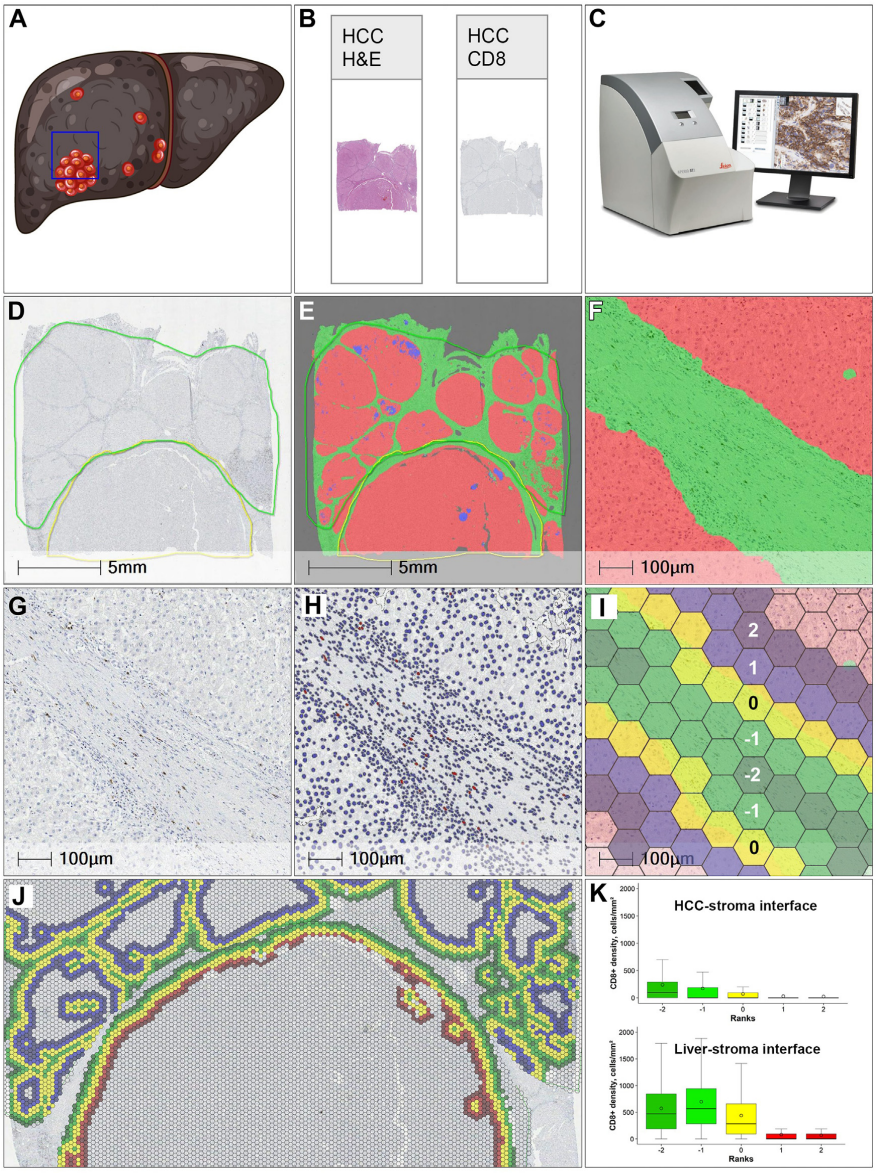

Fig. 1 – Study workflow: (A) explanted liver is sent for pathological examination (image: Freepik.com), (B) hematoxylin-eosin (H&E) and immunohistochemical CD8 slides were used for the study, (C) the slides were scanned using a Leica Aperio ScanScope XT (image: PRNewsfoto/Leica Biosystems), (D) hepatocellular carcinoma (HCC) and adjacent liver parenchyma areas marked by a pathologist on a digitized CD8 slide, (E-F) HALO AI (Indica Labs, USA) automated tissue segmentation, red–epithelium, green–stroma, (G) magnified area of the CD8 immunohistochemistry slide, (H) result of Multiplex IHC (Indica Labs, USA) nuclear segmentation algorithm, red–CD8+ positive cells, (I) overlayed hexagonal grid and ranks, (J) the two interface zones detected based on the selection depicted in Panel D, blue–liver parenchyma, red–HCC, (K) sample CD8+ lymphocyte distribution density charts hexagonal grid and ranks, (J) the two interface zones, blue–liver parenchyma, red–HCC, (K) sample CD8+ distribution density charts across the ranks of the two interface zones.

differences between OS distributions. Cox regression proportional hazards models were utilized to evaluate the independent prognostic significance of immunogradient indicators in relation to clinicopathological variables. Statistical analyses were performed using SAS software (SAS Institute Inc, Cary, North Carolina, USA).

Results

Comparison of OS between the surgical liver resection versus LT for HCC cohorts

The survival data of the previously studied group of HCC patients after liver resection were compared to the new transplant cohort (Fig. 2). The long-term survival probability was significantly higher in the transplant branch ($P < 0.01$), facilitating further detailed analysis of survival determining factors for this cohort.

Univariate predictors of OS

From the characteristics of the patients, only age was found to be a statistically significant univariate predictor: younger age (<51.5 y) negatively associates with OS after transplantation (hazard ratio [HR] 0.18, 95% CI 0.03-0.91, $P = 0.02$). The 3 HCC nodules compared to 1-2 HCC nodules revealed by magnetic resonance imaging and computed tomography scans had a negative association with survival (HR 7.29, 95% CI 1.21-43.85, $P = 0.03$). Hospitalization time or the duration of transplantation procedure did not associate with OS. After testing the findings of the complete preoperative blood test, only the platelet count >70.8 $\times$ 10^9/L showed a statistically significant positive association with OS (HR 0.15, 95% CI 0.03-0.81, $P = 0.01$). The preoperative coagulation panel revealed that activated partial thromboplastin time <40.1s (HR > 100, 95% CI 0-inf, $P = 0.01$) positively influences OS. Analysis of preoperative laboratory findings revealed that albumin >32.8 g/L (HR < 0.01, 95% CI 0-inf, $P = 0.04$), total bilirubin <45 μmol/L (HR 5, 95% CI 0.97-25.90, $P = 0.03$), and creatinine >63 μmol/L (HR 0.13, 95% CI 0.02-1.12, $P = 0.02$) had a statistically significance on OS. The indicators of lower CD8+ lymphocyte density in the nonmalignant areas: both the low global CD8 density across the entire epithelial or stromal aspects of the explanted liver parenchyma and the low mean CD8+ lymphocyte density indicators in the automatically extracted IZ were associated with a shorter OS time in univariate analysis. Table 3 contains the statistically significant results of the univariate OS analysis with the HR and log-rank test. Figure 3 shows the Kaplan–Meier survival probability plots for variables.

Independent predictors of OS

The statistically significant univariate predictors OS were further assessed through Cox multivariate regression analysis. The results indicated that two factors were independently predictive of OS: the mean density of CD8+ at the TE of the nonmalignant IZ (HR 0.0291, $P = 0.03$) and the preoperative platelet count (HR 0.0291, $P = 0.03$). The model demonstrated strong statistical significance, with a likelihood ratio of 11.32 and a P value of <0.01.

Prognostic scoring

In the previous study of patients with HCC after liver resection, a combined risk score was developed.[14] According to this system, 2 (7%) patients in the transplanted cohort would be classified as having a low risk, eleven (39%) as having intermediate risk, and fifteen (54%) would fall into the high-risk

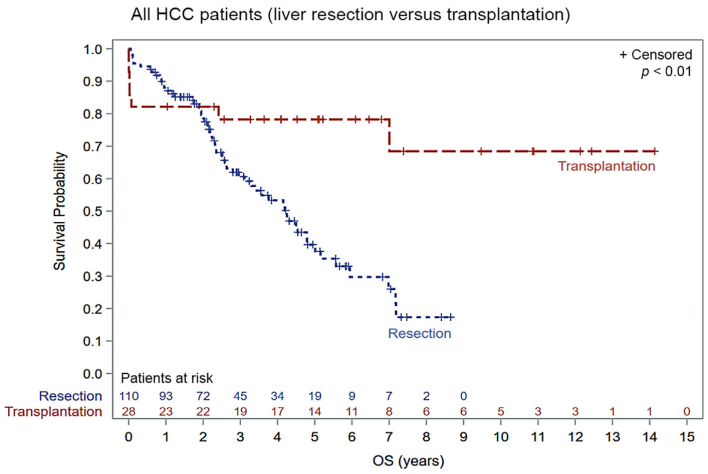

Fig. 2 – Kaplan-Meyer chart for overall survival of hepatocellular carcinoma (HCC) patients treated at the Vilnius University Hospital Santaros Clinics between 2007 and 2020: LTs (red curve) *versus* liver resections (blue curve).

Table 3 – Statistically significant univariate predictors of overall survival of the patients who underwent LT for HCC at the Vilnius University Hospital Santaros Clinics between 2007 and 2020.

Variable	Cutoff	HR	95% CI	P-value
Age, years	51.5	0.18	0.03-0.91	0.02
Number of HCC nodules	3 (vs 1-2)	7.29	1.21-43.85	0.03
Activated partial thromboplastin time, s	40.1	>100	0-∞	0.01
Serum albumin, g/l	32.8	<0.01	0-∞	0.04
Creatinine, μmol/l	63	0.13	0.02-1.12	0.02
Total bilirubin, μmol/l	45	5.00	0.97-25.90	0.03
Platelet count, $\times 10^9$/L	70.8	0.15	0.03-0.81	0.01
Global CD8 density in the epithelial aspect of the nonmalignant liver parenchyma, cells/mm^2	112.3278	0.13	0.01-1.08	0.03
Global CD8 density in the stromal aspect of the nonmalignant liver parenchyma, cells/mm2	630.4228	0.16	0.02-1.29	0.05
Mean CD8 density in the epithelial aspect of the nonmalignant IZ, log-transformed	4.712474	0.13	0.01-1.08	0.03
Mean CD8 density at the epithelial edge (TE) of the nonmalignant IZ, log-transformed	5.803012	0.15	0.03-0.82	0.01
Standard deviation of the mean CD8 density at the epithelial edge of the nonmalignant IZ, log-transformed	5.842227	0.15	0.03-0.82	0.01

HCC = hepatocellular carcinoma; IZ = interface zone.

category. No deaths were recorded in the low-risk group, five patients died in the intermediate-risk, and two in the high-risk group, yet if early (<30 d after transplantation) deaths are excluded, both intermediate and high-risk groups contain a single terminal event each. Combining patients into a low-risk group with 100% 5-y OS, and an intermediate-high-risk group with 77% 5-y OS provided a wider OS curve separation, yet the result is not statistically significant, as the number of patients is very low (see Fig. 4).

Cause-of-death analysis

Seven patients (25%) have died during the study period. Characteristics and causes of death are presented in Table 4. We divided deceased patients into two groups according to the MELD score (MELD ≤ 20 and > 20) (Table 5). In our cohort, only one patient had HCC recurrence with 340 d of recurrence-free survival, which fits the time described in the literature. However, this patient died 6 mo after the diagnosis of recurrence. The patient was listed for LT 1 y after the diagnosis of hepatitis C viral liver cirrhosis. The patient was on a waiting list for 176 d, during this period since HCC was diagnosed. At the time of transplantation, the patient still met the Milan criteria. One year after LT, multifocal HCC recurred in the liver and radiofrequency ablation was performed. Despite treatment, a few months later, multifocal lung metastasis was found. GEMOX chemotherapy was initiated, but a few months later the patient died. From a pathological explanted liver report, it is known that this patient had pathologically confirmed macrovascular invasion and a preoperative tumor size of 4.9 cm. The patient also had a preoperative AFP on the higher side: 181.00 kU/l (cohort range 2.11-474.00 kU/l, median

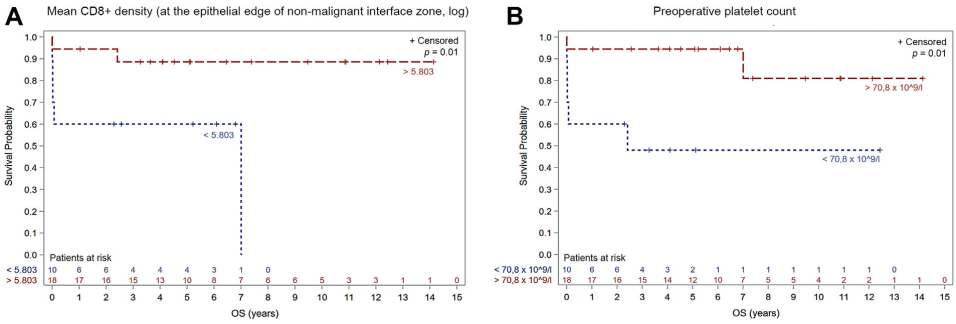

Fig. 3 – Kaplan–Meier overall survival (OS) plots of hepatocellular carcinoma (HCC) patients who underwent LT at the Vilnius University Hospital Santaros Clinics between 2007 and 2020: (A) mean CD8+ density at the epithelial edge of non-malignant interface zone, log-transformed, (B) preoperative peripheral blood platelet count.

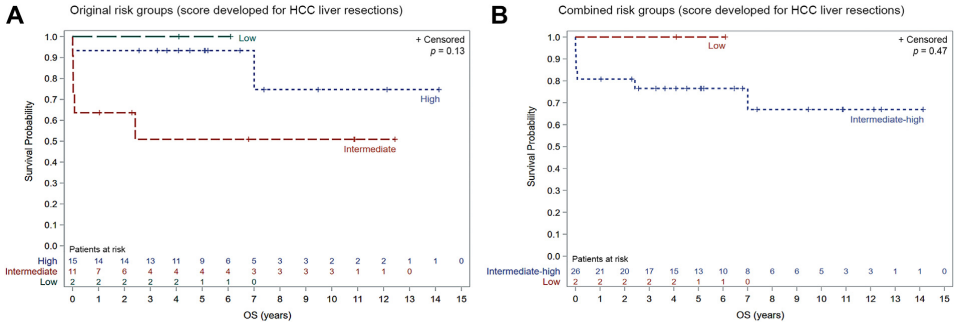

Fig. 4 – Kaplan–Meier overall survival (OS) plots of hepatocellular carcinoma (HCC) patients who underwent LT at the Vilnius University Hospital Santaros Clinics between 2007 and 2020: (A) classified according to the previously developed risk scoring system for HCC patients who underwent liver resections. (B) combining high and intermediate risk groups into a single category.

7.38). From the CD8 + immune response point of view, the patient did not have a single unique value in any of the CD8+ immunogradient indicators (both in the tumor or in the liver).

Discussion

Liver transplantation provides excellent long-term outcomes for certain patients with HCC, pushing to not simply rely on tumor size and number.[20] Although centers use strict selection criteria, there is a risk of recurrence, reaching up to 20% which is mostly observed within 2 y following procedure, bringing the survival between 7 and 16 mo.[21] While tumor recurrences are encountered in patients who underwent either liver resection or transplantation, the correct selection of candidates for the chosen treatment is essential to decrease tumor recurrence while maximizing posttransplantation survival rates.[22] Compared to LT, liver resection for localized HCC is associated with higher rates of recurrence and disease-related mortality.[23] Furthermore, postoperative morbidity is higher after liver resection than after LT for HCC under Milan criteria for cirrhotic patients.[7] Despite the limitations mentioned above, LT is considered the best treatment option for HCC in the cirrhotic liver as it cures both the underlying liver disease and the tumor.[24] Despite restrictive criteria for LT, HCC recurrence affects around 6%-20% of patients after transplantation.[25,26] Recurrence of HCC is a significant predictor of survival after LT. Several risk factors before and after transplantation influence the frequency of HCC recurrence. Risk factors include Milan criteria restrictions (number and size of nodules and vascular invasion), hepatitis B virus or hepatitis C virus viral infection, bridging therapy response, time to transplantation, the alpha-fetoprotein level, histopathological examination, immunosuppression, adjuvant, etc.[25] The majority of HCC recurs within 2 y after LT with a median of 17.8 mo time to recurrence and overall median survival being 12.4 mo after recurrence.[27] Primarily, the extrahepatic sites of recurrence are lungs and bones, while only one-third of recurrences are seen in the liver.[25,27] Since there are no established guidelines for the management of HCC recurrence post-LT, it is considered to be individualized. Potentially the most effective radical treatment for HCC recurrence after LT is surgical resection and repeated LT is not recommended. Other treatment options include ablation, palliative options such as intra-arterial therapies (chemo- or radioembolization), and systemic chemotherapy.[25,26]

The prognostic value of TILs for survival in patients with HCC is still contradictory. Separate subsets of TILs have a different effect on the progression of HCC, contributing to a different prognosis. CD8+ is a surface antigen of cytotoxic T

Table 4 – Deceased patients who underwent LT for HCC at the Vilnius University Hospital Santaros Clinics between 2007 and 2020.

ID	Age	Gender	LVI	Recurrence	Survival	Reported cause of death
HCC-012	50	Female	No	No	1 d	K75 other inflammatory liver diseases
HCC-114	46	Male	No	No	2 d	K72.1 Chronic hepatic failure
HCC-096	57	Male	No	No	8 d	B18.2 Chronic viral hepatitis C
HCC-051	43	Female	No	No	9 d	K74.6 other and unspecified cirrhosis
HCC-113	48	Male	Yes	No	27 d	B18.1 Chronic viral hepatitis B
HCC-131	56	Female	Yes	340 d	883 d	C22. 0 liver cell carcinoma
HCC-110	50	Male	No	No	2559 d	Y83.0 late transplant complications

lymphocytes that play a key role in the antitumor immune response.[13] A meta-analysis suggests that CD8+ lymphocytes could not only be a promising prognostic factor for OS but also low levels of CD8+ can predict a larger tumor size and a later TNM stage. Moreover, patients with higher infiltration of CD8+ cells tend to have better OS in the groups with Asian patients and better disease-free survival in all subgroups, including ethnicity.[28] HCC patients with a high number of CD8+ tumor infiltrating lymphocytes are prone to have a lower recurrence rate and less microvascular invasion.[11] CD8+ lymphocyte infiltration can be assessed by immunohistochemistry from a preoperative liver biopsy, in order to identify patients at high risk of recurrence who could be considered for LT rather than liver resection.[29]

In our study the prognostic value of CD8+ lymphocyte infiltration for the OS of patients after LT due to HCC was explored separately in tumor and peritumoral liver parenchyma along the conventional clinicopathological parameters. We have observed that none of the tumor parameters independently influenced the OS of the patients after LT. The two independent predictors of a longer OS are the higher mean CD8+ density at the TE of the automatically detected nonmalignant IZ, and a higher preoperative platelet count.

Data on patients after liver resection show that high CD8+ lymphocyte density in the center of the tumor and at the tumor margin had better OS, a lower rate of recurrence and a prolonged relapse-free survival.[12,30] Another study shows that a high density of CD8+ cells in the invasive front and peritumor tissue tends to have more prolonged progression-free survival.[11] These studies suggested reassessing the value of CD8+ lymphocytes in transplanted patients. Our previous study of the prognostic value of CD8+ lymphocyte distributions in resected liver samples found that the higher mean density of CD8+ lymphocytes within the epithelial aspect of the perineoplastic liver-stroma interface was an independent predictor of worse OS.[14] The higher number of CD8+ cells in the peritumor tissue in the resected or explanted liver samples may indicate an active inflammatory process and liver damage. This leads us to consider that a reduced liver function (Child-Pugh 6 and >7, albumin <36 g/L) could be associated with a decreased risk after transplantation, but increased risk after liver resection.[6]

According to our findings, another independent predictor of longer OS is a higher preoperative platelet count. A review article investigating the relationship between platelet count and liver regeneration after liver surgery claims that thrombocytopenia before liver resection could serve as a risk factor for hospital mortality, postoperative morbidity, and HCC recurrence. The same article notes that patients with a preoperative platelet count $<150 \times 10^9$/L (especially $<100 \times 10^9$/L), had a higher incidence of posthepatectomy liver failure and mortality.[31] On the other hand, a high pretransplant platelet count could cause a hypercoagulable state, increasing thromboembolic events after LT.[31] Pretransplant platelet count $>49.5 \times 10^9$/L could be an adverse prognostic predictor of posttransplant portal vein complication and early allograft dysfunction.[32] Interestingly, a high preoperative platelet count value could serve as a protective factor against liver damage and HCC recurrence and at the same time act as a pro

Table 5 – Characteristics of deceased patients who underwent LT for HCC at the Vilnius University Hospital Santaros Clinics between 2007 and 2020 according to MELD score.

Characteristic	MELD ≤20	MELD >20
Patients	5 (100%)	2 (100%)
Age, years		
Mean (range)	50.4 (43-57)	49 (48-50)
Median	50	49
Gender		
Male	3 (60%)	1 (50%)
Female	2 (40%)	1 (50%)
Follow-up time, days		
Median (range)	15 (2-2525)	14 (2-26)
Deceased ≤30 d after Tx	3 (60%)	2 (100%)
Deceased >30 d after Tx	2 (40%)	0
Post Tx HCC recurrence and RFS time, days		
Recurrences	1 (%)	0
Time	340	
HCC grade		
G1	3 (60%)	0
G2	2 (40%)	2 (100%)
G3	0	0
pT stage		
T1	4 (80%)	0
T2	1 (20%)	2 (100%)
T3	0	0
T4	0	0
Milan criteria for Tx		
Within	5 (100%)	2 (100%)
History of viral infection		
HBV	0	1 (50%)
HCV	5 (100%)	0
None	0	1 (50%)
Time between liver disease diagnosis and HCC diagnosis, years		
Mean (range)	5.8 (0-12)	11.5 (6-17)
Median	7	11.5
Time between HCC diagnosis and enrollment in the Tx list, months		
Mean (range)	30 (0-60)	0.8 (0-3)
Median	30	0
Time on the Tx list, days		
Mean (range)	118.8 (2-204)	300.5 (236-365)
Median	163	0
Duration of surgery, min		
Mean (range)	515 (345-720)	467.5 (465-470)
Median	420	467.5
Blood loss during surgery, mL		

(continued)

Table 5 – (continued)

Characteristic	MELD ≤20	MELD >20
Mean (range)	4180 (1100-9000)	2600 (1200-4000)
Median	4500	2600

MELD = model for end-stage liver disease; RFS = relapse-free survival; HCC = hepatocellular carcinoma; Tx = transplantation; pT = pathological T stage.

coagulator. In our study, a higher pretransplant platelet count served as an indicator of longer OS. This leads to a further discussion of preoperative platelet count importance since it could serve differently between patients who underwent liver resection or transplantation. The study has several limitations: a) small sample size and b) preoperative tumor or nontumor liver biopsies were not included for analysis.

Conclusions

We conclude that preoperative platelet count and mean CD8+ cell density at the TE of nonmalignant interface in the explanted liver parenchyma could serve as independent predictors for OS after LT. More studies are needed to validate the findings.

Study Type

Retrospective analysis.

Author Contributions

RS, AiG, AL, KS and AR designed the study. RS collected the samples for the IHC study. AiG, KS, and AgG reviewed and collected the clinical data. RS, DZP, and AR performed digital image analysis. RS and DZP performed statistical analysis. AiG and RS drafted the essential parts of the manuscript. All authors reviewed the analysis results and read and approved the final manuscript.

Acknowledgments

The authors would like to thank their colleagues from the National Center of Pathology for the valuable help in producing IHC slides, diagnostic work on the cases, IT support, and significantly contributing to many other technical tasks that enabled the publication of these results. Images from Freepik.com and PRNewsfoto/Leica Biosystems were used for Figure 1A and C, respectively.

Disclosure

The authors declare that the research was conducted in the absence of any commercial or financial relationship that could be construed as a potential conflict of interest.

Funding

This research partly is funded by the European Social Fund resources allocated for the project "Development of Doctoral Studies" implemented by Research Council of Lithuania, project No. 09.3.3-ESFA-V-711-01-0001, under the Specific objective "Strengthen the Skills and Capacities of Public Sector Researchers for Engaging in High Level R & D Activities" of Priority Axis 9 "Educating the Society and Strengthening the Potential of Human Resources" within the framework of the Operational Program for the European Union Funds' Investments in 2014-2020.

Availability of Data

The raw data supporting the conclusions of this article will be made available by the authors, without undue reservation.

Meeting Presentation

The data was presented at the Academic Surgical Congress, 2023, Session 54- Clinical/Outcomes: Transplantation Quickshot Session I. Presentation Name: "Value of CD8+ and Feasibility of Liver Transplantation for Hepatocellular Carcinoma" (Abstract ID: ASC20230902), presenter- Aiste Gulla.

Ethics Statement

The Vilnius Regional Bioethics Committee approved (permit number 2021/6-1354-843, issued 2021-06-29) the study design and waived the requirement of individual informed consent according to the International Ethical Guidelines for Health-related Research Involving Humans.[16]

REFERENCES

1. McGlynn KA, Petrick JL, El-Serag HB. Epidemiology of hepatocellular carcinoma. *Hepatology*. 2021;73:4–13.
2. Chidambaranathan-Reghupaty S, Fisher PB, Sarkar D. Hepatocellular carcinoma (HCC): epidemiology, etiology and molecular classification. *Adv Cancer Res*. 2021;149:1–61.
3. Kulik L, El-Serag HB. Epidemiology and management of hepatocellular carcinoma. *Gastroenterology*. 2019;156:477–491.e1.
4. Yang JD, Hainaut P, Gores GJ, Amadou A, Plymoth A, Roberts LR. A global view of hepatocellular carcinoma: trends, risk, prevention and management. *Nat Rev Gastroenterol Hepatol*. 2019;16:589–604.
5. Sugawara Y, Hibi T. Surgical treatment of hepatocellular carcinoma. *Biosci Trends*. 2021;15:138–141.
6. Eilard MS, Naredi P, Helmersson M, et al. Survival and prognostic factors after transplantation, resection and ablation in a national cohort of early hepatocellular carcinoma. *HPB*. 2021;23:394–403.
7. Krenzien F, Schmelzle M, Struecker B, et al. Liver transplantation and liver resection for cirrhotic patients with

hepatocellular carcinoma: comparison of long-term survivals. *J Gastrointest Surg*. 2018;22:840–848.
8. Salehi O, Vega EA, Kutlu OC, et al. Poorly differentiated hepatocellular carcinoma: resection is equivalent to transplantation in patients with low liver fibrosis. *HPB (Oxford)*. 2022;24:1100–1109.
9. Oura K, Morishita A, Tani J, Masaki T. Tumor immune microenvironment and immunosuppressive therapy in hepatocellular carcinoma: a review. *Int J Mol Sci*. 2021;22:5801.
10. Nam D, Chapiro J, Paradis V, Seraphin TP, Kather JN. Artificial intelligence in liver diseases: improving diagnostics, prognostics and response prediction. *JHEP Rep*. 2022;4:100443.
11. Du M, Yin YL, Xiao L, Cai YM, Ji Y. Evaluating tumor-infiltrating lymphocytes in hepatocellular carcinoma using hematoxylin and eosin-stained tumor sections. *World J Clin Cases*. 2022;10:856–869.
12. Yao W, He JC, Yang Y, et al. The prognostic value of tumor-infiltrating lymphocytes in hepatocellular carcinoma: a systematic review and meta-analysis. *Sci Rep*. 2017;7:7525.
13. Ding W, Xu X, Qian Y, et al. Prognostic value of tumor-infiltrating lymphocytes in hepatocellular carcinoma a meta-analysis. *Medicine (United States)*. 2018;97:e13301.
14. Stulpinas R, Zilenaite-Petrulaitiene D, Rasmusson A, et al. Prognostic value of CD8+ lymphocytes in hepatocellular carcinoma and perineoplastic parenchyma assessed by interface density profiles in liver resection samples. *Cancers*. 2023;15:366.
15. Rasmusson A, Zilenaite D, Nestarenkaite A, et al. Immunogradient indicators for antitumor response assessment by automated tumor-stroma interface zone detection. *Am J Pathol*. 2020;190:1309–1322.
16. Council for International Organizations of Medical Sciences (CIOMS) in collaboration with the World Health Organization (WHO). *International ethical guidelines for health-related research involving Humans*. 4th Ed. Geneva, Switzerland: Council for International Organizations of Medical Sciences (CIOMS); 2016.
17. Milan criteria for liver transplantation. MDCalc. Available at: https://www.mdcalc.com/calc/3900/milan-criteria-liver-transplantation . Accessed February 18, 2023.
18. Zilenaite D, Rasmusson A, Augulis R, et al. Independent prognostic value of intratumoral heterogeneity and immune response features by automated digital immunohistochemistry analysis in early hormone receptor-positive breast carcinoma. *Front Oncol*. 2020;10:950.
19. Budczies J, Klauschen F, Sinn BV, et al. Cutoff finder: a comprehensive and straightforward web application enabling rapid biomarker cutoff optimization. *PLoS One*. 2012;7:e51862.
20. Mehta N, Bhangui P, Yao FY, et al. Liver transplantation for hepatocellular carcinoma. Working group report from the ILTS transplant oncology consensus conference. *Transplantation*. 2020;104:1136–1142.
21. Sarici B, Isik B, Yilmaz S. Management of recurrent HCC after liver transplantation. *J Gastrointest Cancer*. 2020;51:1197–1199.
22. Amado V, González-Rubio S, Zamora J, et al. Clearance of circulating tumor cells in patients with hepatocellular carcinoma undergoing surgical resection or liver transplantation. *Cancers*. 2021;13:2476.
23. Akcam AT, Saritas AG, Ulku A, Rencuzogullari A. Oncological outcomes of hepatic resection vs transplantation for localized hepatocellular carcinoma. *Transplant Proc*. 2019;51:1147–1152.
24. Lang SA, Bednarsch J, Czigany Z, et al. Liver transplantation in malignant disease. *World J Clin Oncol*. 2021;12:623–645.
25. Straś WA, Wasiak D, Łągiewska B, et al. Recurrence of hepatocellular carcinoma after liver transplantation: risk factors and predictive models. *Ann Transplant*. 2022;27:e934924.
26. Agarwal PD, Lucey MR. Management of hepatocellular carcinoma recurrence after liver transplantation. *Ann Hepatol*. 2022;27:100654.
27. Goldaracena N, Mehta N, Scalera I, et al. Multicenter validation of a score to predict prognosis after the development of HCC recurrence following liver transplantation. *HPB*. 2019;21:731–738.
28. Xu X, Tan Y, Qian Y, et al. Clinicopathologic and prognostic significance of tumor-infiltrating CD8+ T cells in patients with hepatocellular carcinoma: a meta-analysis. *Medicine (United States)*. 2019;98:e13923.
29. Ramzan M, Sturm N, Decaens T, et al. Liver-infiltrating CD8+ lymphocytes as prognostic factor for tumour recurrence in hepatitis C virus-related hepatocellular carcinoma. *Liver Int*. 2016;36:434–444.
30. Gabrielson A, Wu Y, Wang H, et al. Intratumoral CD3 and CD8 T-cell densities associated with relapse-free survival in HCC. *Cancer Immunol Res*. 2016;4:419–430.
31. Takahashi K, Liang C, Oda T, Ohkohchi N. Platelet and liver regeneration after liver surgery. *Surg Today*. 2020;50:974–983.
32. Li Q, Wang Y, Ma T, et al. Preoperative platelet count predicts posttransplant portal vein complications in orthotopic liver transplantation: a propensity score analysis. *BMC Gastroenterol*. 2021;21:1.

4th publication / 4 publikacija

Rokas Stulpinas, Ieva Jakiunaite, Agne Sidabraite, Allan Rasmusson, Dovile Zilenaite-Petrulaitiene, Kestutis Strupas, Arvydas Laurinavicius, Aiste Gulla

Low CD8 Density Variation and R1 Surgical Margin as Independent Predictors
of Early Post-Resection Recurrence in HCC Patients Meeting Milan Criteria.

Curr Oncol. 2024 Sep 10;31(9):5344-5353

doi: 10.3390/curroncol31090394. PMID: 39330022; PMCID: PMC11431076.

https://pubmed.ncbi.nlm.nih.gov/39330022/

Current Oncology

MDPI

Article

Low CD8+ Density Variation and R1 Surgical Margin as Independent Predictors of Early Post-Resection Recurrence in HCC Patients Meeting Milan Criteria

Rokas Stulpinas [1,2,*], Ieva Jakiunaite [3], Agne Sidabraite [3], Allan Rasmusson [1,2], Dovile Zilenaite-Petrulaitiene [1,2,4], Kestutis Strupas [5], Arvydas Laurinavicius [1,2] and Aiste Gulla [5,6]

[1] Institute of Biomedical Sciences, Department of Pathology and Forensic Medicine, Faculty of Medicine, Vilnius University, 03101 Vilnius, Lithuania
[2] National Center of Pathology, Affiliate of Vilnius University Hospital Santaros Clinics, 08406 Vilnius, Lithuania
[3] Faculty of Medicine, Vilnius University, 03101 Vilnius, Lithuania
[4] Institute of Informatics, Faculty of Mathematics and Informatics, Vilnius University, 03225 Vilnius, Lithuania
[5] Institute of Clinical Medicine, Centre for Visceral Medicine and Translational Research, Faculty of Medicine, Vilnius University, 01513 Vilnius, Lithuania
[6] Department of Surgery, School of Medicine and Health Sciences, The George Washington University, Washington, DC 20052, USA
* Correspondence: rokas.stulpinas@vpc.lt

Abstract: Our study included 41 patients fulfilling the Milan criteria preoperatively and aimed to identify individuals at high risk of post-resection HCC relapse, which occurred in 18 out of 41 patients (43.9%), retrospectively. We analyzed whole slide images of CD8 immunohistochemistry with automated segmentation of tissue classes and detection of CD8+ lymphocytes. The image analysis outputs were subsampled using a hexagonal grid-based method to assess spatial distribution of CD8+ lymphocytes with regards to the epithelial edges. The CD8+ lymphocyte density indicators, along with clinical, radiological, post-surgical and pathological variables, were tested to predict HCC relapse. Low standard deviation of CD8+ density along the tumor edge and R1 resection emerged as independent predictors of shorter recurrence-free survival (RFS). In particular, patients presenting with both adverse predictors exhibited 100% risk of relapse within 200 days. Our results highlight the potential utility of integrating CD8+ density variability and surgical margin to identify a high relapse-risk group among Milan criteria-fulfilling HCC patients. Validation in cohorts with core biopsy could provide CD8+ distribution data preoperatively and guide preoperative decisions, potentially prioritizing liver transplantation for patients at risk of incomplete resection (R1) and thereby improving overall treatment outcomes significantly.

Keywords: CD8; digital pathology; hepatocellular carcinoma (HCC); tumor-infiltrating lymphocytes; Milan criteria; liver transplantation

check for updates

Citation: Stulpinas, R.; Jakiunaite, I.; Sidabraite, A.; Rasmusson, A.; Zilenaite-Petrulaitiene, D.; Strupas, K.; Laurinavicius, A.; Gulla, A. Low CD8+ Density Variation and R1 Surgical Margin as Independent Predictors of Early Post-Resection Recurrence in HCC Patients Meeting Milan Criteria. *Curr. Oncol.* **2024**, *31*, 5344–5353. https://doi.org/10.3390/curroncol31090394

Received: 19 July 2024
Revised: 4 September 2024
Accepted: 8 September 2024
Published: 10 September 2024

1. Introduction

Liver cancer is one of the five most lethal malignancies and ranks sixth in global morbidity rates [1,2]. The most common type of liver cancer is hepatocellular carcinoma (HCC), comprising over 90% of cases, with only 10–15% of patients achieving a five-year survival rate worldwide [3]. The incidence of HCC increases annually; furthermore, relapse occurs in 30–50% of patients during the first two years after resection [1,4]. Known risk factors for early relapse include male gender, large tumor size, tumor multifocality, high serum alpha-fetoprotein level and many others [4,5].

The complex tumor microenvironment plays a critical role in the progression and metastasis of HCC [6]. The host immune response, particularly involving CD8+ lymphocytes or cytotoxic T cells, can significantly influence tumor recurrence and patient survival

outcomes in HCC [7,8]. Higher densities of CD8+ cells often indicate a robust anti-tumoral immune response that can suppress tumor growth and prevent recurrence. While some earlier studies found no prognostic value in CD8+ cell densities [9], others suggested that high tumor infiltrating lymphocyte (TIL) levels could contribute to HCC development and relapse [10]. However, more recent evidence indicates a positive association between high TIL densities and improved outcomes [8,11]. Emerging research not only examines the average density of tumor-infiltrating lymphocytes but also the spatial heterogeneity of their infiltration. For example, the study by Li et al. determined that both intratumoral and peritumoral lymphoid clusters (tertiary lymphoid structures (TLS)) play crucial roles in HCC, with high peritumoral TLS density correlating with increased immune cell infiltration and a better patient prognosis [12]. Understanding and measuring the precise spatial distribution of tumor-infiltrating lymphocytes is essential for advancing treatment strategies and improving outcomes for HCC patients.

Currently, liver transplantation (LT) is regarded as the first-line treatment option for patients with HCC who meet the Milan criteria [13]. Liver transplantation, when performed as an initial treatment, has the potential to simultaneously remove both the tumor and the underlying disease, typically cirrhosis, thereby offering superior long-term outcomes compared to liver resection (LR). This advantage is demonstrated by a 5-year disease-free survival (DFS) rate of up to 96.8% for LT, compared to 64.3% for LR, and a nearly 50% reduction in mortality rate, although some of the numbers do seem overly optimistic and could be biased [14,15]. Even though the risk of HCC recurrence after LR is threefold that of LT, a shortage of cadaveric organs limits the selection of this therapeutic modality [15]. Salvage liver transplantation (SLT) serves as a crucial alternative curative approach, demonstrating comparable DFS rates between primary liver transplantation (PLT) and SLT–LR groups [16].

Since the introduction of the Milan criteria in 1996 (a single tumor with a diameter $\leq$5 cm; or no more than three tumors, each $\leq$3 cm in size; and no vascular invasion; and no extrahepatic involvement) into clinical use, survival rates after LT for HCC have improved significantly [17]. Despite the strict adherence to these criteria, tumor recurrence occurs in up to 20% of HCC patients who have undergone LT, with 75% of the recurrences emerging during the first 2 years after the LT [18,19]. Stratifying individuals who meet the Milan criteria into distinct risk categories may aid the decision-making process for LT as the next line of therapeutic intervention.

This study aims to improve the prediction of post-resection HCC recurrence in patients meeting the Milan criteria preoperatively using paraffin-embedded tissue, CD8 immunohistochemistry, AI tissue segmentation and hexagonal grid subsampling-based image analytics. If further validated on biopsy material, our findings suggest that integrating CD8+ T cell density variability into preoperative predictive models could aid in decision-making, particularly in considering liver transplantation for patients at risk of incomplete (R1) resection.

2. Materials and Methods

2.1. Study Population

The cohort for this retrospective study comprised consecutive patients, totaling 41 individuals, who underwent liver resection for HCC between 2007–2020 at Vilnius University Hospital Santaros Clinics (Vilnius, Lithuania) and, at the time of surgery, fulfilled the Milan criteria for liver transplantation preoperatively. The resected tissue was processed, analyzed and archived in the National Center of Pathology (Vilnius, Lithuania). The study was approved by the Vilnius Regional Biomedical Research Ethics Committee (permit number 2021/6-1354-843).

2.2. Immunohistochemistry

A pathologist (RS) reviewed the archived slides stained with hematoxylin and eosin to identify the optimal formalin-fixed paraffin-embedded (FFPE) tissue block. The selected

samples, cut to 3 µm in thickness, were mounted on positively charged slides and immunohistochemically stained for CD8 using Dako's C8/144B antibody (dilution 1:100, Dako, Glostrup, Denmark). Staining was performed on a Roche Ventana BenchMark ULTRA automated stainer with the ultraView Universal DAB Detection kit (Ventana Medical Systems, Oro Valley, AZ, USA).

2.3. Digital Image Analysis and Indicator Extraction

The detailed process workflow is explained in our previously published paper [20]. Briefly, slides were digitized at 20× magnification (0.5 µm per pixel) using an Aperio® AT2 DX scanner (Leica Aperio Technologies, Vista, CA, USA). A pathologist (RS) marked the tumor and residual liver parenchyma areas by placing annotations. The HALO®AI (Indica Labs, Albuquerque, NM, USA) system was subsequently trained to segment tissue into epithelial/hepatocytes, stroma and background/debris classes, with CD8+ cell segmentation performed using the HALO® Multiplex IHC algorithm. We further processed the HALO®AI outputs by using a hexagonal grid tiling method (having a side length of 65 µm in this study) as described by Rasmusson et al. [21].

The number of CD8+ cells and the area of tissue classes in each hexagon were aggregated for the malignant (HCC) and non-malignant (residual liver parenchyma) parts of the slide. Based on the abrupt change in tissue class proportions across the grid, we identified hexagons on the extracted epithelial edge and assigned them a rank of 0. The remaining epithelial hexagons (representing HCC or liver depending on the area analyzed) are assigned positive ranks, whereas hexagons on the stromal side received negative ranks corresponding to their distance from the nearest edge. Immune response indicators were extracted from five hexagon-wide interface zones (ranks −2, −1, 0, 1, 2) of the non-neoplastic liver and HCC to reflect CD8+ cell density profiles in both tissue compartments, including mean density, standard deviation (SD), the center of mass and immunodrop ratio (the ratio of CD8+ cell quantities at ranks −1 and 1, indicating abrupt change in cell density at the tumor edge) (see Figure 1).

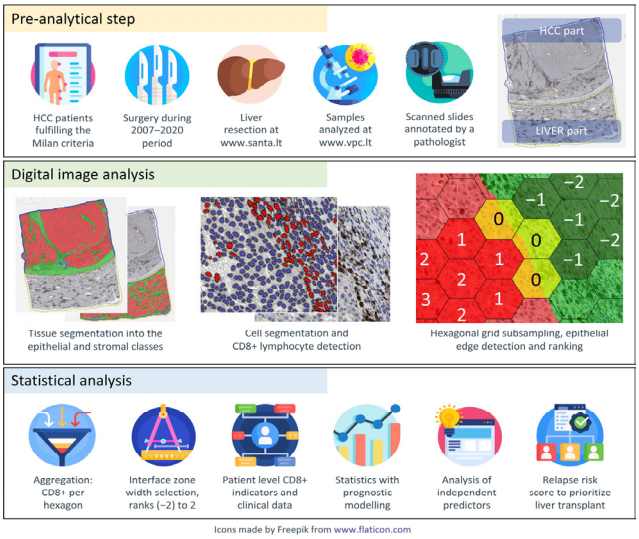

Figure 1. Study workflow. Pre-analytical step: HCC patients meeting the Milan criteria underwent liver resection between 2007–2020. Samples were analyzed and scanned slides were annotated by a

pathologist. Digital image analysis: tissue samples were segmented into epithelial and stromal classes, and CD8+ lymphocytes were detected using HALO® AI (Indica Labs, USA). Hexagonal grid subsampling was applied for epithelial edge detection. Statistical analysis: aggregated CD8+ data per hexagon were combined with clinical data for prognostic modeling. Independent predictors were analyzed, and a relapse risk score was developed to prioritize liver transplant candidates.

2.4. Statistical Analysis and Modeling

To meet the assumptions of normality and homoscedasticity, the initial aggregated data underwent a logarithmic transformation of the CD8+ density values. For improved readability, the 'log' prefix is omitted in the subsequent text. Significance levels were set at $p < 0.05$. Univariate Cox regression was used to evaluate the prognostic significance of conventional clinicopathologic predictors, which were represented by either continuous or categorical variables. Then, a multivariate Cox regression with stepwise likelihood ratio (LR) testing was performed to assess the independent prognostic value of the CD8+ lymphocyte distribution indicators, represented as continuous variables, in the context of the statistically significant conventional predictors identified in the univariate analysis. An integrated Recurrence Risk Score was derived by summing the negative impacts of the independent predictors of recurrence-free survival (RFS). RFS was estimated using the Kaplan–Meier method, followed by log-rank testing to compare the statistical significance of the RFS distributions. SAS (version 9.4; SAS Institute Inc., Cary, NC, USA) and R version 4.3.2 (R Foundation for Statistical Computing, Vienna, Austria), along with the survminer and ggplot2 packages, were employed for data analysis in this study.

3. Results

3.1. Summary of Patient Cohort Characteristics

Patient gender, age, tumor grade, pT stage, intravascular invasion (as reported in the pathology report), resection margin, number of tumors, largest tumor size, the presence of cirrhosis, duration of surgery, hospitalization time and the date of HCC recurrence were collected from hospital records and are presented in Table 1.

Table 1. Patient demographics and clinical characteristics.

Characteristic	Value (%)
Patients	41 (100%)
Age, years:	
Mean (SD)	64.4 (9.16)
Median (IQR)	66 (12)
Age distribution	
<50 years	1 (2.4%)
50–59 years	10 (24.4%)
60–69 years	18 (43.9%)
70–79 years	11 (26.8%)
≥80 years	1 (2.4%)
Gender	
Males	28 (68.3%)
Females	13 (31.7%)
Tumor grade	
G1	4 (9.8%)
G2	29 (70.7%)
G3	8 (19.5%)
pT stage:	
pT1	27 (65.9%)
pT2	14 (34.1%)

Table 1. *Cont.*

Characteristic	Value (%)
Intravascular invasion	
LVI present	12 (29.3%)
LVI absent	29 (70.7%)
Resection margin	
R0	33 (80.5%)
R1	8 (19.5%)
Number of tumors	
One tumor	32 (78.0%)
Two tumors	7 (17.1%)
Three tumors	2 (4.9%)
Tumor size in the pathology report, mm	
Mean (SD)	28 (11)
Median (IQR)	25 (20)
Recurrences	
HCC recurrence	18 (43.9%)
No recurrence	23 (56.1%)
RFS time, days	
Mean (SD)	904.4 (702.9)
Median (IQR)	749 (933)

3.2. Predictors of Recurrence-Free Survival

The resulting Cox proportional hazard model of the Milan criteria-fulfilling patient cohort consisted of two independent predictors of a shorter RFS after HCC resection (see Table 2). One predictor was a histologic feature of immune response, specifically a low SD of CD8+ density along the tumor edge (HR = 0.246 (95% CI 0.078–0.779), $p = 0.0171$, see Figure S1 "Representative images demonstrating CD8+ cell density variation at the tumor edge"), the second—a conventional parameter, the R1 resection as defined in the final pathology report (HR = 7.162 (95% CI 2.213–23.185), $p = 0.0010$). None of the other patient or tumor characteristics had a statistically significant impact on RFS.

Table 2. Independent predictors of recurrence-free survival (RFS) in Milan criteria-fulfilling patients based on multivariate Cox regression modelling.

Indicator	DF	Parameter Estimates	Standard Error	Chi-Square	*p*-Value	Hazard Ratio	95% Hazard Ratio Confidence Limits	
R1 resection	1	1.96882	0.59935	10.7909	0.0010	7.162	2.213	23.185
SD of CD8 at tumor edge	1	−1.40113	0.58769	5.6842	0.0171	0.246	0.078	0.779

Likelihood Ratio Test: Chi-square 17.7246, $p = 0.0001$.

Panel (a) of Figure 2 displays the survival probabilities over time for patients categorized by their resection status: R0 (complete resection) and R1 (incomplete resection). The *p*-value for the comparison between R0 and R1 groups is very low ($p < 0.0001$), indicating that patients with complete resection (R0) have a longer RFS compared to those with incomplete resection (R1). Panel (b) of Figure 2 illustrates the RFS probabilities for patients based on the SD of CD8 density at the tumor edge, with groups divided into low (<5.8) = 1 and high (>5.8) = 0. The *p*-value for this comparison is 0.0066, indicating a statistically significant difference between the two groups and implying that a low SD of CD8+ density along the tumor edge has a negative impact on RFS.

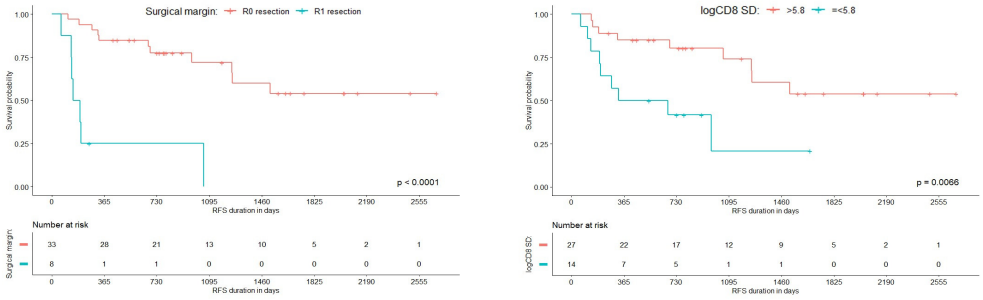

(**a**) (**b**)

Figure 2. The R1 resection (**a**) and low standard deviation of CD8+ density along the tumor edge (**b**) as univariate predictors for shorter RFS.

3.3. Recurrence Risk Score

Based on the findings, a combined prognostic Relapse Score was constructed by summing up the contributions from both independent variables and assigning a value of 1 for a poor and 0 for a good prognosis. Since there are two independent predictors with either a 0 or 1 value, the possible score for each patient is 0 (0 + 0), 1 (1 + 0 or 0 + 1) or 2 (1 + 1). The Kaplan–Meier survival curves for these groups with significant RFS differences are shown in Figure 3. The chart suggests that individuals who exhibit both adverse predictors experience a 100% relapse risk within a relatively short timeframe—less than 200 days.

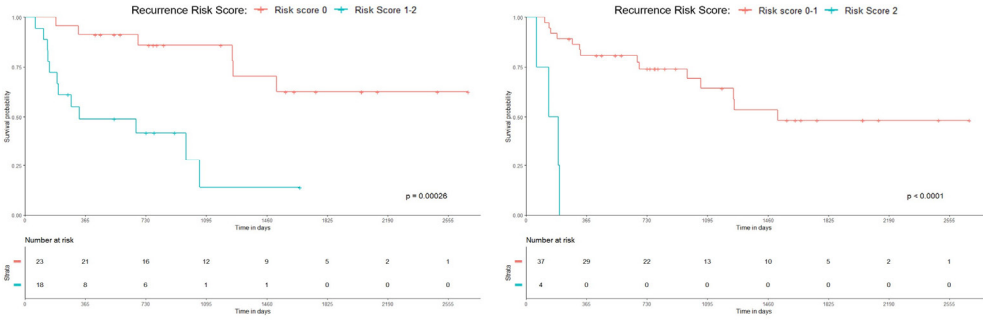

(**a**) (**b**)

Figure 3. HCC Recurrence Risk Score: (**a**) 0 vs. 1–2 ($p = 0.00026$) and (**b**) 0–1 vs. 2 ($p < 0.0001$).

4. Discussion

Our study explored the link between the spatial distribution of CD8+ cytotoxic T cells, the established clinicopathologic adverse factors and the risk of recurrence following liver resection for HCC. The finding that a higher variance (SD) of CD8+ T lymphocyte density at the tumor edge is associated with longer RFS in HCC patients is intriguing. While generally denser and more uniform infiltration of CD8+ T cells is linked to better cancer patient outcomes [22–24], our data suggest a more nuanced relationship. Some studies in other cancers have shown similar trends: for example, Krijgsman et al. (also utilizing a deep learning tissue classifier combined with immunohistochemistry) discovered that

breast cancer patients with high variation (SD) of CD8+ cell density had longer overall survival (OS) [25]. A potential explanation is that the high SD of CD8+ lymphocyte density mathematically reflects the presence of localized, denser immune cell clusters. These clusters, in some cases, might represent the well-established tertiary lymphoid structures (TLS) known to be favorable prognostic markers in HCC [16,26–28]. Uniformly distributed CD8+ lymphocytes at the tumor edge could on the other hand be exhausted T cells that lack the ability to effectively induce an anti-tumoral response [29]. Furthermore, chronic HBV and HCV infection that often precede HCC can lead to the production of immunosuppressive cytokines within the liver microenvironment, which impairs the function of T cells, further contributing to exhaustion [30–32]. To validate this hypothesis, future studies could analyze the expression of immune checkpoint molecules on these CD8+ T cells.

Liver transplantation is the preferred treatment for selected HCC patients, offering markedly improved outcomes in 5-year OS and RFS rates (64.83% and of 70.20%, respectively), compared to liver resection (OS: 50.83%; RFS: 34.46%) [33]. Meanwhile, as patients remain on the waiting list for a donor, interim management strategies such as liver resection, ablation and transarterial interventions are employed to control disease progression [34]. Liver resection is considered a curative procedure for individuals diagnosed with HCC, though it is associated with significant recurrence rates, with 60% of cases relapsing within three years. Moreover, resection yields tissue essential for the pathological evaluation of key independent predictors of HCC recurrence and post-transplantation survival, namely the presence of satellite nodules, the degree of tumor differentiation and microvascular invasion [35]. Although the ideal margin width remains a topic of debate, surgical resection for HCC is generally not advised for patients whose tumors cannot be completely removed with negative (R0) margins [35].

The identification of a positive margin (R1) as a significant independent predictor of a shorter RFS is consistent with the established knowledge that incomplete removal of neoplastic tissue increases the likelihood of recurrence. In our cohort, when a safe surgical margin was unattainable based on intraoperative findings, surgical resection was carried out, ensuring the complete macroscopic removal of the tumor. The overall recurrence rate was observed to be 43.9%, with relapses occurring significantly more frequently in the R1 group (87.5%) compared to the R0 group (33.3%), $p = 0.0133$. Numerous studies have evaluated the influence of surgical margins on the outcomes of HCC following liver resection [36–38]. Although these studies vary in nature, they consistently report that the width of the resection margin does not impact postoperative recurrence rates following hepatectomy for HCC. Poon et al. concluded that a positive margin correlates with an increased risk of postoperative recurrence and is frequently associated with underlying venous invasion or the presence of microsatellites [39].

The Recurrence Risk Score, combining CD8+ density variability (represented by the standard deviation) at the tumor edge and resection margin status, offers a potential tool to identify patients at high risk of early relapse. In addition, although formally eligible for transplantation, patients over 70 years of age demonstrate poorer post-transplantation outcomes than younger cohorts, warranting cautious consideration of liver transplantation in this age group [40]. Liver transplantation should always be considered for eligible patients; however, investigating the factors influencing CD8+ cell distribution and their utility as prognostic biomarkers for recurrence and long-term survival is crucial prior to relying on them for treatment decisions.

Limitations

This study is subject to several limitations that should be acknowledged. First, the sample size of 41 patients, particularly within certain subgroups ($n = 4$), is relatively small, which may limit the generalizability of our findings. Additionally, the still somewhat heterogeneous nature of the study cohort could introduce variability that impacts the ro-

bustness of the results. These factors necessitate caution when interpreting the data. Future validating studies with larger cohorts and/or biopsy core tissues are highly encouraged.

5. Conclusions

In conclusion, our study contributes to the understanding of the immune response's role in predicting HCC recurrence following liver resection. By integrating CD8+ spatial distribution indicators with resection margin status, we present a potentially novel methodology for identifying high-risk HCC patients who meet the Milan criteria preoperatively. Subsequent validation in cohorts using core biopsy material could provide preoperative CD8+ distribution data, thereby guiding preoperative decisions and potentially prioritizing liver transplantation for patients at risk of incomplete resection (R1). This approach could significantly improve overall treatment outcomes. Although significant trends were observed, further research with larger and more diverse cohorts is necessary.

Supplementary Materials: The following supporting information can be downloaded at: https://www.mdpi.com/article/10.3390/curroncol31090394/s1, Figure S1: Representative images demonstrating CD8+ cell density variation at the tumor edge.

Author Contributions: Conceptualization, R.S., A.L. and A.G.; Data curation, R.S.; Formal analysis, R.S., A.R. and D.Z.-P.; Funding acquisition, A.L.; Investigation, R.S., I.J., A.S. and A.G.; Methodology, A.L.; Resources, I.J., A.S. and K.S.; Software, A.R.; Supervision, K.S., A.L. and A.G.; Visualization, R.S. and A.R.; Writing—original draft, R.S., I.J., A.S. and A.G.; Writing—review & editing, A.R., D.Z.-P., K.S. and A.L. All authors have read and agreed to the published version of the manuscript.

Funding: This research is in part funded by the European Social Fund resources allocated for the project "Development of Doctoral Studies " implemented by Research Council of Lithuania, project No. 09.3.3-ESFA-V-711-01-0001, under the Specific objective "Strengthen the Skills and Capacities of Public Sector Researchers for Engaging in High Level R & D Activities" of Priority Axis 9 "Educating the Society and Strengthening the Potential of Human Resources" within the framework of the Operational Programme for the European Union Funds' Investments in 2014–2020.

Institutional Review Board Statement: The Lithuanian Bioethics Committee approved (permit number 2021/6-1354-843, issued 29 June 2021) the study design.

Informed Consent Statement: Patient consent was waived by the Vilnius Regional Biomedical Research Ethics Committee according to the International Ethical Guidelines for Health-related Research Involving Humans.

Data Availability Statement: The data presented in this study are available on request from the corresponding author. The data are not publicly available due to permit restrictions.

Acknowledgments: The authors would like to thank their colleagues from the National Center of Pathology for their valuable help in producing IHC slides, diagnostic work on the cases and IT support and significantly contributing to many other technical tasks that enabled the publication of these results.

Conflicts of Interest: The authors declare no conflicts of interest. The funders had no role in the design of the study; in the collection, analyses, or interpretation of data; in the writing of the manuscript; or in the decision to publish the results.

References

1. Siegel, R.L.; Miller, K.D.; Jemal, A. Cancer statistics, 2018. *CA Cancer J. Clin.* **2018**, *68*, 7–30. [CrossRef] [PubMed]
2. Sung, H.; Ferlay, J.; Siegel, R.L.; Laversanne, M.; Soerjomataram, I.; Jemal, A.; Bray, F. Global Cancer Statistics 2020: GLOBOCAN Estimates of Incidence and Mortality Worldwide for 36 Cancers in 185 Countries. *CA Cancer J. Clin.* **2021**, *71*, 209–249. [CrossRef]
3. Marrero, J.A.; Kulik, L.M.; Sirlin, C.B.; Zhu, A.X.; Finn, R.S.; Abecassis, M.M.; Roberts, L.R.; Heimbach, J.K. Diagnosis, Staging, and Management of Hepatocellular Carcinoma: 2018 Practice Guidance by the American Association for the Study of Liver Diseases. *Hepatology* **2018**, *68*, 723–750. [CrossRef]
4. Chan, A.W.H.; Zhong, J.H.; Berhane, S.; Toyoda, H.; Cucchetti, A.; Shi, K.Q.; Tada, T.; Chong, C.C.N.; Xiang, B.D.; Li, L.Q.; et al. Development of pre and post-operative models to predict early recurrence of hepatocellular carcinoma after surgical resection. *J. Hepatol.* **2018**, *69*, 1284–1293. [CrossRef]

5. Nevola, R.; Ruocco, R.; Criscuolo, L.; Villani, A.; Alfano, M.; Beccia, D.; Imbriani, S.; Claar, E.; Cozzolino, D.; Sasso, F.C.; et al. Predictors of early and late hepatocellular carcinoma recurrence. *World J. Gastroenterol.* **2023**, *29*, 1243–1260. [CrossRef] [PubMed]
6. Kotsari, M.; Dimopoulou, V.; Koskinas, J.; Armakolas, A. Immune System and Hepatocellular Carcinoma (HCC): New Insights into HCC Progression. *Int. J. Mol. Sci.* **2023**, *24*, 11471. [CrossRef]
7. Schoenberg, M.B.; Li, X.K.; Li, X.Y.; Han, Y.S.; Hao, J.C.; Miksch, R.C.; Koch, D.; Börner, N.; Beger, N.T.; Bucher, J.N.; et al. The predictive value of tumor infiltrating leukocytes in Hepatocellular Carcinoma: A systematic review and meta-analysis. *EJSO-Eur. J. Surg. Oncol.* **2021**, *47*, 2561–2570. [CrossRef] [PubMed]
8. Xu, X.Z.; Tan, Y.L.; Qian, Y.; Xue, W.B.; Wang, Y.B.; Du, J.G.; Jin, L.; Ding, W. Clinicopathologic and prognostic significance of tumor-infiltrating CD8+T cells in patients with hepatocellular carcinoma A meta-analysis. *Medicine* **2019**, *98*, e13923. [CrossRef]
9. Ikeguchi, M.; Oi, K.; Hirooka, Y.; Kaibara, N. CD8+lymphocyte infiltration and apoptosis in hepatocellular carcinoma. *Eur. J. Surg. Oncol.* **2004**, *30*, 53–57. [CrossRef]
10. Ramzan, M.; Sturm, N.; Decaens, T.; Bioulac-Sage, P.; Bancel, B.; Merle, P.; Nhieu, J.T.V.; Slama, R.; Letoublon, C.; Zarski, J.P.; et al. Liver-infiltrating CD8+ lymphocytes as prognostic factor for tumour recurrence in hepatitis C virus-related hepatocellular carcinoma. *Liver Int.* **2016**, *36*, 434–444. [CrossRef]
11. Ding, W.; Xu, X.Z.; Qian, Y.; Xue, W.B.; Wang, Y.B.; Du, J.G.; Jin, L.; Tan, Y.L. Prognostic value of tumor-infiltrating lymphocytes in hepatocellular carcinoma A meta-analysis. *Medicine* **2018**, *97*, e13301. [CrossRef]
12. Li, H.; Liu, H.L.; Fu, H.Y.; Li, J.X.; Xu, L.; Wang, G.S.; Wu, H. Peritumoral Tertiary Lymphoid Structures Correlate With Protective Immunity and Improved Prognosis in Patients With Hepatocellular Carcinoma. *Front. Immunol.* **2021**, *12*, 648812. [CrossRef] [PubMed]
13. Mehta, N.; Bhangui, P.; Yao, F.Y.; Mazzaferro, V.; Toso, C.; Akamatsu, N.; Durand, F.; Ijzermans, J.; Polak, W.; Zheng, S.S.; et al. Liver Transplantation for Hepatocellular Carcinoma. Working Group Report from the ILTS Transplant Oncology Consensus Conference. *Transplantation* **2020**, *104*, 1136–1142. [CrossRef] [PubMed]
14. Karakas, S.; Yilmaz, S.; Ince, V.; Akbulut, S.; Dalda, Y.; Akatli, A.N.; Kahraman, A.S.; Kutlu, R.; Carr, B.I. Comparison of liver resection and living donor liver transplantation in patients with hepatocellular carcinoma within Milan criteria and well-preserved liver function. *Hepatol. Forum* **2023**, *4*, 47–52. [CrossRef] [PubMed]
15. Koh, J.H.; Tan, D.J.H.; Ong, Y.; Lim, W.H.; Ng, C.H.; Tay, P.W.L.; Yong, J.N.; Muthiah, M.D.; Tan, E.X.; Pang, N.Q.; et al. Liver resection versus liver transplantation for hepatocellular carcinoma within Milan criteria: A meta-analysis of 18,421 patients. *Hepatobil. Surg. Nutr.* **2022**, *11*, 78. [CrossRef]
16. Anselmo, A.; Siragusa, L.; Brigato, P.; Riccetti, C.; Collini, A.; Sensi, B.; Tisone, G. Primary versus Salvage Liver Transplantation after Curative-Intent Resection or Radiofrequency Ablation for Hepatocellular Carcinoma: Long-Term Oncological Outcomes. *Cancers* **2023**, *15*, 5030. [CrossRef]
17. Mazzaferro, V.; Regalia, E.; Doci, R.; Andreola, S.; Pulvirenti, A.; Bozzetti, F.; Montalto, F.; Ammatuna, M.; Morabito, A.; Gennari, L. Liver transplantation for the treatment of small hepatocellular carcinomas in patients with cirrhosis. *N. Engl. J. Med.* **1996**, *334*, 693–699. [CrossRef]
18. Filgueira, N.A. Hepatocellular carcinoma recurrence after liver transplantation: Risk factors, screening and clinical presentation. *World J. Hepatol.* **2019**, *11*, 261–272. [CrossRef]
19. Tabrizian, P.; Holzner, M.L.; Mehta, N.; Halazun, K.; Agopian, V.G.; Yao, F.; Busuttil, R.W.; Roberts, J.; Emond, J.C.; Samstein, B.; et al. Ten-Year Outcomes of Liver Transplant and Downstaging for Hepatocellular Carcinoma. *JAMA Surg.* **2022**, *157*, 779–788. [CrossRef]
20. Stulpinas, R.; Zilenaite-Petrulaitiene, D.; Rasmusson, A.; Gulla, A.; Grigonyte, A.; Strupas, K.; Laurinavicius, A. Prognostic Value of CD8+Lymphocytes in Hepatocellular Carcinoma and Perineoplastic Parenchyma Assessed by Interface Density Profiles in Liver Resection Samples. *Cancers* **2023**, *15*, 366. [CrossRef]
21. Rasmusson, A.; Zilenaite, D.; Nestarenkaite, A.; Augulis, R.; Laurinaviciene, A.; Ostapenko, V.; Poskus, T.; Laurinavicius, A. Immunogradient Indicators for Antitumor Response Assessment by Automated Tumor-Stroma Interface Zone Detection. *Am. J. Pathol.* **2020**, *190*, 1309–1322. [CrossRef] [PubMed]
22. Orhan, A.; Khesrawi, F.; Madsen, M.T.; Vogelsang, R.P.; Dohrn, N.; Fiehn, A.M.K.; Gogenur, I. Tumor-Infiltrating Lymphocytes as Biomarkers of Treatment Response and Long-Term Survival in Patients with Rectal Cancer: A Systematic Review and Meta-Analysis. *Cancers* **2022**, *14*, 636. [CrossRef] [PubMed]
23. Rodrigo, J.P.; Sánchez-Canteli, M.; López, F.; Wolf, G.T.; Hernández-Prera, J.C.; Williams, M.D.; Willems, S.M.; Franchi, A.; Coca-Pelaz, A.; Ferlito, A. Tumor-Infiltrating Lymphocytes in the Tumor Microenvironment of Laryngeal Squamous Cell Carcinoma: Systematic Review and Meta-Analysis. *Biomedicines* **2021**, *9*, 486. [CrossRef] [PubMed]
24. Zheng, X.Q.; Jin, W.J.; Wang, S.S.; Ding, H.G. Progression on the Roles and Mechanisms of Tumor-Infiltrating T Lymphocytes in Patients With Hepatocellular Carcinoma. *Front. Immunol.* **2021**, *12*, 729705. [CrossRef]
25. Krijgsman, D.; van Leeuwen, M.B.; van der Ven, J.; Almeida, V.; Vlutters, R.; Halter, D.; Kuppen, P.J.K.; van de Velde, C.J.H.; Wimberger-Friedl, R. Quantitative Whole Slide Assessment of Tumor-Infiltrating CD8-Positive Lymphocytes in ER-Positive Breast Cancer in Relation to Clinical Outcome. *IEEE J. Biomed. Health* **2021**, *25*, 381–392. [CrossRef] [PubMed]
26. Jia, W.L.; Yao, Q.Y.; Wang, Y.F.; Mao, Z.Z.; Zhang, T.C.; Li, J.H.; Nie, Y.; Lei, X.J.; Shi, W.; Song, W.J. Protective effect of tertiary lymphoid structures against hepatocellular carcinoma: New findings from a genetic perspective. *Front. Immunol.* **2022**, *13*, 1007426. [CrossRef]

27. Jia, W.L.; Zhang, T.C.; Yao, Q.Y.; Li, J.H.; Nie, Y.; Lei, X.J.; Mao, Z.Z.; Wang, Y.F.; Shi, W.; Song, W.J. Tertiary Lymphatic Structures in Primary Hepatic Carcinoma: Controversy Cannot Overshadow Hope. *Front. Immunol.* **2022**, *13*, 870458. [CrossRef]
28. Li, J.H.; Nie, Y.; Jia, W.L.; Wu, W.L.; Song, W.J.; Li, Y.X. Effect of Tertiary Lymphoid Structures on Prognosis of Patients with Hepatocellular Carcinoma and Preliminary Exploration of Its Formation Mechanism. *Cancers* **2022**, *14*, 5157. [CrossRef]
29. Zhu, Q.Q.; Yang, Y.M.; Deng, X.Q.; Chao, N.N.; Chen, Z.H.; Ye, Y.X.; Zhang, W.Y.; Liu, W.P.; Zhao, S. High CD8+ tumor-infiltrating lymphocytes indicate severe exhaustion and poor prognosis in angioimmunoblastic T-cell lymphoma. *Front. Immunol.* **2023**, *14*, 1228004. [CrossRef]
30. Ma, J.; Zheng, B.; Goswami, S.; Meng, L.; Zhang, D.; Cao, C.; Li, T.; Zhu, F.; Ma, L.; Zhang, Z.; et al. PD1Hi CD8+ T cells correlate with exhausted signature and poor clinical outcome in hepatocellular carcinoma. *J. Immunother. Cancer* **2019**, *7*, 331. [CrossRef]
31. Li, K.K.; Adams, D.H. Antitumor CD8+ T Cells in Hepatocellular Carcinoma: Present but Exhausted. *Hepatology* **2014**, *59*, 1232–1234. [CrossRef] [PubMed]
32. Barsch, M.; Salié, H.; Schlaak, A.E.; Zhang, Z.; Hess, M.; Mayer, L.S.; Tauber, C.; Otto-Mora, P.; Ohtani, T.; Nilsson, T.; et al. T-cell exhaustion and residency dynamics inform clinical outcomes in hepatocellular carcinoma. *J. Hepatol.* **2022**, *77*, 397–409. [CrossRef] [PubMed]
33. Drefs, M.; Schoenberg, M.B.; Börner, N.; Koliogiannis, D.; Koch, D.T.; Schirren, M.J.; Andrassy, J.; Bazhin, A.V.; Werner, J.; Guba, M.O. Changes of long-term survival of resection and liver transplantation in hepatocellular carcinoma throughout the years: A meta-analysis. *EJSO-Eur. J. Surg. Oncol.* **2024**, *50*, 107952. [CrossRef]
34. Donadon, M.; Terrone, A.; Procopio, F.; Cimino, M.; Palmisano, A.; Viganò, L.; Del Fabbro, D.; Di Tommaso, L.; Torzilli, G. Is R1 vascular hepatectomy for hepatocellular carcinoma oncologically adequate? Analysis of 327 consecutive patients. *Surgery* **2019**, *165*, 897–904. [CrossRef]
35. Lim, C.; Salloum, C.; Lahat, E.; Sotirov, D.; Eshkenazy, R.; Shwaartz, C.; Azoulay, D. Impact of narrow margin and R1 resection for hepatocellular carcinoma on the salvage liver transplantation strategy. An intention-to-treat analysis. *HPB* **2019**, *21*, 1295–1302. [CrossRef]
36. Field, W.B.S.; Rostas, J.W.; Philps, P.; Scoggins, C.R.; McMasters, K.M.; Martin, R.C.G. Wide versus narrow margins after partial hepatectomy for hepatocellular carcinoma: Balancing recurrence risk and liver function. *Am. J. Surg.* **2017**, *214*, 273–277. [CrossRef] [PubMed]
37. Shi, M.; Guo, R.P.; Lin, X.J.; Zhang, Y.Q.; Chen, M.S.; Zhang, C.Q.; Lau, W.Y.; Li, J.Q. Partial hepatectomy with wide versus narrow resection margin for solitary hepatocellular carcinoma—A prospective randomized trial. *Ann. Surg.* **2007**, *245*, 36–43. [CrossRef]
38. Shimada, K.; Sakamoto, Y.; Esaki, M.; Kosuge, T. Role of the width of the surgical margin in a hepatectomy for small hepatocellular carcinomas eligible for percutaneous local ablative therapy. *Am. J. Surg.* **2008**, *195*, 775–781. [CrossRef]
39. Poon, R.T.P.; Fan, S.T.; Ng, I.O.L.; Wong, J. Significance of resection margin in hepatectomy for hepatocellular carcinoma—A critical reappraisal. *Ann. Surg.* **2000**, *231*, 544–551. [CrossRef]
40. Mohan, B.P.; Iriana, S.; Khan, S.R.; Yarra, P.; Ponnada, S.; Gallegos-Orozco, J.F. Outcomes of liver transplantation in patients 70 years or older: A systematic review and meta-analysis. *Ann. Hepatol.* **2022**, *27*, 100741. [CrossRef]

VILNIAUS REGIONINIS BIOMEDICININIŲ TYRIMŲ ETIKOS KOMITETAS
sui generis darinys prie VILNIAUS UNIVERSITETO

LEIDIMAS
ATLIKTI BIOMEDICININĮ TYRIMĄ

2021 06 29 Nr.2021/6-1354-843

Tyrimo pavadinimas:

Kepenų navikų patologijos prognostinis modeliavimas dirbtinio intelekto metodais

Protokolo Nr.:	HEP-AI-2021
Versija:	1.00
Data:	2021 04 15
Informuoto asmens sutikimo forma:	atleidžiama nuo reikalavimo gauti asmens sutikimą
Pagrindinis tyrėjas:	**Arvydas Laurinavičius**
Įstaigos pavadinimas:	VšĮ Vilniaus Universiteto ligoninė Santaros klinikos
Adresas:	Santariškių g. 2, Vilnius
Leidimas galioja iki:	**2025 04**

Leidimas išduotas Vilniaus regioninio biomedicininių tyrimų etikos komiteto posėdžio, vykusio 2021 m. birželio 29 d. sprendimu (protokolas Nr. 2021/6)

Pirmininkas doc. dr. Alfredas Laurinavičius

Viešoji įstaiga
Universiteto g. 3
01513 Vilnius

Duomenys kaupiami ir saugomi
Juridinių asmenų registre
Kodas 211950810

Komiteto duomenys:
M. K. Čiurlionio g. 21, LT- 03101 Vilnius
Tel. (8 5) 268 6998, el. p. rbtek@mf.vu.lt

NOTES

Vilniaus universiteto leidykla
Saulėtekio al. 9, III rūmai, LT-10222 Vilnius
El. p. info@leidykla.vu.lt, www.leidykla.vu.lt
bookshop.vu.lt, journals.vu.lt
Tiražas 35 egz.